A STUDY OF STRUCTURAL AND MAGNETIC PROPERTIES OF Mg-Cu MIXED SPINEL FERRITES

M.Sc. Thesis

BY

APURBA PODDER

DEPARTMENT OF PHYSICS
KHULNA UNIVERSITY OF ENGINEERING & TECHNOLOGY
KHULNA - 9203, BANGLADESH

APRIL - 2016

A STUDY OF STRUCTURAL AND MAGNETIC PROPERTIES OF Mg-Cu MIXED SPINEL FERRITES

BY

APURBA PODDER
ROLL NO: 1455552
SESSION: JULY - 2014

A THESIS SUBMITED TO THE DEPARTMENT OF PHYSICS,
KHULNA UNIVERSITY OF ENGINEERING & TECHNOLOGY,
KHULNA - 9203 IN PARTIAL FULFILMENT OF THE
REQUIRMENT FOR THE DEGREE OF MASTER OF SCIENCE

DEPARTMENT OF PHYSICS
KHULNA UNIVERSITY OF ENGINEERING & TECHNOLOGY
KHULNA - 9203, BANGLADESH

APRIL - 2016

TO

MY PARENTS

DECLARATION

This is to certify that the thesis work entitled as "**A Study of Structural and Magnetic Properties of Mg-Cu Mixed Spinel Ferrites**" has been carried out in partial fulfillment of the requirement for M.Sc. degree in the department of Physics, Khulna University of Engineering & Technology, Khulna - 9203, Bangladesh. The above research work or any part of this work has not been submitted anywhere for the award of any degree or diploma. No other person's work has been used without due acknowledgement.

1. Supervisor	Candidate
----------------------------	---------------------------------
(Prof. Dr. S. S. Sikder)	(Apurba Podder)

2. Co-Supervisor

(Dr. Sheikh Manjura Hoque)

Acknowledgements

It gives me immense and satisfaction to acknowledge the blessings of the Lord Krishna creator of the universe who is the most gracious compassionate and beneficent to its creature, who beloved me with knowledge and potential to implement my research work.

I express with due respect my deep sense of gratitude and indebtedness to my Supervisor Professor Dr. Shibendra Shekher Sikder, Department of Physics, Khulna University of Engineering & Technology, Khulna for his indispensable guidance, keen interest, constructive and constant inspiration throughout suggestions close supervision and fruitful discussion during the research work.

I am very much indebted to my Co-supervisor Dr. Sk. Manjura Hoque, Head and Principal Scientific Officer, Materials Science Division, Atomic Energy Centre, Dhaka (AECD) for introducing the present research topic and for inspiring guidance and valuable suggestions throughout this research work. It would have not been possible for me to bring out this thesis without her help and constant encouragement.

I am indebted to Professor Dr. Jolly Sultana, Head, Department of Physics, Khulna University of Engineering & Technology for her strong support in various ways during the entire period of my study in this department.

I gratefully acknowledge Professor Dr. Md. Mahbub Alam, Department of Physics, Khulna University of Engineering & Technology, for his co-operation and inspiration during this work. My thanks are also for Md. Kamrul Hasan Reza, Mr. Sujit Kumar Shil, and Mr. Alamgir Hossain Assistant Professor & Suman Kumar Halder, Lecturer, KUET, for their moral support.

My thanks due to Dr. Dilip Kumar Saha, Director, Atomic Energy Centre, Dhaka, for her kind permission to use the laboratory of Materials Science Division, AECD.

I wish to thanks all the scientist of Materials Science Division, especially to Dr. Md. Mahbubul Haque, Dr Nazrul Islam Khan, Mr. Fazul Kamal, Mrs. Samia Islam Liba for their support and scientific discussion to do this research work.

My special thanks to all the staff members of Materials Science Division, AECD, particularly Mrs. Alhamra Parveen, Mrs. Anjuman Ara Begum, Mr. Kamrul Islam, Mr. Anowar Hossain, Mr. Nurul Islam, Mrs. Nazmunnahar Begum, Mrs. Zarna Begum and Mr. Kaiyoum for their sincere help during the preparation of the sample and experimental measurements.

I would like to express my heart full obligation thanks to my parents, and all others family members for their multifaceted support and love no matter distance. Words are not enough to express my feelings and sincere thanks to my loving

I also wish to thank to authority of Khulna University of Engineering & Technology for providing me with the necessary permission for conducting their thesis work.

APURBA PODDER

ABSTRACT

Mg-Cu ferrites are well-known technological magnetic materials finding applications in various electrical devices. The present work is focused on the influence of substitutions and sintering temperature on structural and magnetic properties of Mg-Cu ferrites. $Mg_{1-x}Cu_xFe_2O_4$ where x=0.0, 0.1, 0.2, 0.3, 0.4 and 0.5 samples have been prepared by conventional ceramic method, sintered at 1100°C, 1200°C and 1200°C (quenched). Some physical properties such as lattice parameters, density, porosity, magnetic properties such specific magnetization and hyperfine magnetic field. The structural phase identification was carried out by X-ray diffraction (XRD), microstructure analysis of the samples following scanning electron microscope (SEM), specific magnetization measurement by vibrating sample magnetometer (VSM) and Mössbauer spectroscopy analysis. The X-ray diffraction analysis revealed that all the samples are crystallize in single phase cubic spinel structure. It was found that lattice parameter and porosity decreases with the Cu-content. It was observed from the microstructure study that the grain size increase with the increasing Cu-content. Thoughout the investigation it has also been found that grain size increases with increasing sintering temperature. Magnetization measurements have been accomplished by VSM. It was found that saturation magnetization increases with Cu-content with high value of 36.77 emu/gm for x = 0.5 at sintered temperature 1200°C (quenched), as well as microstructure grain size increases and grain growth clear visible. Interesting experimental results on magnetization at different sintering temperature have been found. Other structural and magnetic properties such as chemical isomer shift, quadruple splitting and hyperfine field were determined by Mössbauer spectroscopy. The velocity scale of a thin ^{57}Fe sample and the isomer shifts are given relative to the centroid of the spectrum. The shifts of Fe atoms in all Mg-Cu ferrites sample behave trivalent ions. The spectrum for the $Mg_{1-x}Cu_xFe_2O_4$ ferrites consists of six lines which are broad as compared with Mössbauer spectrum of a pure ^{57}Fe samples. One of the magnetic signals is a sextet typical of those associated with a good ferromagnetic at room temperature. In a ferromagnetic order all Fe with antiparallel behavior is consistent with a diluted exchange coupling between magnetic Fe-ions on the tetrahedral site to octahedral site.

CONTENTS

Page No.

CHAPTER - I

INTRODUCTION

CHAPTER - II

THEROETICAL BACKGROUND

CHAPTER-III

EXPERIMENTAL PROCEDURE

CHAPTER-IV

RESULTS AND DISCUSSION

CHAPTER-V

CONCLUSION

List of Figures

List of Tables

List of Symbols

XRD = X-Ray Diffraction

VSM = Vibrating Sample Magnetometer

T_m = Melting temperature

K_1 = Anisotropy constant

H_c = Coercive force

μ = Permeability

μ_m = Maximum permeability

μ_i = Initial permeability

μ' = Real part of the complex permeability

μ'' = imaginary part of the complex permeability

D_g = Grain size

B = Magnetic induction

H = Magnetic field

a_0 = Lattice parameter

Tan δ = loss factor or loss tangent.

M_s = Saturation magnetization

T_c = Curie temperature

λ = Wave length of the X-ray

[hkl] = Index of the peak

I = X-ray beam of intensity

SPM = Superparamagnetic

Θ = Weiss constant

M = Magnetization

CHAPTER I

INTRODUCTION

CHAPTER II

THEROETICAL BACKGROUND

CHAPTER III

EXPERIMENTAL PROCEDURE

CHAPTER IV

RESULTS AND DISCUSSION

CHAPTER V

CONCLUSION

REFERENCE

INTRODUCTION

1.1 Introduction

Ferrites are magnetic ceramics containing iron oxide as a major constituent in it. It is now some 80 years since ferrites debuted as an important new category of magnetic materials. These are now very well established group of magnetic materials. The term ferrites mean certain double oxide of iron and another metal, which have two unequal sub lattices and are ordered antiparallel to each other. Magnetic spinals ferrites have the general formula $MO.Fe_2O_3$ where M is a divalent metal ion with an ionic radius approximately between 0.6 Å and 1Å. In the case of simple ferrites, M is one of the divalent ions of the transition elements Mg, Mn, Zn, Ni, Co, Fe and Cu etc. [1.1]. Soft ferrites have been extensively used for many kinds of magnetic devices such as transformers, inductors and magnetic heads for high frequency (ranging from 10^3 to 10^{11} Hz) because their electrical resistivity is higher than those of the soft magnetic alloys ranges from 10^3 to 10^{11} **Ω**-cm which is up to 15 order of magnitude higher than that of metal like iron [1.2]. Low eddy current losses, high initial permeability, high saturation induction, low hysteresis loss and reduced physical size. Due to these reason extensive research activities have been carried out during the past 50 years to enhance their effluence from the application point of view to various technical devices. Ferrites are important component for electrical and electronic, telecommunication and data storage system. Exhaustive research is very much necessary to develop the application of ferrites in electrical and electronic industries in Bangladesh, where market of ferrite is quite large. These application oriented materials are also important candidates, the research on which provides potential opportunity to consolidate the knowledge of fundamental research on ferromagnetism and condensed matter physics.

The magnetic and electrical properties of a spinal structure are controlled by the distribution of cations at the tetrahedral and octahedral sites in the lattice. Spinel ferrites commanded the attention first when S. Hilpert [1.3] focused on the usefulness of ferrites at high frequency application. The ferrites were developed into commercially important materials, chiefly during the years 1933 - 1945 by Snioek [1.4] and his associates at the Philips Research Laboratories in Holland [1.5]. The normal spinal ferrites MFe_2O_4 the divalent ions are all in 'A' sites and the Fe^{3+} ions occupy ‘B’ sites. In spinal structure the magnetic ions are distributed among two different lattices tetrahedral (A) and octahedral (B) sites and are ordered antiparallel to each other cubic spinel ferrites has two sub lattices: Tetrahedral (A) site and Octahedral (B) site in AB_2O_4 crystal structure.

The important structural, electrical and magnetic properties of spinels, responsible for their application in various fields are found to depend on the distribution of cations among to depend on the distribution of cations among the sites. Therefore the estimation of the cation distribution turns out to be important. Various cations can be replaced in A site and B site to tune its magnetic properties. Depending on A site and B site cations it can exhibit various magnetic structures [1.6]. Tetrahedral co-ordinate interstices (called ‘A’ site) which are surrounded by 4 nearest neighboring oxygen ions and octahedral co-ordinate interstices (called ‘B’ sites) which are co-ordinate by 6 nearest neighboring oxygen ions. Structurally spinel can be represented as AB_2O_4. One unit cell of it cations eight formula units of AB_2O_4, where out of 64 ‘A’ sites 8 and out of 32 ‘B’ sites 16 are occupied by cations. Depending on the cation distribution in interstices, the spinel is broadly divided into two groups:

(i) Normal spinel and

(ii) Inverse spinal

Typical example of normal spinal ferrites MFe_2O_4 the divalent ions are all in ‘A’ sites and the Fe^{3+} ions occupy ‘B’ sites. Typical example of normal spinal is $MgFe_2O_4$ and $ZnFe_2O_4$ etc. In inverse spinal the divalent ions occupy some of the ‘B’ sites and the Fe^{3+} ions are divided equally between ‘A’ and ‘B’ sites. Most of the magnetic spinals are inverse type like $NiFe_2O_4$, $CuFe_2O_4$ and $MnFe_2O_4$ etc. Magnetism originates from the spin of unpaired electrons. Cations in ferrite lattice are separated by oxygen anions since cations are separated by oxygen, cation-cation direct (ferromagnetic) interactions are negligible. When cations are bonded covalently to the O^{2-} , P-orbital of oxygen interacts with d-orbital of cations with; $C-\uparrow-\downarrow-O\uparrow-\downarrow-C$ (where-C-represents cation and O represents oxygen) antiparallel spins of cations. This mechanism of indirect interaction is called super exchange. There may be there types of interactions like A-O-B, B-O-B and A-O-A. Among them A-O-B interaction is the strongest one. As the number of unpaired electrons in different cations is not same, the resultant magnetization is thus the difference between the magnetic moments of the octahedral lattice and that of the tetrahedral lattice. This type of magnetism is called ferrimagnetism and Mg-Cu is a ferrimagnetic material.

In ferrites the cations occupy the tetrahedral (A) and octahedral (B) sites of the cubic spinal lattice and experience competing nearest neighbor (J_{AB}) and the next nearest neighbor (J_{AA} and J_{BB}) interactions with $|J_{AB}| \gg |J_{BB}| > |J_{AA}$. The magnetic properties of ferrites are dependent on the type of magnetic ion residing on the A and B sites and the relative strengths of the inter (J_{AB}) and intra sublattice (J_{BB}, J_{AA}) interaction. When the J_{AB} is much stronger than J_{BB} and J_{AA} interactions the magnetic spins have a collinear structure in which the magnetic moments. On the A sublattice are antiparallel to the moments on the B sublattice. But when J_{BB} or J_{AA} becomes comparable with J_{AB}, it may led to non-collinear spin structure [1.7]. When magnetic dilution of the sub lattices is introduced by substituting nonmagnetic ions in the lattice, frustration and/or disorder occurs leading to collapse of the co linearity of the ferromagnetic phase by local spin canting exhibiting a wide spectrum of magnetic ordering e.g. antiferromagnetic, ferromagnetic, re-entrant spin glass, spin glass, cluster spin glass properties [1.8-1.9]. Small amount of site disorder i.e. cation redistribution between A and B site is sufficient to change the super exchange interactions. Which are strongly dependent on thermal history i.e. on sintering temperature time and atmosphere as well as heating rates during the materials is preparation.

Many researchers had worked on Mg substitution in different ferrite systems and found Mg substitution has a significant effect on the structural, electrical and magnetic properties. MgO is a very stable oxide that can be used in a large range of technological application [1.10]. Mg containing composition is preferred to avoid the presence of divalent iron to obtain high resistivity with increasing Mg content only octahedral Fe^{2+} ions are substituted by Mg^{2+} and it decreased with increasing Mg content [1.11]. In the Fe deficient ferrites, the dominant conduction mechanism is due to hole-hopping. At high concentration of Mg^{2+} ions to the hopping process between iron ions [1.12]. Mg is also preferred to increase the rate of densification and to avoid the tendency of discontinuous grain growth [1.13]. It is believed that increase of initial permeability can be obtained by decreasing magnetostriction constant. Magnetostriction constant of Mg-Cu-Zn, ferrites is lower than that of Ni-Cu-Zn [1.14]. MgO has low dielectric loss and low dielectric constant. It is doped with ferroelectric material for high frequency device application [1.15]. So Mg containing ferrites would obtain higher magnetic properties.

Cu is also used in other ferrites as divalent cation for improving electromagnetic properties and for lowering the sintering temperature. Yue *et. al* [1.16] worked on the $(Mg_{0.5-x}Cu_xZn_{0.5})O(Fe_2O_3)_{0.98}$ ferrites are found that the density ,grain size, permeability, Curie temperature increased, resistivity decreased with Cu-content up to x = 0.40. Rezlescu *et. al* [1.17] reported the effect of Cu substitution on the physical properties of $(Mg_{0.5-x}Cu_xZn_{0.5}O)Fe_2O_3$ + 0.5MgO ferrites. They found that the density increased up to x = 0.30 whereas, resistivity increased up to x = 0.10 and permeability increased with Cu content as well. They [1.18] also reported that the sintered density and resistivity of $(Mg_{0.5-x}Cu_xZn_{0.5}O)Fe_2O_3$ ferrite increased up to x=0.3 whereas, permeability increased up to x=0.4. Bhosale *et. al.* [1.19] investigated the effect of Mg in Mg-Cu-Zn ferrite and found that density increased and permeability decreased with Mg^{2+} content. But later they [1.20] reported the ferritization temperature of this system varies with increasing Mg^{2+}. It was also been found that lattice parameter decreased and density, initial permeability increased with increase Mg^{2+} content up to x = 0.2 in $(Mg_xCu_{0.5-x}\ Zn_{0.5})Fe_2O_4$ ferrites. Hiti [1.21] studied the effect of frequency, temperature and composition as the dielectric behavior of $(Mg_xZn_{1-x})Fe_2O_4$ ferrites. The relaxation frequency was found to be shifted to higher values as the temperature increased.

Hoque *et. al* [1.22] reported that the maximization of initial permeability and saturation magnetization at x = 0.2 in $(Ni_{1-x}Cu_x)Fe_2O_4$ ferrites, which could be attributed to the maximum sintered density obtained for this composition, Hoque *et. al* [1.23] worked on Cu substituted Mg-Zn ferrites. They found a remarkable increase in the bulk density with increasing Cu substitution for Mg. By incorporating CuO, the initial permeabilities of the samples increased. Saturation magnetization increased slightly with increasing Cu content up to $x \leq 0.3$ and then it decreased for x = 0.35 Cu substitution is also used in hard ferrites for improving properties [1.24].

The number of magnetically ordered Fe ions increase within few hours of hand milling. This trend can be explained by an induced chemical disorder which results in Fe ions occupying both sublattice of the spinel, and thus the formation of localized magnetic clusters. The size and shape of these magnetic clusters are influenced by the strong J_{AB} interaction between Fe ions on A-sites and Fe-ions on the B-sites. A random arrangement of Fe ions on both sides will yield clusters with different volumes and magnetic order [1.25]. Since the relaxation time is sensitive to volume [1.26]. The Mössbauer spectrum is the sum of spectra with deferent relaxation times. One of the magnetic signals is a sextet typical of those associated with a magnetic order, even through thermal effects at room temperature are apparent from the considerable broadening of the special lines. In principle, in Mössbauer measurements super paramagnetic effects prevail at room temperatures where the fluctuation relaxation time become less then the lamer precession time of the nuclear magnetic moments with the effect being strongly dependent on the volume of single domain magnetic clusters. The line broadening of the β pattern with increasing temperatures originates from different temperatures dependencies of magnetic hyperfine fields at various Fe sites using the molecular field theory [1.27-1.28]. In our earlier work [1.29] spin canting decreases as a result of rare earth substitution was assured to explain this increase in saturation magnetization. However information about spin continuing can be obtained from Mössbauer measurements in high magnetic field [1.30].

Mössbauer spectroscopy, because of the influence of the local environment on the Fe moment, is directly reflected in the hyperfine field distribution studied by Rodmarcq *et. al* [1.31], Chappert et. al. [1.32] and Chain *et. al* [1.33]. The moment variation can be directly derived from the hyperfine field distribution, because the proportionality between hyperfine field and magnetic moment was established from crystalline by Gubbem *et. al* [1.34]. Our studies involve the finding of how the Fe moment is directly reflected in the hyperfine field distribution measurements A-sites to B-sites by Mössbauer spectroscopy because of the influence of the local environment.

Modifications in the properties of Lithium ferrite $Li_{0.5}Fe_{2.5}O_4$ due to the substitution of various ions have been studied by various workers. Various studies can be found in the literature only-Ti, Li-Ge, Li-Cd and Li-Zn ferrites [1.35-1.39]. These are insufficient data on Li-Cu system in the literature. The initial permeability of ferromagnetic materials results from the spin rotational and domain wall motion [1.40-1.41]. It depends upon the magnetization, the ionic structure and the degree of domain wall continuity across the grain boundary layers as shown in Globus. It is found that, initial permeability varies with different condition such soaking time. The sintering temperature, the sintering time and porosity of the defects introduced and atmosphere of firing due to the sintering process [1.42]. Further polycrystalline ferrites having very good dielectric constant. Prakash and Baijlal [1.43] explained the composition dependence of the dielectric constant by using the assumption that the mechanism of dielectric polarization is similar to that of conduction.

In the present work efforts have been taken both Mg and Cu are non magnetic they are used to disproportionate the Fe^{3+} ions on the crystal lattice sites to provide of increase the magnetic moment. Pure Mg ferrites has very high resistivity but the conductivity increases with the addition of Cu. Pure $MgFe_2O_4$ has very high sintering temperature which the addition of $CuFe_2O_4$ lowers the overall sintering temperature and thus performs as fluxing material. Again Cu ferrite and Cu-containing ferrites from an interesting group of ferrites because of their typical electrical and magnetic properties and changes in crystal structure on heating, i. e. they undergo a structural phase transition. There is a possibility of exploiting properties of $MgFe_2O_4$ with the substitution of small percentage of Cu. Commonly Mg-Cu ferrites categorized as microwave ferrites leading to applications in high frequency environment. The effect of sintering temperature and the cooling condition in order to improve the quality of the ferrite which would be produced by the powder metallurgy technique might be established. However, attempts have been made to present a systematic review to various experimental and theoretical observed fast related on this study. To carried out for a complete understanding on these two scientifically interesting systems.

1.2 The Aims and Objectives of the Present Work

The chemical and magnetic structures of Mg-Cu ferrite are well known. It is ferromagnetic in nature and possesses a cubic structure and can be used in various electromagnetic devices due to their high resistivity and high frequency tolerance. In the present work our aim is to study the effect of Cu substitution in Mg ferrite and to investigate the change in physical, magnetic and electric properties are as follows:

(i) To synthesis a series of $Mg_{1-x}Cu_xFe_2O_4$ (where x = 0.0, 0.1, 0.2, 0.3, 0.4 and 0.5) ferrites by standerd double sintering ceramic method.

(ii) To investigate in detail the effects of substitution of Mg^{2+} ions in place of Cu^{2+}ions covering a wide range of concentration on the structural magnetic properties.

(iii) To study site occupancy of various ions on tetrahedral and octahedral sites.

(iv) The prepared samples have been characterized in terms of their crystal structures, unit cell parameters and phase present in the prepared samples with the help of X-ray diffraction (XRD). The porosity of the prepared sample has been calculated from the theoretical density and bulk density of the samples sintered at different temperature are 1100°C, 1200°C and 1200°C (quenched).

(v) To study the microstructure of samples sintered at 1200°C and 1200°C (quenched) by SEM.

(vi) The magnetization of the samples has been measured as a function of field and temperature using Vibrating Sample Magnetometer (VSM).

(vii) To study hyperfine structure of Mg-Cu ferrites with Mössbauer spectroscopy. Mössbauer studies will be performed to analysis the cation distribution. We will also measure the Isomer Shift, Quadruple Splitting and Hyperfine field splitting.

1.3 Reason for Choosing this Research Work

The ferrites in not completely defined by its chemistry and crystal structure but also requires knowledge and control of its parameters such as density, grain size, porosity and their intra and inter granular distribution. It is well known that almost all ferrites decompose at the elevated temperature of we want to melt them under normal conditions. This happens because the oxygen splits off at higher temperature reducing Fe^{3+} to Fe^{2+}. This necessarily implies that ferrites preparation by melting, as in the case of metals is not possible. The normal methods of preparation of ferrites comprise the conventional ceramic method or powder metallurgy, chemical co-precipitation method and sol-gel method. In this thesis work conventional ceramic method will be employed for the preparation of Mg-Cu ferrites for its relative simplicity and availability. Preparation procedure of ferrites generally consists of four major steps such as mixing, preferring, milling and sintering.

The sintered ferrites will be cooled through furnace cooling or quenching method in order to study their effect on the structure and properties of the Mg-Cu mixed spinel ferrites. The structural properties will be evaluated through X-ray diffraction (XRD) and scanning electron microscopy (SEM). These magnetic studies will be performed by the Mössbauer Spectroscopy and Vibrating Sample Magnetometer (VSM). It must be remembered that, the sintering process is irreversible in terms of microstructure, therefore constant care must be maintained to keep conditions constant prior to and during sintering. Our studies involve the finding of how the iron movement is directly reflected in the hyperfine field distribution measurements by Mössbauer spectroscopy because of the influence of the total environment. Mössbauer spectra for Mg-Cu ferrite were not investigated before.

1.4 Application of Ferrites

Ferrites are very important magnetic materials because of their high electric resistivity; they have wide applications in technology, particular at high frequencies. Ferrites are used due to their following properties:

(i) Ferrites are part of low power and high flux transformers which are used in television.

(ii) Soft ferrites were used for the manufacture of inductor core in combination with capacitor circuits in telephone system, but now a day solid state device have replaced them.

(iii) Almost every item of electronic equipment produced such as electromagnets, electric motors, loud speakers, deflection Yokes, generators, radar absorbers, antenna rods, proximity, sensors, humidity sensors, memory devices, recording head, broad band transformer, filters, inductor etc are frequently based on ferrite.

(iv) Ferrites are used in high frequency transformer core and computer memories i.e. computer hard disk, floppy disks, credit cards, audio cassettes, video cassettes and recorder heads.

(v) In computer, non volatile memories are made of ferrite materials. They store information even if power supply fails. Non – volatile memories are made of ferrites materials as they are highly stable against severe shock and vibrations.

(vi) Ferrites are primarily used as inductive components in a large variety of electronic circuits such as low-noise amplifiers, filters, voltage-controlled oscillators, impedance matching networks, for instance. The basic components to produce the inductance are a very soft ferrite and a metallic coil.

(vii) Ferrites are used in microwave devices like circulation, isolators, and switches phase shifters and in radar circuits.

(viii) Ferrites are used to produce low frequency ultrasonic wave by magnetostriction.

(ix) Layered samples of ferrites with piezo electric oxides can lead to a new generation of magnetic field sensors. These sensors can provide a high sensitivity, miniature size, virtually zero power consumption; sensors for AC and DC electric currents can be fabricated.

(x) Ferro-fluids, as a cooling material, in speakers. They cool the coils with vibration.

(xi) Ferrites are used as electromagnetic wave absorbers at low dielectric value.

1.5 Review of the Earlier Research Work

Many investigators have focused their attention on the improvement of electromagnetic properties of the ferrite by divalent ions substitution. Generally, the divalent metal ions (M^{2+}); Ni, Zn, Cu, Mg, Mn, Co or mixtures of these are substituted in different spinel ferrites. Spinel ferrites are extremely important for academic and technological applications. The physical properties such as structural, electrical and magnetic properties are governed by the type of magnetic ion residing on the tetrahedral A –site and octahedral B-site of the spinel lattice and the relative strength of the inter and inter-sub lattice interactions. Divalent ion substitutes have different sitting preferences for the two sites (‘A’ and ‘B’) in the spinel structure and can change many properties as an effect of modified cation distribution in the ferrite. On the basis of site distribution of M^{2+} ions and the strength of the exchange interaction among magnetic ions, the influence of M^{2+} substitution on electromagnetic properties can be explained.

S. F. Mansour *et. al* have observed [1.44] that the dielectric behavior for Mg-Zn ferrites can be explained qualitatively interms of the supposition that the mechanism of the polarization process is electronic polarization. He observed peaks of a certain frequency in the dielectric loss tangent versus frequency curve in all the samples. The peak can be observed when the hopping frequency is approximately equal to that of the extremely applied electric field. Zn^{2+} is used to improve electromagnetic properties as well as densification in the ferrite. It is substituted in spinel ferrite to improve magnetization [1.45]. It also lowers magnetostriction and anisotropy in ferrites [1.46]. Goev *et. al* [1.47] stated that initial permeability increased and hysteresis loss decreased with increasing Zn concentration in ($Ni_{0.85-}$

${}_{y}Cu_{0.15}Zn_{y})Fe_2O_4$ ferrites. Both saturation and remancence magnetization had maximum at y = 0.4. An improved electromagnetic properties were obtained by Low *et. al* [1.48] at high Zn content of $(Ni_{0.02x}Cu_{0.02y}Zn_{0.02Z})Fe_2O_4$; where x + y + z = 50.

M. A. Hakim et. al. [1.49] have synthesized Mg-ferrite nanoparticles by using a chemical Co-precipitation method in three different methods. Metal nitrates were used for preparing $MgFe_2O_4$ nanoparticles. In the first method, they used NH_4OH as the precursor. In second method, KOH was used as precipitating agent and in method three; $MgFe_2O_4$ was prepared by direct mixing of salt solution. They reported that first method is relatively good methods among that three. Average size of the $MgFe_2O_4$ particles was found to be in the range of 17-19nm annealed at temperatures of 500 - 900°C. Cu is also used in other ferrites as divalent cation for improving electromagnetic properties and for lowering the sintering temperature.

Yue *et. al* [1.50] worked on the effect of Cu on the electromagnetic properties of $(Mg_{0.5-x}Cu_xZn_{0.5})O(Fe_2O_3)_{0.98}$ ferrites and found that the density, grain size, permeability, Curie temperature increased; resistivity decreased with Cu content up to x = 0.40. Rezlescu *et .al* [1.51] reported the effect of Cu substitution on the physical properties of $(Mg_{0.5-x}Cu_xZn_{0.5})Fe_2O_4$ +0.5MgO ferrites. They found that the density increased up to x=0.30 whereas, resistivity increased up to x = 0.10 and permeability increased with Cu content as well. They [1.52] also reported that the sintered density and resistivity of $(Mg_{0.5-x}Cu_xZn_{0.5}O)Fe_2O_3$ ferrite increased up to x = 0.30 whereas, permeability increased up to x = 0.40.

Z. H. Mhan *et. al* [1.53] and K. O. Low *et. al* [1.54] reported that Ni-Cu-Zn ferrites are well established soft magnetic material for MLCI applications because of their relatively low sintering temperature, high permeability in the RF frequency region and high electrical resistivity. Z. H. Khan *et. al* [1.55] studied complex permeability spectra of Ni-Cu-Zn ferrites. The particle size increase the sintering temperature is raised. For the composition and different sintering temperature was found that the real permeability in that low frequency region decreases CuO. M. Manjurul Haque *et. al* [1.56] reported the effect of Zn^{2+} substitution on the magnetic properties of $Mg_{1-x}Zn_xFe_2O_4$ ferrites prepared by solid-state reaction method. They observed that the lattice parameter increases linearly with the increase in Zn content. The Curie temperature decreases with the increase in Zn content. The saturation magnetization (Ms) and magnetic moment are observed to increase up to x = 0.40 and thereafter decreases due to the spin canting in B-sites. The initial permeability increases with the addition of Zn^{2+} ions but the resonance frequency shift towards the lower frequency.

S. Noor *et. al* [1.57-1.58] investigated composition dependence of $Co_{1-x}Cd_xFe_2O_4$ sintered at 1050°C/3hrs. They found variation of lattice parameter with Cd content obeys Vagard's law and the linear variation of X-ray densities with Cd-content. Bulk density is found to increase while porosity decreases with increasing Cd-content. Curie temperature decrease linearly with the addition of Cd-ions. The initial permeability increases with Cd content and sintering temperature has little effect on permeability. Saturation magnetization increases with increasing Cd content at $x \geq 0.40$ and then it decreases. The hysteresis behavior and initial permeability reveals the softer ferromagnetic nature of the studied sample. DC electrical resistivity is found to increases with the increase of Cd content.

M. H. Mahmoud and A. A. Satttar [1.59] studied Mössbauer spectra studied of Cu-Zn ferrites substituted with rare earth ions. They observed general trend of decreasing the hyperfine field value in presumably due to the weakening of A-B exchange interaction caused by substitution of magnetic Cu^{2+} with the nonmagnetic Zn^{2+} ions, which also results in a decrease of the Curie temperature. As indicated the samples the exhibit a typical relaxation spectra in room temperature and could be analyzed in terms of the superposition of two sextets and a quadruple split central line. M. A. Hakim *et. al* [1.60] studied hyperfine field of Co-Fe based amorphous ribbon by Mossbauer technique. The Mossbauer spectra for all samples clearly show Lorentizen shaped lines in sextet with broad distribution of magnetic hyperfine field as compared to pure ^{57}Fe foil. A five to six fold increase of the broadening of spectral line with FWHM for the Co-based alloy compared to pure Fe. Magnetic properties of the mixed spinal $CoFe_{1-x}Cr_xO_4$ have been investigated by H. Mohn *et.al* [1.61]. The measured variation of magnetic moment per formula unit at 80k with Cr –content obtained from magnetization and Mössbauer data for x = 0 - 0.6 displays a discrepancy between them thus exhibiting a significant canting on B-sites. Mahmoud *et. al* [1.62] studied the cation distribution and spin canting angles variation $(Cu_{0.5}Zn_{0.5})Fe_2O_4$ ferrites substituted with Sm and Nd using Mössbauer spectra indicate A-sites to B-sites. Dalt *et. al*[1.63] investigated the analysis of nano structure $MgFe_2O_4$ through solution combustion technique. The 30% fuel deficient formulation was selected to synthesized powders at different furnace temperature structural and morphological characterization was performed by using XRD and TEM. Mössbauer spectroscopy and VSM were employed for magnetic measurements. Chul Sung Kim *et. al* [1.64] studied Mössbauer spectra of $Ni_{0.065}Zn_{0.25}Cu_xFe_{2-x}O_4$ that was taken at various temperatures ranging from room temperature to 725K. Mössbauer spectra was observed and interpreted as originating from different temperature dependence of the magnetic hyperfine field at various iron sites. The isomer shifts indicated that the ions where ferrites at the tetrahedral sites (A) and octahedral sites (B). The quadruple shifts showed that the orientation of the magnetic hyperfine field with respect to the principle axes of the electric field gradient was random. The spectra to a medal based on a random distribution of Fe and Zn ions on the A-sites [1.65].

One of the key parameters to increase the permeability in spinel ferrite is lowering the magnetostriction constant. As the magnetostriction constent of Mg-Cu-Zn ferrites is lower than Ni-Cu-Zn [1.66] and decreased with increasing Mg content [1.67]. Mg can be substituted for Ni to increase the permeability in Ni-Cu-Zn ferrites. Mg containing compositions were also preferred to avoid the presence of divalent iron (to obtain high resistivity) and to avoid tendency of discontinuous grain growth [1.68]. Cu is used in ferrite to decrease the sintering temperature so that it can be co-fired with Ag internal electrode. However, Cu decreases the resistivity of the ferrite, which is not desirable for high frequency applications. So, optimization of Cu content with respect to densification and resistivity of the ferrite is very important. All these suggest that the Cu substitution may improve the electromagnetic properties in Mg-Cu ferrite categorized as microwave ferrite leading to high frequency application.

1.6 Outline of the Thesis

The thesis has been configured into five chapters which are as follows:

Chapter 1: Introduction

In this chapter, a brief introduction to Mg-Cu ferrites and organization of thesis. This chapter incorporates background information to assist in understanding the aims and objectives of this investigation, and also reviews recent reports by other investigators with which these results can compared.

Chapter II: Theoretical Background

In this chapter, a briefly describe theories necessary to understand magnetic materials as well as ferrites, classification of ferrites, cation distribution, super exchange interaction, two sublattice modules etc have been discussed in details.

Chapter III: Experimental Background

In this chapter, the experiment procedures are briefly explained along with description of the sample preparation, raw materials. This chapter deals with mainly the design and construction of experimental and preparation of ferrite samples. The fundamentals and working principles of measurement set up are discussed.

Chapter IV: Result and Discussion

In this chapter, result and discussion are thoroughly explained. The various experimental and theoretical studies namely structural magnetic properties and Mössbauer analysis of $Mg_{1-x}Cu_xFe_2O_4$ $(0 \leq x \leq 0.5)$ ferrites are presented and discussed step by step.

Chapter V: Conclusion

In this chapter, the results obtained in this study are summarized. Suggestions for future works on these studies are included.

References are added at the end of each chapter.

THEROETICAL BACKGROUND

2.1 Origin of Magnetism

The origin of magnetism lies in the orbital and spin motions of electrons and how the electrons interact with one another with the concept of electron spin introduce by Goud Smit in 1925 and Ublen Beck in 1926, the origin of magnetism was explained spin corresponds to movement of electric charge in the electron hence on electric current which produces a magnetic moment in the atom. Figure 2.1 illustrated the magnetism in solids arise due to orbital and spin motions of electrons as well as spins of the nuclei of an atom. The motion of electrons is equivalent to an electric current which produces the magnetic effects. The best way to introduce the different types of magnetism is to describe how materials respond to magnetic fields. This may be surprising to some, but all matter is magnetic. It is just that some materials are much more magnetic than others. The main distinction is that in some materials. There is no collective interaction of atomic magnetic moments, whereas in other materials there is a very strong interaction between atomic moments.

The major contribution comes from the spin of unpaired valence electron which produces permanent electronic magnetic moments. A number of unpaired valence electrons present in the atoms of the solid and on the relative orientations of the neighboring magnetic moments. The net magnetic moment is the vector sum of the individual spin and orbital moments of the electrons in the outer shells [2.1].

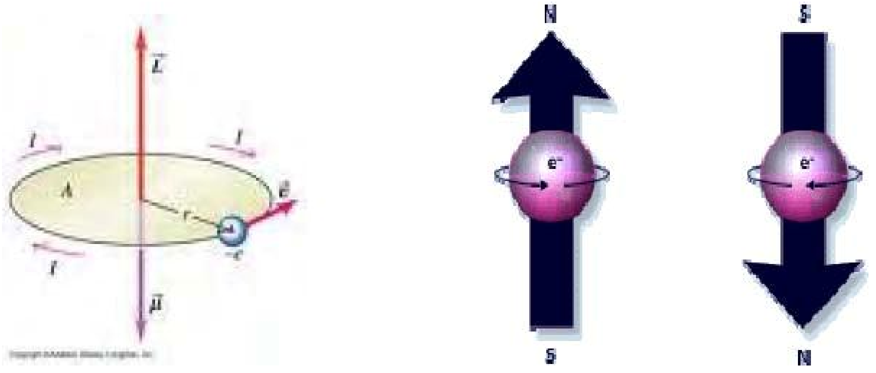

Figure 2.1 (a) Electron orbit around the nucleus (b) Electron spin

The circulating electron produces its own orbital magnetic moment, measured in Bohr Magnetrons (μ_B) and there is also a spin magnetic moment associated with it due to the electron itself spinning. In most materials there is resultant magnetic moment, due to the electron being grouped in pairs causing the magnetic moment to be cancelled by its neighbor. Figure 2.1 (b) illustrate these two phenomena the electron spin can be represented in two modes pointed up or down.

(i) In an atom, with opposed paired spins cancel and do not result in magnetic moment, while

(ii) The unpaired spins will give rise to a net magnetic moment.

The magnetism in solids can be clarified into the following five major groups are:

- Diamagnetism
- Para magnetism
- Ferromagnetism
- Anti ferromagnetism
- Ferrimagnetism

2.1.1 Diamagnetism

Diamagnetism substances consist of atoms or molecules with no net angular momentum. When an external magnetic field is applied, there creates a circulating atomic current that produces a very small bulk magnetization opposing the applied field [2.2]. When a material is placed in a magnetic field, electrons in the atomic orbital tend to oppose the external magnetic field by moving the induced magnetic moment in a direction opposite to the external magnetic field. This may view as an atomic version of Lenz’s law induced magnetic field tend to oppose the change which created them. Materials in which effect is the only magnetic response are called diamagnetic. The other characteristic behavior of diamagnetic materials is that the susceptibility is temperature independent. The typical aloes of small negative susceptibility are in the order of 10^{-5} to 10^{-6}. A superconductor will be a perfect diamagnet, since there is no resistance to the forming of the current loops. Due to this fact, a diamagnetic material is weakly repelled in the magnetic field. When the field is removed, its magnetization becomes zero. Most of the material is diamagnetic, including Au, Ag, Hg, Cu, B, S, N_2, Zn and most of organic compounds [2.3].

2.1.2 Paramagnetism

In certain materials, each atoms or molecules posses permanent magnetic moment individually due to its orbital and spin magnetic moment. In the absence of an applied magnetic field in dipole moments are randomly oriented showing figure [2.2(a)]; therefore the materials have no net macroscopic magnetization. In an applied magnetic field these moments start to align parallel to the field. Materials that are paramagnetic become magnetized in the same direction as that of an applied magnetic field and the amount of magnetization is proportional to that of the applied magnetic field [2.4-2.8]. Paramagnetism occurs in materials with permanent magnetic dipole moment, such as atomic or molecular with an odd number of electrons, atoms or ions in unfilled orbital's.

Paramagnetism is found in atoms, molecules and lattice defects possessing an odd number of electrons as the total spin of the system cannot be zero. Metals, free atoms and ions with partly filled inner shall, transition elements and few compounds with an even number of electrons including oxygen also show Paramagnetism [2.9]. Paramagnetic materials are attracted when subject to an applied magnetic field, hence have a relative magnetic permeability greater than one or equivalently and are very small positive magnetic susceptibility with the order of 10^{-5} to 10^{-3}. These materials show weak magnetism in the presence of an external magnetic field but when the field is removed, thermal motion will quickly disrupt the magnetic alignment.

The alignment at magnetic moments is disturbed by the thermal agitation with the rise in temperature and greater field are required to attain the same magnetization. As a result paramagnetic susceptibility decreases with the rise in temperature. The paramagnetic susceptibility is inversely proportional to the temperature. It can be described by the relation

$$\chi = \frac{C}{T} \tag{2.1}$$

This is called the Curie Law of Paramagnetism. Here χ is the paramagnetic susceptibility; T is the absolute temperature and 'C' is called the Curie constant. Examples of paramagnetic elements are Al, Ca, Cr, Mg, NO and Na etc [2.10]

2.1.3 Ferromagnetism

Ferromagnetism is a phenomenon of spontaneous magnetization. It has the alignment of an appreciable fraction of molecular magnetic moments in some favorable direction in the crystal. In a ferromagnetic material, the exchange coupling between neighboring moments leads the moments to align parallel with each other shown in Figure 2.2(b). A ferromagnetic material has permanent magnetic moment is the result of the co operative interaction of large number of atomic spins what are called domains regions, where all spins are aligned in the Curie temperature, above which it loses its ferromagnetic properties [2.5]. This is because the thermal tendency to disorder overwhelm. The energy lowering due to ferromagnetic order the susceptibility of a ferromagnetic materials dose not follows the Curie Law, but displayed a molified behavior defined by Curie-Weiss law. Shown in Figure 2.3

$$\chi = \frac{C}{T-\Theta} \tag{2.2}$$

Where C is a constant and Θ is called Weiss constant is almost identical to the Curie temperature (T_c). At temperature below T_c, the magnetic moments are ordered whereas above T_c material losses magnetic ordering and show paramagnetic character.

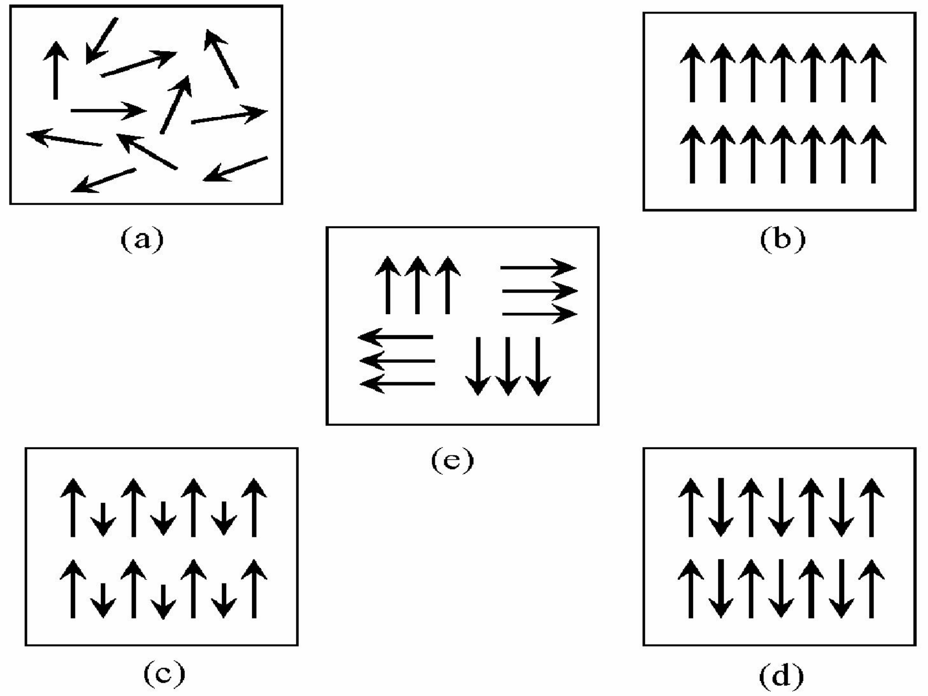

Figure:2.2 Varieties of magnetic orderings (a) Paramagnetic (b) Ferromagnetic (c) Ferrimagnetic (d) Antiferromagnetic and (e) superparamagnetic

Examples of ferromagnetic materials are transition metals Fe, Co and Ni but other elements and alloys involving transition or rare earth elements are also ferromagnetic due to their unfilled 3d and 4f shells. These materials have a large and positive magnetic susceptibility to an external magnetic field. They exhibit a strong attraction to magnetic fields and are able to retain their magnetic properties after the external field is removed.

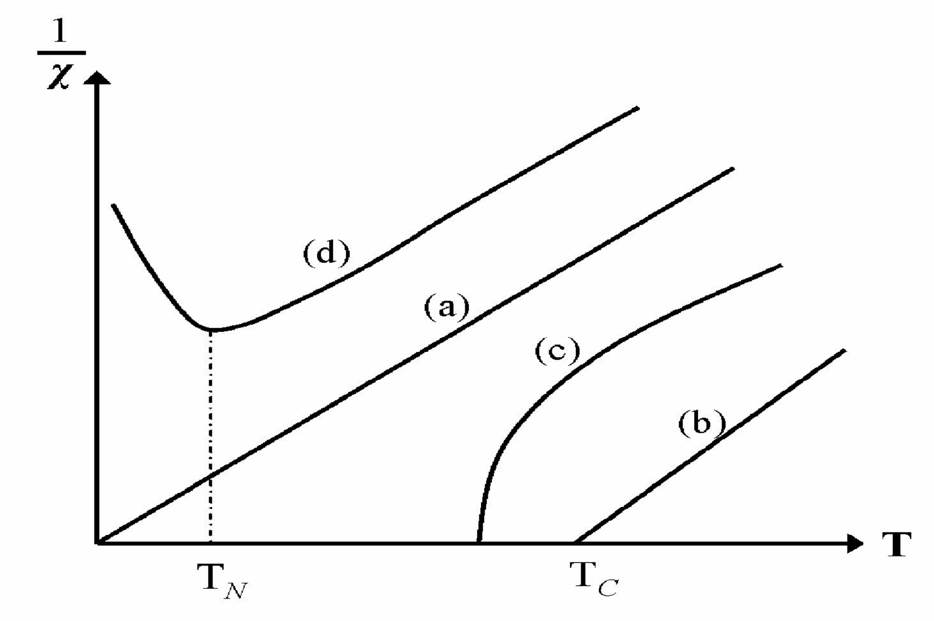

Figure 2.3: The inverse susceptibility varies with temperature T for (a) Paramagnetic (b) Ferromagnetic (c) Ferrimagnetic (d) Anti ferromagnetic, T_N and T_C are Neel Temperature and Curie temperature respectively.

Two distinct characteristics of ferromagnetic materials are

(i) Spontaneous magnetization and

(ii) The existence of magnetic or daring temperature (Cure temperature)

The spontaneous magnetization is the net magnetization that exists inside a uniformly magnetized microscopic volume in the absence of a field. The magnitude of this magnetization, at 0K is dependent on the spin magnetic moments of electrons. Spontaneous magnetization is the term used to describe, the appearance of an ordered spin state at zero applied magnetic filed in a ferromagnetic or ferrimagnetic material below a critical point called the Curie temperature or T_C. This fact leads Weiss to make the bold brilliant assumption that a molecular field acted in a ferromagnetic substance below its T_C as well as above and that this field was so strong that it could magnetize the substance to saturation even in the absence of an applied field. The substance is then self saturation magnetization is an intrinsic property independent of particle size but dependent on temperature. Even though electronic exchange forces in ferromagnetic are very large thermal energy eventually overcomes the exchange energy and produces a random sizing effect. T_C is also an intrinsic property.

2.1.4 Antiferromagnetism

Antiferromagnetic materials are those in which the dipoles have equal moments, but adjacent dipoles point in opposite direction [2.10]. There are also materials with more than two sub lattices with triangular, canted or spiral spin arrangements. Due to these facts, antiferromagnetic materials have small non-zero magnetic moment [2.11]. They have a weak positive magnetic susceptibility of the order of paramagnetic material at all temperatures, but their susceptibility change in a peculiar manner with temperature. This theory of antiferromagnetism was developed chiefly by Neel in 1932. Cr is the only element exhibiting antiferromagnetism at room temperature.

Antiferromagnetic materials are very similar to ferromagnetic materials but the exchange interaction between neighboring atoms leads to the anti-parallel alignment of the atomic magnetic moments figure 2.2 (d). Therefore the magnetic field cancels out and the material appears to behave in the same way as the paramagnetic material. The antiparallel arrangement of magnetic dipoles in antiferromagnetic materials, in the reason for small magnetic susceptibility of antiferromagnetic materials. The inverse susceptibility as a function of temperature is shown in Figure:2.3 (d). The natural state makes it different for the material to become magnetized in the direction of the applied field but still demonstrates a relative permeability slightly greater then above a critical temperature known as the Neel temperature the material becomes paramagnetic [2.8]. Common examples of materials with antiferromagnetic ordering include MnO, FeO, CoO and NiO.

2.1.5 Ferrimagnetism

Ferrimagnetic materials have spin structure of both spin-down components but have a net non-zero magnetic moment in one of these directions [2.12]. The magnetic moments of the atoms on different adjacent sublattice are opposite to each other as in antiferromagnetism; however, in ferrimagnetic materials the opposing moments are unequal shown in figure: 2.2 (c). An overall magnetization is produced but not all the magnetic moment may give a positive contribution to the overall magnetization.

As a result a net magnetic moment remains in the absence of external magnetic field the behavior of susceptibility of a ferrimagnetic material also obeys Curie-Weiss law and has a negative Θ as well as in figure: 2.3 (c). Ferrimagnetism is therefore similar to ferromagnetism. It exhibits all the hall marks to ferrimagnetic behavior like spontaneous magnetization, Cure temperature, hysteresis and remanence. However ferromagnetic and ferrimagnetic have every difference magnetic ordering, while these materials may also demonstrate a relative permeability greater than 1. Their temperature dependence are not as consistent as with ferromagnetic materials and can result is some very unusual results. In ionic compounds, such as oxides more complex forms of magnetic ordering can occur as a result of the crystal structure. The magnetic structure is composed of two magnetic sublattices (called ‘A’ and ‘B’) separated by oxygen. The exchange interactions are mediated by the oxygen anions. When this happens, the interactions are called indirect or superexchange interaction. The magnitude of magnetic susceptibility for ferromagnetic and ferrimagnetic materials in similar, however the alignment of magnetic dipole moments is drastically different.

2.2 Classification of Ferrites and its Relevance

Ferrites are electrically non-conductive ferrimagnetic ceramic compound materials, consisting of various mixtures of iron oxides such as Hematite (Fe_2O_3) or Magnetite (Fe_3O_4) and the oxides of other metal like NiO, CuO, ZnO, MnO, CoO, MgO. The prime property of ferrites is that, in the magnetized state, all the spin magnetic moments are not oriented in the same direction few of them are in the opposite direction. But at the spin magnetic moments are of two types with different values. The net magnetic moments will have some finite value. The molecular formula at ferrites is $M^{2+}O.Fe_2^{3+}O_3$, where M stands for the divalent metal such as Fe, Mn, Co, Ni, Cu, Mg, Zn or Cd. There are 8 molecules per unit cell in a spinel structure. There are 32 oxygen (O^{2-}) ions, 16Fe^{3+} ions and 8M^{2+}ions, per unit cell. Out of them 8Fe^{3+} and 8M^{2+} ions occupy the octahedral sites. Each ion is surrounded by 6 oxygen ions.

The spin of all such ions are parallel to each other. The rest 8Fe^{3+} ions occupy the tetrahedral site which means that each ion is surrounded by 4 oxygen ions. The spin of these 8 ions in the tetrahedral sites, are all oriented antiparallel to the spin in the octahedral sites. The net spin magnetic moment of Fe^{3+} ions is zero as the 8 spin in the tetrahedral sites cancel the 8 antiparallel spins in the octahedral site. The spin magnetic moment of the 8M^{2+} ions contribute to the magnetization of ferrites [2.3]

Ferrites have been studies since 1936. They have an enormous impact over the application of magnetic materials. Ferrites are essentially ceramic materials, compound of iron, boron, barium, strontium, lead, zinc, magnesium or manganese. The ingredients are mixed, preferred, milled/crushed, dried, shaped and finally pressed and fired into their final hand a brittle state. Ferrite are a class of chemical compounds with the formula AB_2O_4 where A and B represent various metal cations usually including iron. These ceramic materials are used in applications ranging from magnetic components in micro electronics. The DC electrical resistivity of ferrites at room temperature can vary depending upon the chemical composition between about $10^{-2}\Omega$-cm and higher than $10^{11}\Omega$-cm [2.13]

Ferrites are classified into two categories based on their coercive field strength. They are:

(i) Soft ferrite with coercive field strength <10 Oe.

(ii) Hard ferrite with coercive field strength >125 Oe.

2.2.1 Soft Ferrites

Soft ferrites are those that can be easily magnetized or demagnetized. These are characterized by low coercive forces and high magnetic permeabilities. The low coercively means the materials magnetization can easily reverse direction without dissipating much energy (hysteresis losses), while the materials high resistivity prevents of energy loss, the generally exhibit small hysteresis losses. At high frequency metallic soft magnetic materials simply con not be used due to the eddy current losses. Therefore soft ferrite, which is ceramic insulators, becomes the most desirable material. These materials are ferromagnetic with cubic crystal structure and the general composition $MO.Fe_2O$, where M is a transition metal such as Ni, Mn, Mg, Zn, Co or Cd. The magnetically soft ferrites first came into commercial production in 1948. Additionally part of the family of soft ferrites are the microwave ferrites e.g. Ytrium-Iron-Garnet. These ferrites are used in the frequency range from 100 MHz to 500GHz for wave guides for electromagnetic radiation and in microwave device such as phase shifter. Application of soft ferrites include: core for electro-magnets, electric-motors, transformers, generators and other electrical equipment. Soft ferrites have certain advantages over other electromagnetic materials including high resistivity and low eddy current losses over wide frequency ranges. They have high permeability and are stable over a wide temperature rang. These advantages make soft ferrites over all other magnetic materials.

2.2.2 Hard Ferrites

Hard ferrites are difficult to magnetize or demagnetize. Hard magnets are characterized by high remanent inductions and high coercivities. They generally exhibit large hysteresis losses, examples are alnico, rare earth metal alloy etc [2.13]. The development of permanent magnets began in 1950S with the introduction of hard ferrites. These materials are ferromagnetic and have quite a low remanence (~400mT). The coercivities of these magnets ($\sim 250 kAm^{-1}$), however, is for in excess other materials. The maximum energy products are only $\sim 40 kJm^{-3}$. Hard ferrites like Ba-ferrites, Sr-ferrites, Pb-ferrites are used in communication device operation with high frequency currents because of their high resistivity negligible eddy currents and lower loss of energy due to Joule heating and hysteresis. These are found useful in many applications including fractional horse-power motors, automobiles, audio and video recorders, earphones, computer peripherals and clocks.

2.3 Types of Ferrites

According to the crystallographic structures ferrites can be clarified into three different types [2.14]

(i) Cubic ferrites of spinel

(ii) Hexagonal ferrites

(iii) Cubic ferrites of garnets.

The present research work is on spinal ferrites therefore it has been discussed in detail the spinel ferrites only.

2.3.1 Cubic Ferrites with Spinel Structure

They are also called ferrites spinal is the most widely used family of ferrites and are sometimes called ferrospinels, because their crystal structure is closely related to that of the natural mineral spinal. The spinal structure of ferrites as possessed by mineral spinel $MgAl_2O_4$ was first determined by Bragg [2.15]. The cubic ferrite has the general formula $MO.Fe_2O_3$, where M is one of the divalent cations of the transition elements such as Mn, Ni, Mg, Zn, Cd, Co etc. A combination of these ions is also possible and it can named as solid solution of two ferrites or mixed spinal ferrites. Generally, M represent a combination of ions which has an average valence of two. The trivalent Fe-ion in $MO.Fe_2O_3$ can partially be replaced by another divalent in such as Mg^{2+} or Cu^{2+} giving rise to mixed crystals.

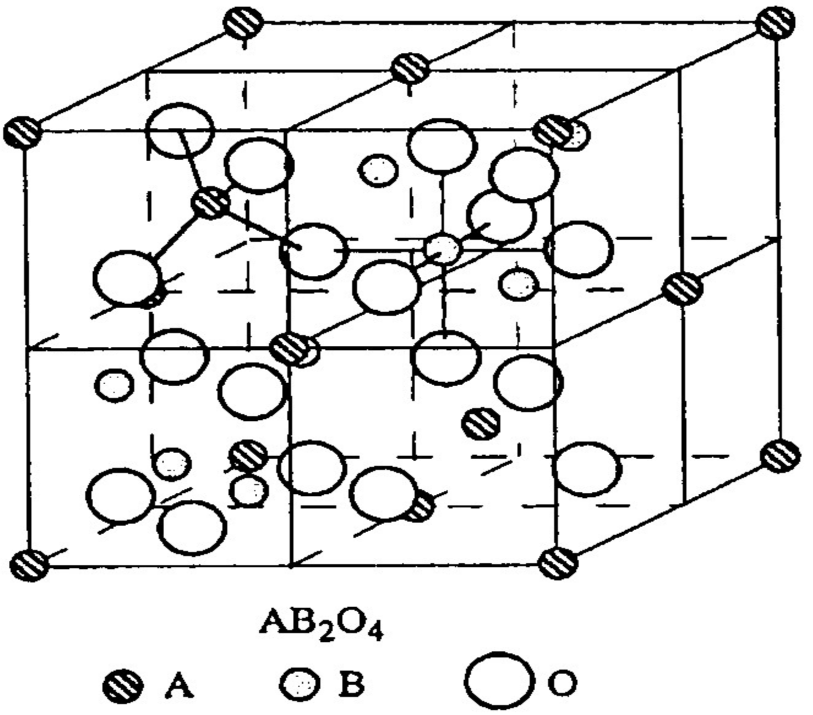

Figure 2.4: Schematic of two sub cells of a unit cell of the spinal structure, showing octahedral or tetrahedral sites.

The crystal structure of ferrite is based on a fcc lattice of the oxygen ions. Each unit cell contains eight formula units. Therefore there are $32O^-$ anions $16Fe^{3+}$ cations and $8M^{2+}$ cations in the cell and the order of 8.50 in each unit cell there are 64 tetrahedral or A-sites and 32 octahedral or B-site. These sites are so named because they are surrounded by four and six oxygen ions at equal distances respectively.

The lattice characteristics of a spinel include a fcc site for the oxygen atoms and two cationic sites occupying A and B sites [2.16-2.17]. In a spinel, there are 64 A sites 32 B sites and 32 oxygen sites in a unit cell. Due to their exchange coupling, spinel ferrites are ferromagnetically aligned where all of the moments of A-sites 34 are aligned parallel with respect to one another while moments of A and B sites are antiparallel to each other. The change neutrality requires the presence of the cations within the structure to counter balance the change of these oxygen anions. These cations rest on two types of interstitial sites to preserve the charge neutrality namely A and B sites. The magnetic properties of spinel ferrites are generally influenced by composition and cation distribution. Variation of cation distribution between the cationic sites leads to different electrical and magnetic properties even if the composition of the spinal is the same. The distribution of cations over A and B sites is determined by their ionic radius, electronic configuration and electrostatic energy in the spinel lattice. The octahedral sites are large than the tetrahedral sites, thus, the divalent ions are localized in the octahedral sites where trivalent ions are in the tetrahedral sites [2.18]. Each type of lattice sites will accept other metal ions with a suitable, 0.65 - 0.80Å at B-sites and 0.40 - 0.64Å at A sites.

The spinal ferrites have been classified into three categories due to the distribution of cation on tetrahedral (A) and octahedral (B) sites.

(i) Normal spinel ferrites
(ii) Inverse spinal ferrites
(iii) Intermediate or Mixed spinal ferrites.

2.3.1.1 Normal Spinel Ferrites

If there is only one kind of cations on octahedral (B) sites, the spinel is normal. In these ferrites the divalent cations occupy tetrahedral (A) sites while the trivalent cations are on octahedral (B) sites. The divalent cation (M^{2+}) are the tetrahedral A-sites and two trivalent (Fe^{3+}) cations are in octahedral B-sites which is represented as $(M^{2+})_A[Fe^{3+}Fe^{3+}]_BO_4$. A typical example of normal spinel ferrite is bulk $ZnFe_2O_4$.

2.3.1.2 Inverse Spinel Ferrites

In this structure half of the trivalent (A) sites and half octahedral (B) sites, the remaining cations being randomly distributed among the octahedral (B) sites. In this case divalent (M^{2+}) cations are in octahedral B- sites and the trivalent (Fe^{3+}) cations are equally divided between A and B sites. The divalent and trivalent ions normally occupy the B-sites in a random fashion i.e. they are disordered. These ferrites are represented by the formula $[Fe^{3+}]_A[M^{2+}Fe^{3+}]_BO_4$. A typical example of inverse spinal ferrite is Fe_3O_4 in which divalent cations of Fe occupy the octahedral (B) sites [2.19]

2.3.1.3 Intermediate or Mixed Spinel Ferrites

X-ray and neutron diffraction experiments and magnetization measurements show that there is a whole range of cation distribution between the normal and inverse structure spinel with ionic distribution, intermediate between normal and inverse are known as mixed spinel. The arrangement of the form $(M_\delta^{2+}Fe^{3+}_{1-\delta})[M^{2+}_{1-\delta}Fe^{3+}_{1+\delta}]_BO_4^{2-}$, where δ is called inversion parameter. Quantity δ depends on the method of preparation and nature of the constituents of the ferrites. For complete normal spinel ferrites $\delta = 1$, for complete inverse spinal ferrites $\delta = 0$, of mixed spinal ferrite δ range these two extreme values. For completely mixed ferrites $\delta = \frac{1}{3}$. If there unequal number of each kind of cations on octahedral sites, the spinal is called mixed. Typical example of mixed spinal ferrite are $MgFe_2O_4$ and Mn Fe_2O_4 [2.20].

The factor affecting the cation distribution over A and B sites are as follows [2.21-2.22]

- The size of the cations
- The electronic configuration of cations
- The electronic energy
- The saturation magnetization of the lattice

Smaller cations (trivalent ions) prefer to occupy the A-sites.the cations have special preference for A and B sites and the preference depends on the following factors:

- Ionic radius
- Size of interstices
- Temperature
- Orbital preference for the specific coordination.

The preference of cations is according to Verway - Heilmar Scheme [2.23]

- Ions with strong preference for A-sites Zn^{2+}, Cd^{2+}, Ga^{2+},In^{3+}, Ge^{4+}.
- Ions with strong preference for B-sites Ni^{2+}, Cr^{3+}, Ti^{4+}, Sn^{4+}.
- In different ions are Mg^{2+}, Al^{3+}, Fe^{3+}, Co^{2+}, Mn^{2+}, Fe^{3+}, Cu^{2+}.

Moreover the electrostatic energy also affects the cation distribution in the spinel lattice.

Neel suggested that magnetic moments in ferrites are sum of magnetic moments of individual sublattices. In spinel structure, exchange interaction between electron of ions in A and B sites have different values. Usually interaction between magnetic ions of A and B sites (A-B interaction) is the strongest. The interaction between A-A is almost ten times of weaker than that of A-B interaction whereas the B-B interaction is the weakest. The dominant A-B sites interaction results into complete or partial (non compensated) antiferromagnetic known as ferrimagnetism [2.24]. The dominant A-B interaction having greatest exchange energy, produces antiparallel arrangement of cation between the magnetic moments in the two types of sublattices and also parallel arrangement of the cations within each sublattices despite of A-A or B-B antiferromagnetic interaction [2.25].

2.3.2 Hexagonal ferrites

This was first identified by Went, Rathenau Gorter and Van Oostershout in 1952 [2.14] and Jonken, Wijin Z Braunin 1956. Hexaferrite are hexagonal or rhombohedral ferromagnetic oxides with formula $MFe_{12}O_4$, where M is an element like Barium, Lead or Strontium. The third type of ferrites are often called the barium ferrites these compounds usually contain BaO, in addition to Fe_2O_3, as the basic component oxide. They are also known as magneto plumbites. The common chemical formula of barium ferrites is l(BaO) . m(MO). $N(Fe_2O_3)_n$ or $Ba^{3+}M_m{}^{2+}Fe_{2n}{}^{3+}O_{l+m+3n}$, where l is much more complex than the previous two in both in terms of composition of barium ferrites may be changed one is to vary the M^{3+} ions. Mg, Mn, Fe, Co, Ni, Cu, and Zn are found suitable for the formation of hexagonal ferrites. Another way is to alter the values of l, m, and n. Basic combinations are found at 1-0-6 (M), 1-2-8 (M_2W), 2-2-6 (M_2Y) and 3-2-12 (M_2Z). Compounds formed under these combinations are termed classical hexagonal ferrites. Still another way is to substitute for Ba with Pb or Sr and or substitute for Fe with Al, Ga, Cr or Mn. A fourth way to vary the composition of barium ferrites is to mix two or more of the classical hexagonal ferrite in different proportions. They are widely used as permanent magnets and have high coercivity. They are used at very high frequency. Their hexagonal ferrite lattice is similar to the spinal structure with closely packed oxygen ions, but there are also metal ions at some layers with the same ionic radii as that of oxygen ions, hexagonal ferrites have larger ions than that of garnet ferrites and are formed by the replacement of oxygen ions. Most of these ions are Ba, Sr, or lead.

2.3.3 Cubic Ferrites of Garnet

The mineral garnet refers to group of mixed oxides, of which the widely known one has the chemical formula $Mn_3Al_2Si_{13}O_{12}$, or equivalently $3MnO.Al_2O_3.3Si_2O_3$ single magnetic garnets have the general formula $3M_2O_3.5Fe_2O_3 = 2M_3^{3+}Fe_5^{3+}O_{12}$. It is to be noted that in magnetic garnets, the 24 positive charge units per formula units are divided unequally between the ferrites ions (15 units) and another species of trivalent ions (9 units). Technically useful garnets are those with M = Sm, Eu, Gd, Tb, Dy, Ho, Er, Tm, Yb or Y. They are known as rare earth garnets. Figure 2.5 shows the cubic ferrite of garnet.

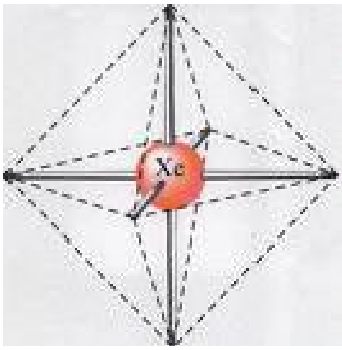

Figure 2.5: Cubic ferrite of garnet.

A code system has been adopted to name them: REG stands for the rare-earth garnet, GdIG for the gadolinium- iron-garnet ($Gd_3Fe_5O_{12}$), YIG for the Yttrium-iron garnet ($Y_3Fe_5O_{12}$) etc. Garnets crystallize in the cubic system with two fifths of the ferric ions forming a bcc lattice, like ferrospinals, the garnets too, pace a large number (160) of ion in eight units formula unit cell. The lattice constant is ≈12.5Å about 50% larger than those ferrospinal. Also the crystal structure of garnets is more complicated than the spinal structure because of the size (0.85-1.10Å) of the M^{3+} ions. They are too large to be accommodated at the interstitial sites between the oxygen ions. Hence the oxygen ions are prohibited from forming a close packed structure as in the spinal. The general formulas for the unit cell of a pure iron garnet have eight formula units of $M_3Fe_5O_{12}$, where M is trivalent rare earth ions (Y, Gd, Dy). Their cell shape is cubic and the edge length is about 12.5 Å. They have complex crystal structure. They are important due to their application in memory structure.

2.4 Magnetic Properties of Ferrites

Ferromagnetic materials are characterized by a high magnetization (Magnetic moments per unit volume) which can be achieved even in polycrystalline materials by the application of relatively small magnetic field. In a ferromagnetic material the individual atomic (atom with partially filled 3d or 4f shells) or ionic moment arising from unpaired spins are permanent and interact strongly with one another in a manner which tends to cause parallel alignment of the nearby moments.

The moment of a large number of neighboring ions are thus parallel, even in the absence of an applied field. These regions or domains, of spontaneous magnetization exit in both single and polycrystalline materials and within a domain the value of the saturation magnetization, M_s is the maximum that can be achieved in the material at interaction lies in the so-called quantum mechanical exchange [2.26-2.27], but in a phenomenological description of magnetism, it is possible to regard that the obliging forces are arising from an internal magnetic field called the molecular filed [2.28]. Weiss assumed that spontaneous magnetization properties disappear at the Curie point when the thermal energy is equal to the energy of the individual ionic moment in Weiss induction field. Then,

$$B_W = k_B T_C + \mu B_m \qquad (2.3)$$

Where k_B is Boltzmann constant, T_c is Curie temperature, μ is permeability and B_m is the Weiss molecular field. It is convenient to write $B_m = \mu_0 H$, below the Weiss molecular field H is used. Weiss assumed that that the molecular field H_m was proportional to the magnetization M

$$H_m = \gamma M \qquad (2.4)$$

Where M is the magnetization is the material and γ is the constant proportionality called molecular field co-efficient.

A ferrite may be defined as the one which below a certain temperature bears a spontaneous magnetization that arise from non-parallel arrangement of the strongly coupled atomic dipole. Ferrites are the substance consists of two sublattices with magnetic moments of one sublattice tending to antiparallel to those of other. The term ferromagnetism has been used in broad sense in order to include the material with more than two sublattices and with other spin configuration, such as triangular or spinel configuration. It is usually assumed that a ferromagnetic material has an appreciable net magnetization although no precise definition of the term appreciable has been given. The two sublattice are denoted by A- and B-sites are denoted by A and B. If the magnetic moment of the ions at A and B sites are unequal, this inequality may be due to

(i) Presence of elements indifferent ionic state, e.g. Fe^{3+}and Fe^{2}+

(ii) Different elements in the same or different ionic states, e.g. Fe^{3+} and Mg^{2+}

(iii) Different crystalline field acting at two sites

The competition between the forces on the B spins may lead to the triangular configuration.

2.4.1 Magnetic Dipole

A dipole is a pair of electric charges or magnetic poles of equal magnitude but opposite polarity, separated by a small distance. Dipoles can be characterized by their dipole moment, a vector quantity with a magnitude equal to the product of the charge as magnetic strength of one of the poles and the distance separating the two poles. The Earth’s magnetic field which is approximately a magnetic dipole. However, the N-pole and S-pole are labeled here geographically, which is the opposite of the convention for labeling the poles of a magnetic dipole moment. In physics, there are two kinds of dipoles:

(i) An **electric dipole** is a separation of positive and magnetic charges. The simplest example of this is a pair of electric charges of equal magnitude but opposite sign, separated by some (usually small) distance. A permanent electric dipole is called electrets.

(ii) A **magnetic dipole** is a closed circulation of electric current. A simple example of this is a single loop of wire some constant current flowing through it [2.29-2.30].

2.4.2 Magnetic Field

A magnetic field (H) is a vector field which is created with moving charges or magnetic materials. It is also be defined as a regions in which the magnetic lines of force is present. The magnetic field vector at a given points in space is specified by two properties:

(i) Its direction which is along the orientation of a compass needle.

(ii) Its magnitude (also called strength), which is proportional to how strength the compass needle orients along that direction.

In matter, atomic circular currents may occur. Their strength is characterized by the magnetization **M**, which is the magnetic moment per cm^3. Then the matter provide the magnetic field is

$$H = 4\pi M \tag{2.5}$$

The S.I. units for magnetic field strength Am^{-1}.

2.4.3 Magnetic Moment

A magnet's magnetic moment (μ) is a vector that characterizes the magnets overall magnetic properties. For a bar magnet; the direction of the magnetic moment points from the magnetic south pole to its north pole; and the magnitude relates to how strong and how far apart these poles are. In S.I. units, the magnetic moment is specified interms of $A\text{-}m^2$. A magnet both produces its own magnetic field and it responds to magnetic fields. The magnetic moment is a measure of the strength of a magnetic source. In the simplest case of a current loop, the magnetic moment is defined as

$$\mu_m = I\int dA \tag{2.6}$$

Where, A is the vector area of the current loop, and the current, I is constant.

In the more complicated case of a spinning charged solid, the magnetic moment can be found by the following equation:

$$\mu_m = \frac{1}{2}\int r \times J d\tau \tag{2.7}$$

Where, $d\tau = r^2 \sin\theta dr d\theta d\varphi$, J is the current density. In addition, when the magnet is put into an external magnetic field, produced by a different source, it is subject to a torque tending to orient the magnetic moment parallel to the field. The amount of this torque is proportional both to the magnetic moment and the external field. A magnet may also be subject to a force driving it in one direction or another according to the positions and orientations of the magnetic and source. If the field is uniform in space, the magnet is subject to no net force, although it is subject to a torque.

2.4.4 Magnetic Moment of Ferrites

The determination of saturation moments of simple ferrites having the formula $M^{2+}Fe^{3+}O_4$, where M^{2+} is the divalent cation, such as Cu, Co, Ni, Fe, Mg, Mn etc agrees with the Neel's collinear model. The A-B interaction is much larger than the A-A and B-B interaction respectively. The two kinds of magnetic ion from two sublattices each saturated and magnetized in opposite direction at absolute zero.

Saturation magnetic moments of some selected spinels [2.24] are listed in the Table:2.1, the first six ferrites are the inverse type i.e $Fe^{3+}[Me^{2+}Fe^{3+}]O_4$. The magnetic moments of two Fe^{+3} cations compensate each other and the ferrite magnetization becomes equal to $M^{2+}(\mu_B) = 2S_M^{+2}(cal)$. These values are listed in the Table:2.1 and the experimental and calculated shows good agreement, except Cobalt and copper series. The Li ferrite is also completely inverse and its moment is calculated based on the cation distribution Fe $[Li_{0.5}Fe_{2.25}]$ O_4 is equal to 2.5 (μ_B); per molecule is in good agreement with the measured value. These are two possible reasons for the discrepancies observed between calculated and observed magnetic moments are mentioned in the Table:2.1.

(i) The orbital moments of the divalent ions may not be neglected: the crystal field effects therefore become important.

(ii) The cation distribution must be taken into account.

Table 2.1: Experiment and calculated saturation moments of spinals

Ferrites	M (μ_B)	$2S_M^{2+}$(cal)
$MnFe_2O_4$	5 - 4.4	5
$FeFe_2O_4$	4.2 - 4.08	5
Co Fe_2O_4	3.3 - 3.9	3
Ni Fe_2O_4	2.3 - 2.40	2
Cu Fe_2O_4	1.3 - 1.37	1
Mg Fe_2O_4	1.1 - 0.86	1.1
$Li_{0.5}$ $Fe_{2.5}O_4$	2.6	2.5

2.5 Magnetic Exchange Interaction

In physics, the exchange interaction is a quantum mechanical effect without classical analogue which increases or decreases the expectation value of the energy or distance between two or more identical particles when their were functions overlap. The exchange interaction is the mechanism responsible for ferromagnetism, among other consequences.

The electron spins of the two atoms S_i and S_j which is proportional to their products. The exchange energy can be written as universally in terms of Heisenberg Hamiltonian [2.32]

$$H = -\Sigma J_{ij} S_i S_j = -\Sigma J_{ij} S_i S_j \cos\phi \quad (2.8)$$

Where, J_{ij} is the exchange integral represents the strength of the coupling between the spin angular momentum i and j and ϕ is the angle between the spins. It is well known that the favored situation is the one with the lowest energy and it turns out that there are two ways in which the wave functions can combine i.e. there are two possibilities for lowering the energy by $E_{ex.}$

These are:

(i) If J_{ij} is positive and the spin configuration is parallel, then ($\cos\phi = 1$) the energy is minimum. This situation leads to ferromagnetism.

(ii) If J_{ij} is negative and the spins are antiparallel ($\cos\phi = -1$) then energy is minimum. This situation leads to antiferromagnetism or ferrimagnetism.

2.5.1 Super exchange Interactions in Spinel Ferrites

Magnetic interactions in spinel ferrites as well as in some ionic compounds are different from the one considered above because the cations are mutually separated by bigger anions (oxygen ions). These anions obscure the direct overlapping of the cation charge distributions, sometimes partially and sometimes completely making the direct exchange interaction very weak. The magnetic interaction in magnetic oxide cannot be explained on the basis of direct reaction because of the following facts:

(i) The magnetic ions are located too far apart from each other shielded by the non magnetic anion i.e. oxygen. This is because these are not band type semiconductor [2.33]. The non magnetic anion such as oxygen is situated in the line joining magnetic cations.

(ii) Super exchange interaction appears, i.e. indirect exchange via anion P-orbital that may be strong enough to order the magnetic moments. The P orbital of an anion (center) internet with the d-orbital of the transitional metal cations.

Three major types of superexchange interactions in spinel ferrites are: J_{AB}, J_{BB} and J_{AA}.

Ferromagnetic oxides are one kind of magnetic system in which there exist at least two in equivalent sublattice for the magnetic ions. The antiparallel alignment between these sublattices (ferrimagnetic ordering) may occur provided the inter sublattice (J_{AB}) exchange interaction are antiferromagnetic and some requirements concerning the signs and strength of the intra-sublattice (J_{AA}, J_{BB}) exchange interaction are fulfilled since usually in ferromagnetic oxides the magnetic cations are surrounded by bigger oxygen anion (almost excluding the direct overlap between cation orbital) magnetic interaction occur via indirect superexchange interaction depends both on the electronic structure of the cations and their geometrical arrangement [2.34].

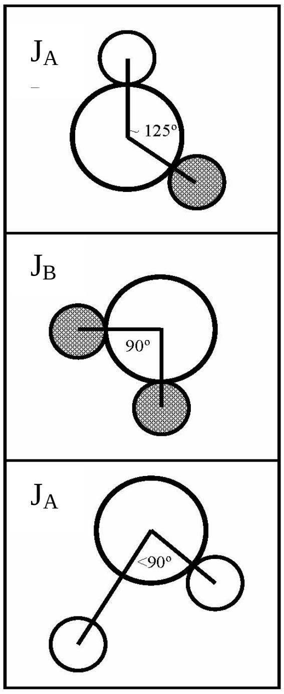

Figure 2.6: Three major types of superexchange interactions in spinel ferrites are as follows: J_{AB}, J_{BB} and J_{AA}. The small empty circle is A-site, the small solid circle is B-site, and the large empty circle is oxygen anion.

The magnitude of negative exchange energies between two magnetic ions M and $M^{/}$ depend upon the distances from these ions to the oxygen ion O^{2-} via which the super exchange take place and on the angle $M\text{-}OM^{/}(\phi)$. According to the super exchange theory the angle $\phi=180°$ gives rise to the greatest exchange energy, and this energy decrease vary rapidly as the distance between the ions increases. The magnetic properties of the spinel ferrites are governed by the type of magnetic ions residing on the A and B sites and relative strengths of the inter-sublattice (J_{AB}) and intra-sublattice (J_{AA}, J_{BB}) exchange interaction are shown in figure 2.6

2.5.2 Neel's Collinear Model of Ferrites

Neel [2.35] assumed that a ferromagnetic crystal lattice could be split into two sublattices such as A (tetrahedral) and B (octahedral) sites. He supposed the existence of only one type of magnetic ions in the material of which a fraction λ appeared on A-sites and the rest fraction μ on B-sites.

$$\text{Thus } \lambda + \mu = 1 \qquad (2.8)$$

The remaining lattice sites were assumed to have ions of zero magnetic moments. A-ion as well as B-ion have neighbors of both A and B types there are several interaction between magnetic ions as A-A, B-B, A-B and B-A. it is supposed that A-B and B-A interactions are identical and predominant over A-A or B-B interaction and four the alignment of the magnetic moment of each A-ion more [2.33]. Neel defined the interactions within the material from the Weiss molecular field viewpoint as

$$H = H_0 + H_m \qquad (2.9)$$

Where H_0 is the external applied field and H_m is the internal field arises due to the interaction of other atoms or ions in the material. When the molecular field concept is applied to a ferromagnetic material we have

$$H_A = H_{AA} + H_{AB} \qquad (2.10)$$

$$H_B = H_{BB} + H_{BA} \qquad (2.11)$$

Here molecular field H_A on A-sites is equal to the sum of the molecular field H_{AA} due to neighboring A-ions and H_{AB} due to neighboring B-sites. The molecular field components can be written as,

$$H_{AA} = \gamma_{AA} M_A, \quad H_{AB} = \gamma_{AB} M_B \qquad (2.12)$$

A similar definition holds for molecular field H_B, acting on B-ions. Molecular filed components can also be written as

$$H_{BB} = \gamma_{BB} M_B,\ \ H_{BA} = \gamma_{BA} M_A \qquad (2.13)$$

Here J's are molecular field Co-efficient and M_A and M_B are magnetic moments of A and B sublattice or an identical sublattices

$$\gamma_{AB} = \gamma_{BA},\ \text{but}\ \gamma_{AA} \neq \gamma_{BB} \qquad (2.14)$$

In the presence of the applied magnetic field H_a, the total magnetic field on the sublattice, can be written as

$$H_a = H_o + H_A$$

$$= H_o + \gamma_{AA} M_A + \gamma_{AB} M_B \qquad (2.15)$$

$$H_b = H_o + H_B$$

$$= H_o + \gamma_{BB} M_B + \gamma_{AB} M_A \qquad (2.16)$$

2.5.3 Non-collinear Model of Ferrimagnetism

In general, all the interactions are negative (anti ferromagnetic) with $|J_{AB}| >> |J_{BB}| > |J_{AA}|$. In such situation, collinear or type of ordering is obtained. Yafet and Kittel [2.36] theoretically considered the stability of the ground state of magnetic ordering, taking all the three exchange interactions into account and concluded that beyond a certain value of $\frac{J_{BB}}{J_{AB}}$, the stable structure was a non-collinear triangular configuration of moment where in the B-site moments are oppositely canted relative to the A-sites moments. Later on Leyons *et.a l*[2.37] extending these theoretical considerations showed that for the value of $\frac{3J_{BB}S_B}{2J_{BB}S_A}$ greater than unity. Initially one can understand why the collinear Neel structure gets perturbed when $\frac{J_{BB}}{J_{AB}}$ increases. Since all these three exchange interactions are negative (favoring anti ferromagnetic alignment of moments) the inter- and intra-sublattice exchange interaction complete with each other in aligning the moment direction in the sublattice. This is one of the origins of topological frustration in the spinel lattice. By selective one can effectively decreases the influence of J_{AB} vis – a - vis J_{BB} and thus perturb the Neel ordering.

It was found that ferrites which have been substituted sufficiently with non magnetic atoms showed significant departure from Neel collinear model. These theoretical models have been used to explain thus departures:

(i) A paramagnetic center model in which a number of magnetic nearest neighbors determine whether a magnetic ion remains paramagnetic or contributes to the magnetization.

(ii) A uniform spin canting relative to the average magnetization and

(iii) A localized canting where the canting angle of a magnetic ion spin depends on the local magnetic environment.

The discrepancy in the Neel's theory was resolved by Yatet and Kitten [2.36] and they formulated the non-collinear model of ferrimagnetism. They concluded that the ground state at 0K might have one of the following configurations:

- Have an antiparallel arrangement of the spins on two sites.
- Consists of triangular arrangements of the spins on the sublattices and
- An antiferromagnetic in each of the sites separately.

2.6 Magnetization Process

A review of magnetization process, namely the response of ferromagnetic or ferrimagnetic material (bulk) to an applied field with a semi-microscopic approach is presented. In ferromagnetic or ferrimagnetic material, the magnetization curves, especially in low magnetic fields differ widely from sample to sample and as a function of the magnetic history of the sample i.e. of the previous fields which have been successively applied.

2.6.1 Magnetization Curve

For unmagnetization bulk material, there is a zero net magnetic moment. It can be predicted that there will be an infinite number of degree of magnetization between the unmagnitized and saturation condition, when the material is subjected to an external magnetic field. These extreme situations correspond respectively to random orientation of domains complete alignment is one direction with elimination of domain walls. If we start with the applied magnetic field, the bulk material will be progressively magnetized by the domain dynamics, the magnetization of the sample will follow the course as shown in figure 2.7 (2.38).

The slop from the origin to a point on the curve or the ratio $(\frac{M}{H})$ is defined as magnetic susceptibility. The curve is called magnetization curve. This curve is greatly perceived as being made of three major portions.

The first, the lower section, is in the initial susceptibility region and is characterized by reversible domain wall movements and rotations. By reversible means that after the magnetization slightly with an increase in field the origin at magnetization conditions can be reversed if the field is reduced to initial value. The combination of the displacement walls to an initial permeability is entirely dependent on the short of material studied.

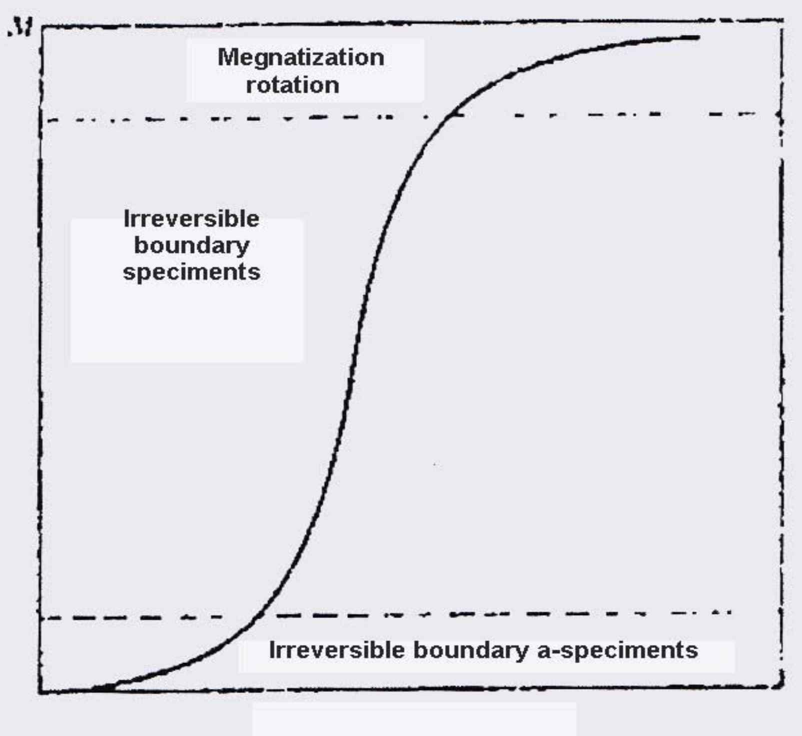

Figure 2.7: Domain dynamics during various parts of the magnetization curve.

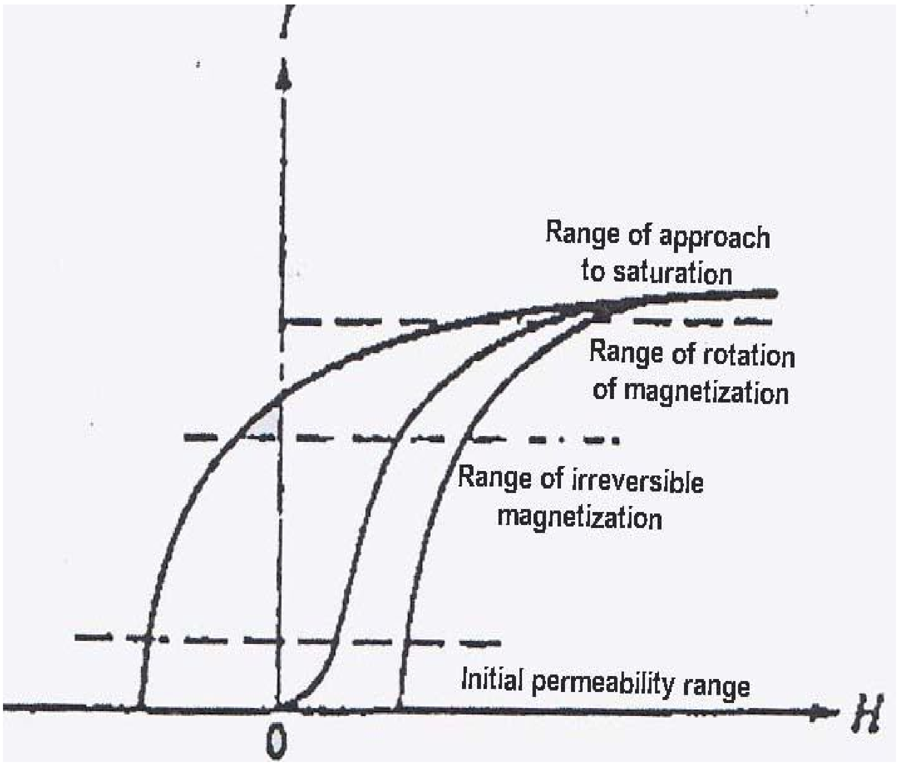

Figure 2.8: Magnetization curve and the classification of magnetization mechanism.

In the second stage magnetization curve, of the field is increased, the intensity of the magnetization increases more drastically, is called the irreversible magnetization range. This range is obtained mainly by the irreversible domain will motion from one stable state to another.

If the field is increased further, the magnetization curve becomes less steep and its process become reversible once more. In the third section of magnetization take place by rotation magnetization. This range is called rotation magnetization range. Beyond this range the magnetization gradually approaches to saturation magnetization shown in figure: 2.8.

2.6.2 Magnetization and Temperature

The influence of temperature on magnetic material can be determinate in the magnetic properties of dose materials. Rising the temperature of a solid, result in the increase of the thermal vibration of atoms, with this the atomic magnetic moments are free to rotate. This phenomenon the atoms tend to randomize the directions of any moments that may be aligned [2.39]. With increasing temperature, the saturation magnetization diminishes gradually and abruptly drops to zero at what called the Curie temperature (T_c). The Curie point of a ferromagnetic material is the temperature above which it loses its characteristic ferromagnetic ability. At temperature below the Curie point the magnetic moments are partially aligned within magnetic domains in ferromagnetic materials. As the temperature is increased from below the Curie point, thermal fluctuations increasingly destroy this alignment, until the net magnetization becomes zero at and above the Curie point.

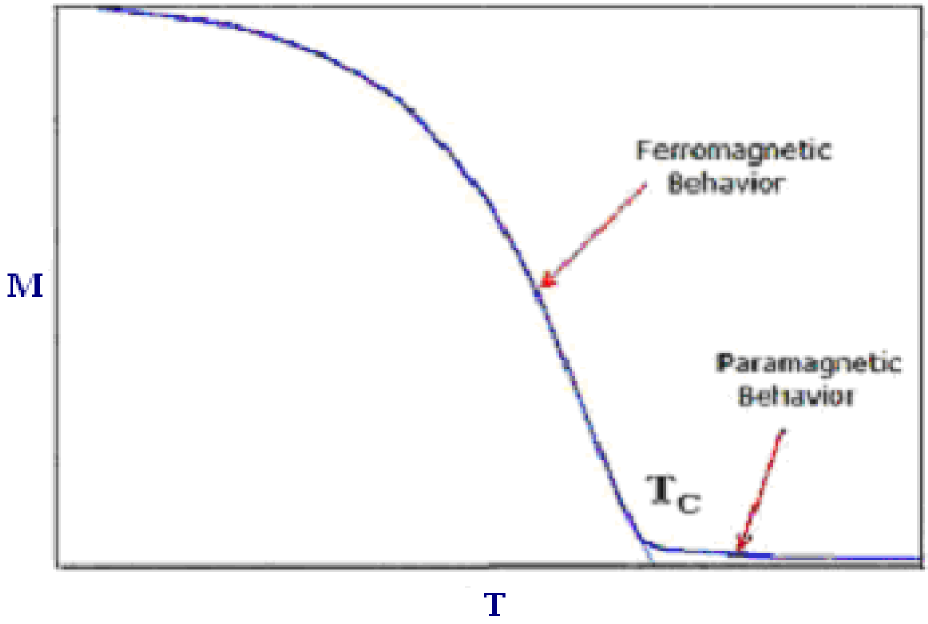

Figure 2.9: Typical M-T curve for magnetic material.

Above the Curie point, the material is purely paramagnetic. At temperature below the Curie point, an applied magnetic field has a paramagnetic effect on the magnetization, but the combination of paramagnetism leads to the magnetization following a hysteresis curve with the applied field strength.

2.7 Mössbauer Spectroscopy

Mössbauer spectroscopy can gives very precise information about the chemical, structural, magnetic and time- dependent properties of a material. Key to the success of the technique is the discovery of recoilless γ-ray emission and absorption, now referred to as the “Mössbauer effect”, after its discover Rudolph

Mössbauer, who first observed the effect in 1957 and received the Nobel Prize in physics in 1961 for his work.

In the content of magnetization one learns about the internal magnetic field and hence magnetic moment, at the local sites of the resonant nucleus. Careful analysis can also fell about the relative orientation of the magnetic moments. Mössbauer spectroscopy yields information on the magnetic properties of individual atoms rather than on assemblies of atoms as in conventional magnetization measurements. Mössbauer spectroscopy is used for the identification of magnetic field distribution of magnetic atoms in magnetic materials by the evaluation of the collected spectra. This is a very useful technique for studying the nature and the number of nearest magnetic neighbors in magnetic alloys.

The Mössbauer effect provides information about the local magnetic and electronic environment of Mössbauer nuclei (i.e. ^{57}Fe or ^{119}Sn) in a sample. Since this technique does not require the application of an external field, it is possible to observe very weak magnetic interactions, without the perturbing effect of the external field.

Mössbauer spectroscopy has also been used to determine the average direction of magnetization by using the well known fact that for the ^{57}Fe, The intensity of the six lines of the hyperfine spectra have an area ratio 3: Z: 1:1: Z: 3, Where Z $= \frac{4}{1+\cot^2\theta}$, θ being the angle between the direction of magnetic field at the nucleus and the direction of γ-ray emission [2.40]. In ^{57}Fe the strength of this magnetic field is H = 33T [2.41] at room temperature. The value Z varies from 0 for the axis magnetization in the sample phase to 4 for the axis of magnetization in sample plane.

Mössbauer spectroscopy is a technique which enables these energy levels to be investigated since the recoil free processes arising from the Mössbauer effect lead to the resonant absorption of γ-rays with an extremely precise energy. Hence, small changes in energy levels because of the hyperfine interactions between the nucleus and surrounding changes can be detected with the technique. A Mössbauer spectrum is characterized by the number, shape, position and relative intensity of the various absorption lines.

2.7.1 Mössbauer Effect

The principle of the Mössbauer effect is essentially the observation of fine structure in the transition between different nuclear energy levels, e.g. of ^{57}Fe or ^{119}Sn nuclei, by means of nuclear resonance absorption or fluorescence radiation. In the experiment a source containing ^{57}Co nuclei provides a convenient supply of excited ^{57}Fe nuclei, which decay into the ground state accompanied by a γ-ray emission.

Nuclear transitions emitting γ-radiation, which are no preceded by phonon transitions. These zero-phonon γ-transitions, take place between the excited and ground state nuclear energy levels of the nucleus which is bound in a solid matrix as reported by Mössbauer [2.42]. Therefore, the nucleus is no longer isolated, but fixed with the lattice. In this situation the recoil energy may be less than the lowest quantized lattice vibration energy and consequently the γ-ray energy may be emitted without any loss of energy due to the recoil of nucleus. This is known as the Mössbauer effect. The frequency spreads of such transition which occur between nuclear exited states are solely determined by the energy uncertainty of the nuclear excited stats involved. The Mössbauer γ-ray has a finite spread in energy which is quantized by a line width, defined as the full width at half maxima of maximum intensity and related to the life time of the nuclear excited state. The line width restricts the number of isotopes in which the Mössbauer effect is observed.

The important parameters which can be measured by using Mössbauer spectroscopy are describing the interaction of the nucleus with the surrounding atomic electrons, these parameters give information about the nature of the chemical bonds, electric field gradient and magnetic ordering moments. The Hamiltonian for the interaction between the nucleus and the surrounding changes may be written as [3.43]

$$H = E_0+M_1+E_2+ \qquad (2.17)$$

Where E_0 represents electric monopole coulombing interaction between nuclear charges and the electron clouds which affect the nuclear energy levels, M_1 refers to magnetic dipole interaction between nuclear magnetic moments and the effective magnetic field at the nucleus and E_2 represents the electric quadrupole interaction between electric field gradient at the nucleus. Higher order terms are usually very small and can be neglected.

This is most often achieved by oscillating a radioactive source with a velocity of a few mm/s recording the spectrum in discrete velocity steps. Fractions of mm/s compared to the speed of light (3×10^{11} mm/s) gives the minute energy shift necessary to observe the hyperfine interaction for convenience the energy seal of Mössbauer spectrum is thus quoted in terms of the source velocity, as shown in figure:2.10

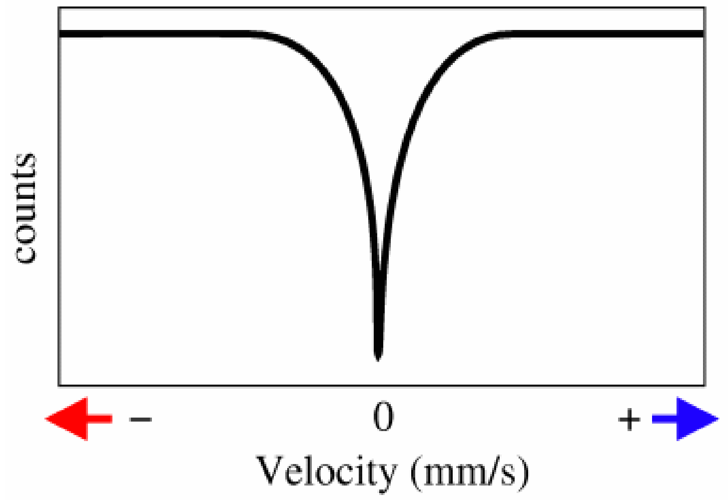

Figure 2.10: simple spectrum showing the velocities scale and motion of source relative to the absorber.

In figure: 2.10 the absorption peak occurs at 0 mm/s, where source and absorber are identical. The energy levels in the absorbing nuclei can be modified by their environment in three main ways: by the Isomer Shift, Quadrupole Splitting and Magnetic Splitting.

2.7.1.1 Isomer Shift

The isomer shift arises due to the slight change in the Coulomb interaction between the nuclear and electronic charge distributions over the nuclear volume which is associated with the slight increase of the ^{57}Fe nucleus in the $I = \frac{3}{2}$ state. In a Mössbauer spectrum the isomer shift is the velocity of the center of gravity of the spectrum with respect to zero velocity. The hyperfine splitting scheme for the ^{57}Fe Mössbauer transition induced by Coulomb interaction (Isomer shift) is shown in Fig. 2.11(a). This shift, first observed in Mössbauer experiment by Kistner and Sunyar (1960) [3.44] is on account of the difference in the nuclear volume of the ground and excited states and the difference between the electron densities at the Mössbauer nucleus in different materials. The nuclear excited and ground states in the absence of hyperfine interaction except the electric monopole interaction are un split but their centers of gravity and shifted not the same source and absorber by an amount known as the isomer shift.

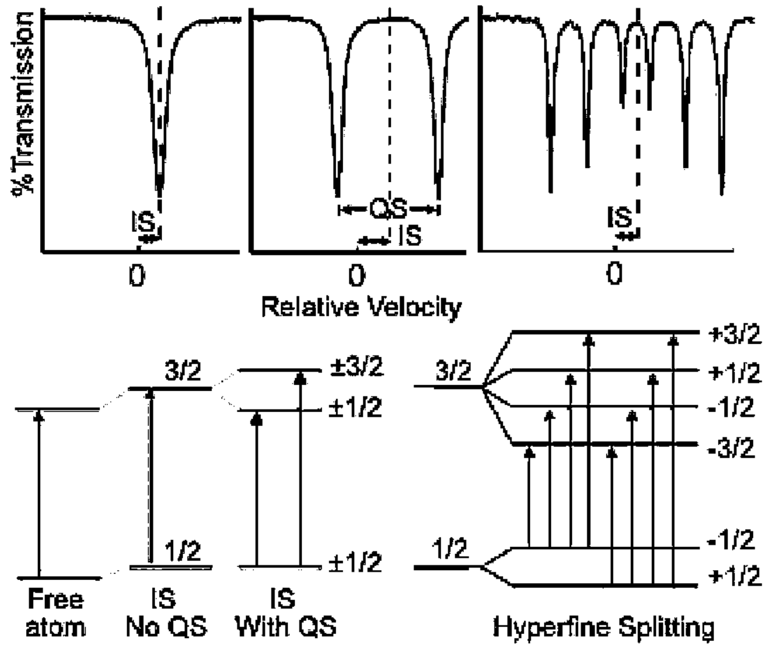

Figure 2.11: Hyperfine splitting scheme for the ^{57}Fe Mössbauer transition induced by (a) Coulomb interaction (Isomer Shift), (b) Quadrupole interaction and (c) Hyperfine Splitting interaction between the nucleus and the electrons.

Isomer shift is not an absolute quantity since it represents the difference between the electric monopole interaction in the source and the absorber. Therefore, the zero velocity of the spectrum of a standard absorber is determined first and the isomer shifts of different absorbers expressed relative to that of the standard absorber. Thermal vibration of the nuclei will also shift the γ-ray energy. As these thermal vibrations are temperature dependent, the temperature of both the source and absorber should be considered when quoting isomer shifts.

Measurement of isomer shifts have been performed in a variety of compounds. Expression in velocity until the isomer shift is given by

$$V = C\,[\psi(0)_s^2 - \psi(0)_A^2] \qquad (2.18)$$

Where $\psi(0)^2$ is the difference of electron densities at the nuclear sites for the sources and absorbers used and C is a constant characteristic for the particular γ-transition and is independent of the chemical environment.

The IS arises from the fact that a nucleus has a finite volume and S-electrons spend a fraction of their time inside the nuclear region. The nuclear charge thus interacts electro statically with the S-electron charge. As a result of this interaction the nuclear energy levels get shifted by a small amount, the shift depends upon the chemical environment. Although, we cannot measure change directly, it is possible to compare values by mean of a suitable reference which can be either the γ-ray source or another standard absorber. The observed range of IS is within an order of magnitude of the natural line width of the transition i.e, 10^{-8} to 10^{-9} ev. Isomer shifts provides important information concerning the nature of the chemical bond because the outer electrons (valence electrons) would be must effected by changes chemical surrounding and consequently the changes in the outer S-electrons densities would contributed must to IS.

Let us consider that the absorber and source lattice are different is chemical composition so that electronic wave function at nuclei differ in the two lattices. This would cause differential shifts in the energy of the γ-rays from the source nuclei and the absorber nuclei. This difference in the energy can be written as [2.41]

$$\begin{aligned}\text{IS} &= \Delta E_A - \Delta E_S \\ &= \left(\frac{2\pi}{5}\right)Ze^2(R_{ex}^2 - R_g^2)[|\psi(0)|_A^2 - |\psi(0)|_S^2] \\ &= \left(\frac{2\pi}{5}\right)Ze^2R^2\left(\frac{dR}{R}\right)[|\psi(0)|_A^2 - |\psi(0)|_S^2] \qquad (2.19)\end{aligned}$$

Where dR = R_{ex} - R_g and R = $\frac{R_{ex}+R_g}{2}$, here R_{ex} and R_g are the nuclear radii of the excited and ground states, R is the average charge radius and $|\psi(0)|_A$ and $|\psi(0)|_s$ refer to the electron densities at the nuclei of absorber and the source respectively.

The expression shows that the IS is the product of two parameters

(i) $\frac{dR}{R}$, a nuclear parameter and

(ii) $|\psi(0)|_A^2 - |\psi(0)|_S^2$ an atomic or chemical parameter.

IS can be positive or negative, depending on whether $\frac{dR}{R}$ is positive or negative, and

$$|\psi(0)|_A^2 > |\psi(0)|_s^2 \text{ or } |\psi(0)|_A^2 < |\psi(0)|_s^2$$

There is well defined range for IS for high spin complex. For an atom, the IS relative to iron metal are 0.8 to 1.5 mm/s for divalent iron and 0.2 to 0.5mm/s for trivalent iron[2.39-2.41]. A large change in IS is observed when the co-ordination number changes from 6 to 4. IS for octahedral Fe^{3+} is high spin complexes because in octahedral site co-ordination number is 6 whereas in tetrahedral site the co-ordination number is 4. As we know, increasing the sheared electrons at octahedral Fe^{3+} nucleuses causing more IS at octahedral Fe^{3+} site that at tetrahedral Fe^{3+} site.

2.7.1.2 Electric Quadruple Splitting

The interaction of the quadruple moment of a nucleus with an electric field gradient (EFG) established at its site by the surrounding environment causes quadruple splitting in nuclear levels [2.39-2.40]. An oblate (flattened) nucleus has a negative quadruple moment while a prolate (elongated) one has a positive moment. Nuclei whose spin is up or $\frac{1}{2}$ are spherical symmetric and have zero quadruple moment and thus the ground state of ^{57}Fe with I = $\frac{1}{2}$ does not exhibit quadrupole splitting. While determining the isomer shift; it is assumed that the nuclear charges distribution is spherical. However, nuclei in states with a nuclear angular moment which are greater than $\frac{1}{2}$ have in general non-spherical charge distributions which are characterized by a nuclear quadruple moment. When the nuclear quadruple moment experiences an asymmetric electric field produced by the arrangement of asymmetric electronic charge distribution and characterized by the electric field gradient (EFG), an electric quadruple interaction occurs which gives rise to a splitting of the nuclear energy levels corresponding to different alignments of the quadruple moment with respect to the principal axis of the nuclear quadruple is fixed for a certain nucleus and hence the EFG can be determined from the Mössbauer Spectrum.

The valance electrons of the Mossbauer atoms and the asymmetry in the electronic structure contribute to the EFG and this is known as valence contributions. Lattice contribution is due to the asymmetric arrangement of Legend atoms in non-cubic Lattices. Molecular orbits and the polarization of the core electrons also modify the EFG. For the EFG, the greatest contribution comes from the electrons on the ion. The polarizable nature of the electron cloud may change the EFG by increasing or decreasing it and is described quantitatively by the sternheimer anti shielding factors

[2.51]. For the open shell ion (non S-state) such as Fe^{+2}, the principal source of q; namely q_{val} comes from integrating over the valence electrons on the Mössbauer ion itself, plus a secondary contribution of q_{lat} from the rest of the crystal (usually assumed to be a sum over point charges).

Therefore

$$q = (1-R)q_{val} + (1-\gamma_\alpha)q_{lat} \qquad (2.20)$$

Where Sternheimer factor R and γ_α denote the fraction of each EFG arising from deformed closed sub shells in the Mössbauer atom.

The quantum mechanical expression that describes the interaction between a nucleus with quadrupole moment eQ and EFG q is given by the Hamiltonian operator

$$H = \frac{eqa}{4I(2I-1)}[3I_z^2 - I(I+1) + \frac{n}{2}(I_+^2 - I_-^2)] \qquad (2.21)$$

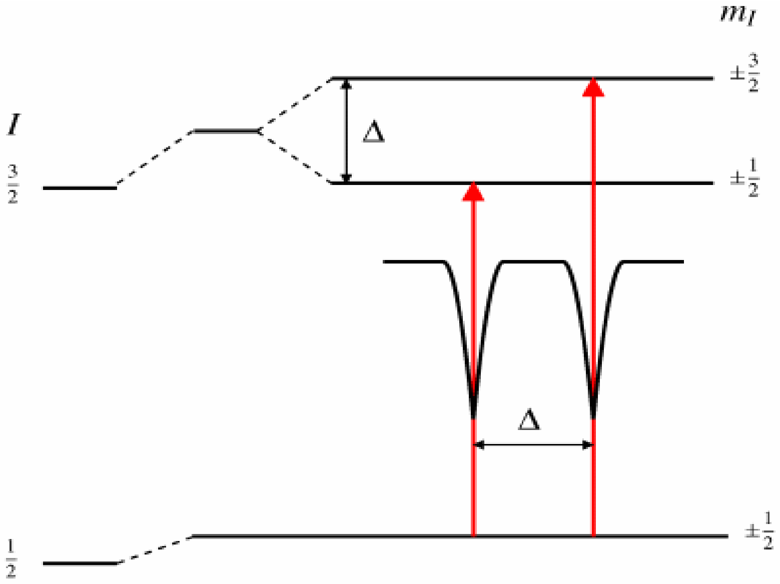

Fig. 2.12: Quadrupole splitting for a $\frac{3}{2}$ to $\frac{1}{2}$ transition. The magnitude of quadrupole splitting, Δ is shown.

Where I_+ and I_- are the raising and lowering operators for the conventional spin operators. For direct determination of quadruple moment values, we discuss the determination of the quadruple moment of the $\frac{3}{2}$, 14.4 Kev state of Co^{57}. For the ferrous Fe^{2+} states, the EFG is predominantly because of lattice contribution in the expression

$$q=(1-R)q_{val}+(1-\gamma_{\alpha})q_{lat} \tag{2.22}$$

$m_I = \pm\frac{1}{2}$ and $m_I = \pm\frac{3}{2}$. This is shown in Figure: 2.12

For ferric (Fe^{2+}) iron, the quadruple splitting in O-Fe_2O_3 was studied. Since this ion is in the ${}^6S_{3/2}$ state; no contribution is expected from q_{val} and only q_{lat} must be considered. The Mössbauer spectrum shows a magnetic six-line pattern. The quadrupole interaction shifts the spectrum asymmetrically.

In the case of an isotope with a $I=\frac{3}{2}$ excited state, such as ^{57}Fe or ^{119}Sn, the excited state is split into two sub states The magnitude of splitting, Delta, is related to the nuclear quadruple moment, Q, and the principle component of the EFG, V_{zz}, by the relation

$$\Delta=\frac{eQV_{ZZ}}{2} \tag{2.23}$$

2.7.1.3 Magnetic splitting

The hyperfine Hamiltonian for a nuclear magnetic dipole ia a magnetic field H is given by

$$H_M=-\mu.H \qquad (\text{Since } \mu=g\mu_N I)$$

$$H_M=-g\mu_N I.H \tag{2.24}$$

Where μ_N is the nuclear magnetron $\left(\frac{e\hbar}{2m_N c}\right)$, m_N is the mass the nucleus and g is the gyro magnetic ratio. The energy levels are

$$E_M=-\frac{m_N H m_l}{I}=gm_N H m_l \qquad [m_l = l, l-1............] \tag{2.25}$$

This indicates that 2l+1 magnetic sublevel are equally spaced with a separation of gM_NH between the levels.

When a nucleus experiences a magnetic field, a magnetic dipole interaction takes place between the nuclear magnetic moment and the magnetic field. This interaction splits the nuclear state (with I > 0) into two sub states and the excited state with $I = \frac{3}{2}$ splits into four sub states. The selection rules with $m_I = 0, \pm 1$ allows six possible transitions between these sets of excited and ground state leading to six-line Mössbauer spectrum.

The magnetic splitting is proportional to the magnetic field at the nucleus. The intensities of the absorption lines depend on the transitions probabilities between the different substates. Contribution for magnetic hyperfine field can come from all electrons that are present within the atom, the molecule and the lattice. The effects of magnetic hyperfine fields are observed in the Mössbauer spectra of magnetically ordered systems if the electron spin relaxation times are long. Magnetic splitting can arise due to magnetic hyperfine field and any external applied field and the field at the nucleus is a vector sum of two.

This magnetic field splits nuclear levels with a spin of l into (2l+1) sub states. This is shown in Figure: 2.11 for ^{57}Fe. Transitions between the excited state and ground state can only occur where m_I changes by 0 or 1. This gives six possible transitions for a $\frac{3}{2}$ to $\frac{1}{2}$ transition, giving a sextet as illustrated in Figure: 2.13, with the line spacing being proportional to B effective magnetic field at the nucleus.

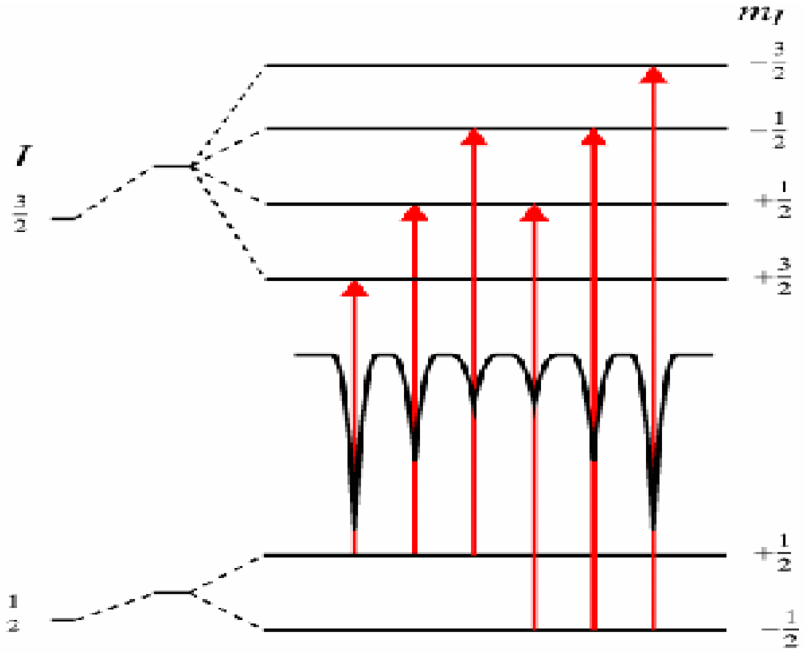

Figure 2.13: Magnetic splitting of the nuclear energy levels

The line positions are related to the splitting of the energy levels, but the line intensities are related to the angle between the Mössbauer γ-ray and the nuclear spin moment. The outer, middle and inner line intensities are related by:

$$3:\frac{4\sin^2\theta}{1+\cos^2\theta}:1$$

meaning the outer and inner lines are always in the same proportion but the middle lines can vary in relative intensity between 0 and 4 depending upon the angle the nuclear spin moments make to the γ-ray. In polycrystalline samples with no applied field this value averages to 2 but in single crystals or under applied fields the relative line intensities can give information about moment orientation and magnetic ordering as shown in Figure: 2.12.

2.7.1.4 Magnetic Hyperfine Interaction

The internal magnetic field at the nucleus has its origin from the spin and radial and angular distribution of the electron density in the atom. The magnetic field is given by [2.46-2.47]

$$\mathrm{H} = -\frac{8}{3} n\mu_B \left|\psi_{\uparrow}(0)\right|^2 \bar{s} - 2\mu_B \left\langle \bar{l} \right\rangle \left\langle \frac{1}{r^3} \right\rangle - 2\mu_B \frac{\left\langle 3\left(\bar{r}.\bar{\Delta}\right)\bar{r} - r^2\bar{s} \right\rangle}{r^5} \qquad (2.26)$$

Where μ_B is Bhor magnetron, s and l are operators for the spin and orbital moment of the electron and $\left|\psi_{\uparrow}(0)\right|^2$ is the electron density at the nucleus with $+\frac{1}{2}$ spin projection.

The first term, in this expression is known as Fermi contact term which describes the contact magnetic interaction between the s-electrons and a nucleus, only S- electron contribute to the Fermi contact term since the S- electron have a non-zero charge density at the nucleus. The field resulting from this source is very large compared to that from other sources. The Fermi contact field mainly arises from the polarization of the spins of paired S- electrons by the unpaired 3d electrons via exchange attraction that emits between electrons of like spins [2.48-2.49]. The inner core electrons (1S and 2S) produce a large negative field, whereas 3s and 4s electron produce smaller positive fields resulting in a net negative field almost of the nuclei [2.50]. The second term in the above expression is known as orbital current field and it is produce due to an interaction of the unquenched orbital moment of the electron with the nuclear magnetic moment.

The third term known as Dipolar field arises due to dipole-dipole interactions operation between the electron spin and the nuclear magnetic moment. For observing a well resolved Zeeman splitting in the Mössbauer spectrum, two conditions have to satisfied

$$\tau_0 > \tau_L \text{ And } \tau_s > \tau_L ; \qquad (2.27)$$

Where τ_0 the life time of the nuclear is excited state, τ_s is the electron spin correlation time and τ_L is the Larmour precession time of the nucleus. The first conditions state that the Zeeman splitting must be larger than the natural line width. The second condition states the relationship between the spin correlation time and nuclear Larmour procession time. In paramagnetic system the spin correlation time is so small, of the order of 10^{-12} and 10^{-14} gu. That during on Larmour precession, the electron of spin undergoes several fluctuation and hence the nuclei will not experience any hyperfine field to presses around and hence no magnetic splitting will be absorbed. In magnetically ordered system, the strong exchange interaction helps to increase the spin correlations times, thus the direction of the hyperfine field is steady and the nucleus spin process round it to lift the degeneracy of the nuclear levels yielding hyperfine split spectrum.

EXPERIMENTAL PROCEDURE

3.1 Methodology of Ferrite Preparation

Sample preparation technique is an important part of ferrites sample. Knowledge and control of the chemical composition, homogeneity and microstructure are very crucial. The preparation of polycrystalline ferrites with optimized properties has always demanded delicate handling and cautions approach. The ferrites is not completely defined by its chemistry and crystal structure but also requires knowledge and control of parameters of its microstructure such as grain size, porosity, intra- and inter-granular distribution. As most of the properties needed for ferrite applications are not intrinsic but extrinsic, preparations of samples has to encounter added complexity. There are many processing methods such as solid state reaction method [3.1]; high energy ball milling [3.2]; sol-gel [3.3]; chemical co-precipitation method [3.4]; microwave sintering method [3.5]; auto combustion method [3.6] etc for the preparation of polycrystalline ferrite decompose at the elevated temperature if we want to melt them under normal conditions. This happens because the oxygen splits off at higher temperature reducing Fe^{3+} to Fe^{2+}. This necessarily implies that ferrite preparation by melting, as in the case of metals, is not possible. The normal methods of preparation of ferrites comprise of the conventional ceramic method i.e. solid state reaction method involving ball milling of reactions following by sintering at elevated temperature range and non-conventional method, also called wet method chemical co-precipitation method and sol-gel method etc examples of wet method. In this thesis work conventional ceramic method has been employed for the preparation of Mg-Cu ferrite for its relative simplicity and availability.

3.1.1 Composition of the Studied Ferrite System

A series of mixed ferrites of composition were fabricated by solid state reaction technique keeping in view of their ionic radial and valences for maintaining the charge neutrality.

In the present work, conventional ceramic method has been employed for a series composition of Mg-Cu ferrites are synthesized, characterized and investigated. The powder preparation process and sintering facility available at the Material Science Division, Atomic Energy Centre, Dhaka has been utilized for the preparation of samples. General formula for sample is $Mg_{1-x}Cu_xFe_2O_4$ with x=0.0, 0.1, 0.2, 0.3, 0.4 and 0.5. The properties of Mg-Cu samples are influenced considerably by sintering temperature and compositions.

3.2 Method of Sample preparation

The sample preparation of polycrystalline ferrites with optimum desired properties is still a complex and difficult task. Ferrites with optimized properties have always demanded delicate handling and cautions approach in materials synthesis and appropriate knowledge of thermodynamics control of the chemical composition and homogeneity. The general preparation procedure of ferrites comprises of the following operation as shown in figure 3.1. The block diagram and the detail of which are described subsequently.

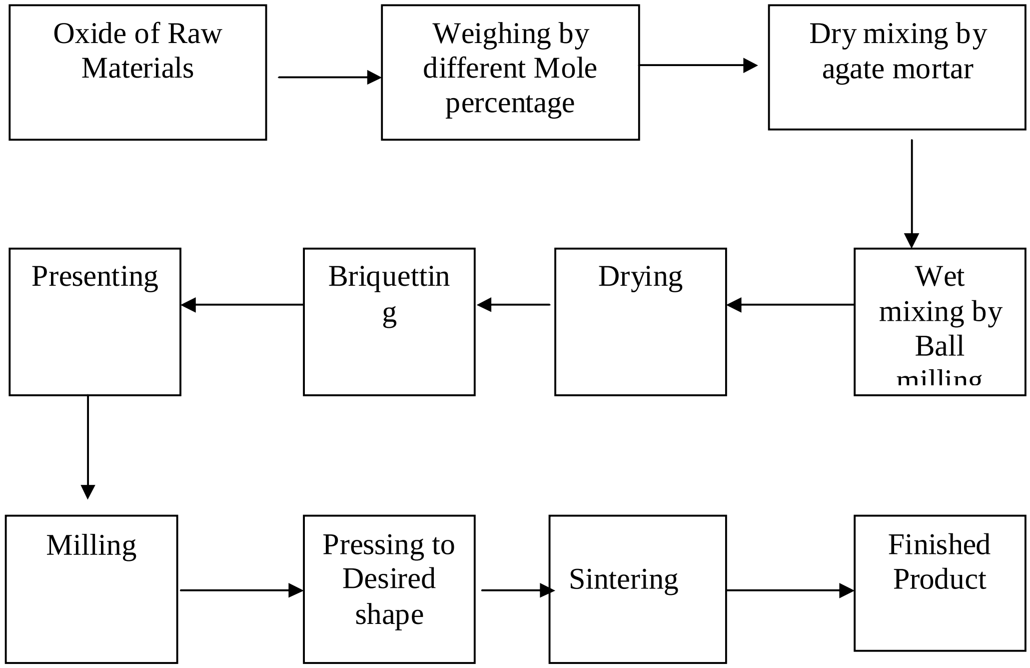

Figure 3.1: Flow chart of ferrite preparation.

The overall preparation process generally comprised of the following four major steps:

(i) Preparing a mixture of materials with the cations in the ratio corresponding to that in the final product.

(ii) Pre-firing the mixture to form ferrite.

(iii) Converting the “raw ferrite” into powder and pressing the powder into the required shapes.

(iv) Sintering to produce a highly densified product.

One thing is to be remembered that, the sintering process is irreversible in terms of microstructure, therefore constant care must be maintained to keep conditions constants prior to and during sintering.

3.2.1 Preparing the Mixture of Mg-Cu Ferrites

The extent of the work in this step varies greatly, depending on the starting materials. When component oxides are used, the corresponding step involves a mere mixing of the oxides by wet milling for 6 hours. To avoid iron contamination, mixing is done with stainless steel balls in a steel ball milling machine and a fluid such as distilled water is used to prepare the mixture into slurry.

The raw materials for the preparation of Mg-Cu ferrite were oxide of iron, copper and magnesium. The purity of raw materials used in the present work is analytical research grade oxides supplied by the manufacturer E. Mark of Germany. The constituent in required stoichiometric proportions were weighed first and then thoroughly mixed using ceramic mortar and pestle.

3.2.2 Pre-firing the Mixture to form ferrite

The slurry prepared in step 1 is dried, palletized and then transferred to a porcelain crucible for pre-firing at temperature 1200°C for $MgFe_2O_4$ and at temperature 1100°C for the rest. This was performed in a furnace named Gallen Camp at Materials Science Division AECD. As far as the final composition of the ferrite is concerned step-2 is most crucial because subsequent steps would not change the composition substantially. For this reason, it is important to understand how a ferrite is formed from its component oxides.

The solid state reaction leading to the formation of ferrites is actually achieved by counter diffusion. This means the diffusion involves two or more species of ions which move in opposite direction initially across the interface of two contacting particles of different component oxides. In 1965 Carter and Kooy made careful studies of the position of inter markers in diffusions couples and computer that the counter diffusion essentially involves the movements of cations through a more or less rigid lattice of oxygen anions.

During the pre-firing stage, the reaction of Fe_2O_3 with metal oxide (say MO or M'_2O_3) takes place in the solid state to form spinel according to reactions

$$MO + Fe_2O_3 \longrightarrow MFe_2O_4\text{(spinel)}$$

$$2M^{/}{}_2O_4 + 4Fe_2O_4 \longrightarrow 4M^{/}\ Fe_2O_4\text{(spinel)} + O_2$$

The MgO creep into Fe_2O_3 to form an intermediate phase and finally Cu ions are introduced to form Mg-Cu ferrites.

In order to produce chemically homogeneous and magnetically better material, this pre-fired lump material was crushed. This oxide mixture was then milled thoroughly for 6 - 8 hours to obtain homogeneous mixture. It is to be mentioned that the size can be reduced to ≈ 1 micron by prolong normal ball milling. However some fraction of the particles in that case may be reduced to even sub micron level.

3.2.3 Converting Raw Ferrite into Powder and Pressing Powder

Besides reducing the particle size to ≈ 1 micron, grinding also eliminates intra particle pores and homogenizes the ferrite by mixing. To promote successful sintering in the next steps, the powder must be well characterized after grinding with respect to such factors, as particle size and distribution, particle shape, homogeneity, absorbed gases, impurities and intra-particle porosity. Iron contamination due to continuous wear of the mill wall and steel ball need to be closely watched and minimized. Now to the ground homogeneous powder, polyvinyl alcohol is added as a binder. Pressing the powder into compacts of desired shapes is done either by conventional method in a die-punch assemble or by hydrostatic or iso-static compaction.

We made use of the former one. Pressing a uniformly dense body by this method is difficult owing to the friction gradient of the powder at the wells of the die and between the particles themselves. This problem is somewhat overcome by the addition of external and internal lubricant to the powder such as stearic acid. Mainly, we made two types of samples: disk shape and torodial shown in figure 3.3. Specimen was prepared by a hydraulic press shown in figure:3.2 with a pressure of 2 ton/cm^2. The die was made of nonmagnetic stainless steel, designed and made in the workshop of AECD.

Figure 3.2 Hydraulic press used to make different shaped samples.

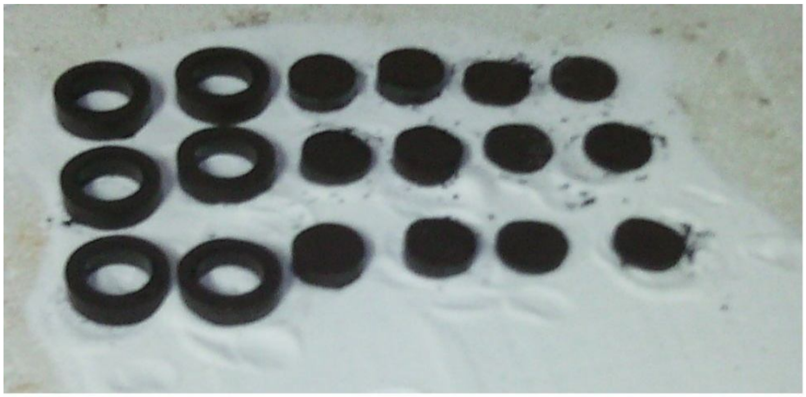

Figure 3.3: Toroid and disk shapes

3.2.4 Sintering

Sintering is the final and a very critical step of preparing properties. The sintering time, temperature and the furnaces atmosphere play very important role the magnetic property of final materials. Sintering commonly refers to processes involved in the heat treatment by which a mass of compacted powder is transformed into a highly densified object by heating it in a furnace below its melting point. Ceramic processing is based on the sintering of powder compacts rather than melting /solidifications /cold working (characteristic for metal) because:

(a) Ceramics melt at high temperatures

(b) As solidified microstructures cannot be modified through additional plastic deformation and re-crystallization due to brittleness

(c) The resulting coarse grains would act as fracture initiation of ceramics.

(d) Low thermal conductivities of ceramics (< 30 - 50 W/mk) in contract to high thermal conductivity of metals (in the range 50-300 w/mk) cause large temperature gradients, and thus thermal stress and shock in melting solidification of ceramics.

Sintering involves the thermal treatment of a powder or compact at a temperature below the melting point of the main constituent, for the purpose of increasing its strength by bonding together of the particles. In this process atomic mobility of the compact is sufficient to permit the decrease the free energy associated with the grain boundaries. Sintering may result in densification, depending on the predominant diffusion pathway. It is used in the fabrication of metal and ceramic components, the agglomeration of ore fines for further metallurgical processing and occurs during the formation of sand stones and glaciers. Sintering must fulfill three requirements.

(i) To bind the particles togather so as to impart sufficient strength to product.

(ii) To dense the grain compacts by elimination of the pores

(iii) To homogenize the materials by completing the reaction left unfinished in the preferring step.

The first two requirements are closely related as far as their mechanisms are concerned. The following figure shows the simple way to bond tour spherical particles to form neck at the contacts by volume diffusion.

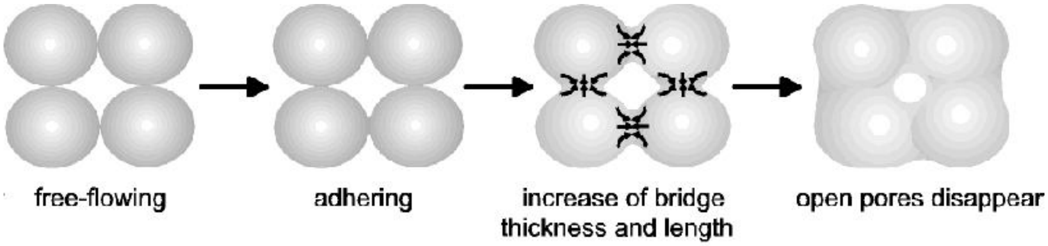

Figure 3.4 Volume diffusions.

One the basis of volume diffusion induced under surface tension, an important equation for the initial stage of sintering process is given by:

$$\frac{\Delta L}{L} = \left[\left(\frac{AD^{*}\gamma\Omega}{r^{3}KT}\right)t\right] \tag{3.1}$$

Where, $\frac{\Delta L}{L}$ is the shrinkage of the compact, Ω is the volume of a single vacancy, D^{*} is the co-efficient of self diffusion for the slowest species, γ is the surface energy, γ is the average radius of the particles, t is sintering time and A is a constant with the approximate value of unity. The above equation indicates that sintering fulfills the requirements (a) and (b) more efficiently when compact features high surface energy and self diffusivity and the particles are fine.

For densification, Bruke made two important observations. One is that the formation of neck only makes the initial stage sintering; an intermediate stage begins when grain growth occurs with the compact density at around 60% of the theoretical value and ends when the pore phase become discontinuous and the density reaches a value of approximately 95%. Another observation of Bruke [3.7] deals with the final stage of sintering. Of discontinuous grain grows occur at the intermediate stage, migration of grain boundaries will leave the remaining isolated pores trapped inside the grains, thus preventing further shrinkage of these intra particle pores and practically stopping the sintering process. In this operation, the cooling rate slays an important role on which structural modification is mainly based. Sintering of crystalline solids follows the following empirical relationship regarding rate of grain growth [3.8]

$$D = Kt^{n} \tag{3.2}$$

Where d is the mean grain diameter, t is sintering time, n is about $\frac{1}{3}$ and K is a temperature dependent parameter.

In the present thesis we have used a programmable furnance NABER (Model HT 08/16 Germany) at AECD. The temperature of the furnace could be maintained within the accuracy of ±1°C.

For sintering we followed more or less the following program.

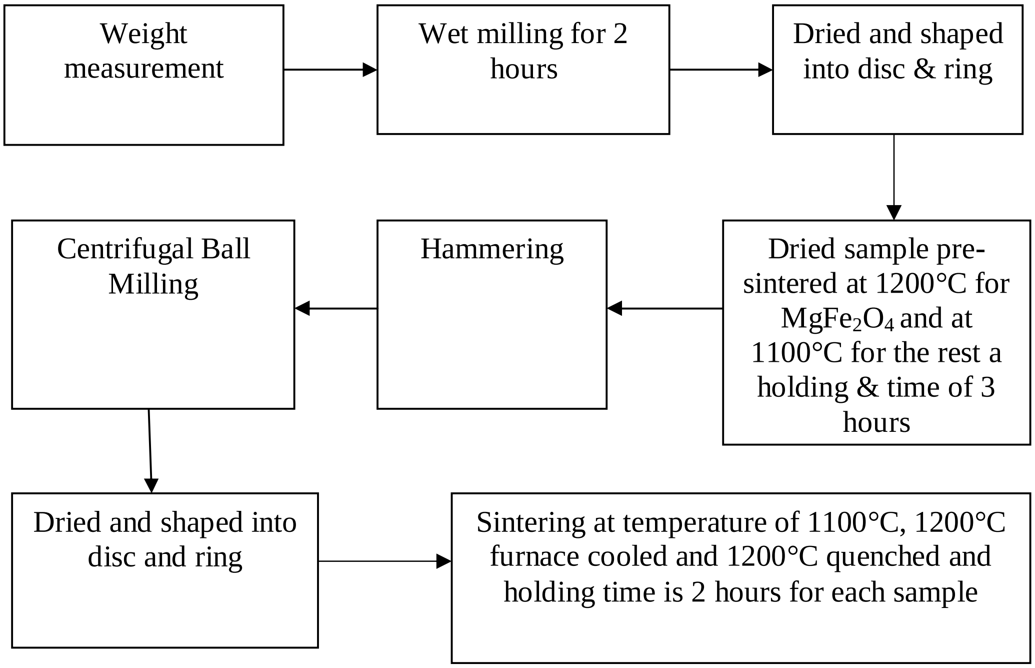

Figure 3.5 Flow chart of sintering

3.3 X-ray Diffraction

To study the crystalline structure of solids, X-ray diffraction (XRD) is a versatile and non-destructive technique that provides detailed information about the materials. A crystal lattice is a regularly arranged three-dimensional distribution (cubic, rhombic etc.) of atoms in space. They are fashioned in such a way that they from a series of parallel plane separated from one another by a distance d (inter-planer or inter –atomic distance) which varies according to the nature of the material. XRD is a rapid analytical technique primarily used for phase identification of a crystalline material and can provide information on unit cell dimensions. The analyzed material is finely ground, homogenized and average bulk composition is determined.

X-rays are the electromagnetic waves whose wavelength is in the neighborhood of 1Á. The wavelength of an X-ray is that the same order of magnitude as the lattice constant of crystals and it is this which makes X-ray so useful in structural analysis of crystals. When X-ray beam is incident on a material, the photons primarily interact with the electrons in atoms and get scattered. Diffracted waves from different atoms can interfere with each other and the resultant intensity distribution is strongly modulated by this interaction. If the atoms are arranged in a periodic fashion, as in crystals, the diffracted waves will consist of sharp interference maxima (peaks) with the same symmetry as in the distribution of atoms. Measuring the diffraction pattern therefore allows us to deduce the distribution of atoms in a material. It is to be noted here that, in diffraction experiments, only X-rays diffracted via elastic scattering are measured.

The peaks in an X-ray diffraction pattern are directly related to the atomic distance. Let us consider an incident X-ray beam interacting with the atoms arranged in a periodic manner as shown in two dimensions in figure: 3.6. The atoms, represented as spheres in the illustration, can be viewed as forming different sets of planes in the crystal. For a given set of lattice planes with an inter-plane distance of d, the condition for a diffraction (peak) to occur can be simple written as

$$2d \sin n\theta = n\lambda \tag{3.3}$$

This is known as Braggs's law.

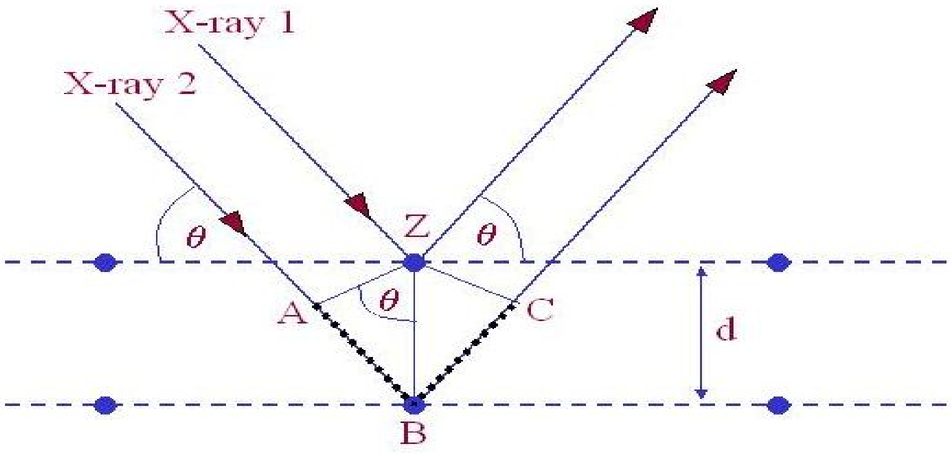

Figure 3.6 Bragg's diffraction pattern

In the equation (3.3), λ is the wavelength of the X-ray, θ is the scattering angle, and n is an integer representing the order of the diffraction peak. The Bragg's Law is one of the most important laws used for interpreting X - ray diffraction data. From the law, we find that the diffraction is only possible when $\lambda < 2d$ [3.9].

In the present work A PHILIPS PW3040 X'Pert PRO X-ray diffractometer was used to study the crystalline phases of the prepared samples in the Materials Science division, Atomic Energy Centre, Dhaka.

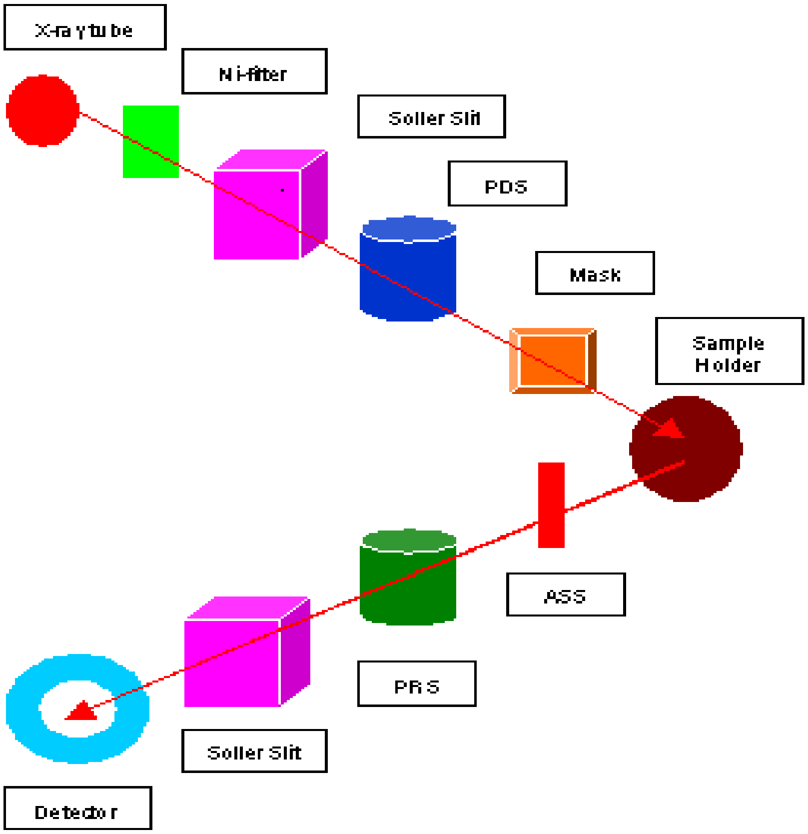

Figure: 3.7 Block diagram of the PHILIPS PW3040 X'Pert PRO XRD system

Figure: 3.7 shows the inside view of the PHILIPS X'Pert PRO XRD system. The powder diffraction technique was used with a primary beam powder of 40 kV and 30 mA for Cu-K_α radiation. A nickel filter was used to reduce Cu-K_β radiation and finally Cu-K_α radiation was only used as the primary beam. The experimental has been performed at room temperature. A 2θ scan was taken from 25^o to 75^o to get possible fundamental peaks with the sampling pitch of 0.02^o and time for each step data collection was 1.0 sec. Both the programmable divergence and receiving slits were used to control the irradiated beam area and output intensity from the powder sample, respectively. An anti scatter slit was used just after the tube and in front of the detector to get parallel beam only. All the data of the sample were stored in the computer memory and later on analyzed them using computer “software” X’Pert HIGHS CORE”. For XRD experiment each sample was set on a glass slide and fixed the sample by putting adhesive typed the two ends of the sample.

For each composition, the cylindrical samples of weight more than 2 gm are converted into powder. For XRD experiment each sample was set on a glass slide and fixed the sample by putting adhesive tape at the two ends of the sample X-ray diffraction patterns were carried out to confirm the crystal structure. Instrumental broadening of the system was determined from θ - 2θ scan of standard Si. At (311) reflections position of the peak, the value of instrumental broadening was found to be 0.07°. This value of instrumental broadening has subtracted from the pattern. After that using the X-ray data, the lattice constant (a) and hence the X-ray densities were calculated.

3.3.1 Different Parts of the PHILIPS X’ Pert PRO XRD System

Figure: 3.8 shows the inside view of the X’- pert PRO XRD system. A complex of instruments of X- ray diffraction analysis has been established for both materials research and specimen characterization. These include facilities for studying single crystal defects, and a variety of other materials problems.

The PHILIPS X’ Pert PRO XRD system comprised of the following parts

(i) Cu-Tube” with maximum input power of 60 kV and 55 mA
(ii) “Ni- Filter” to remove Cu-K_α component
(iii) “Solar slit” to pass parallel beam only
(iv) “Programmable Divergent slits(PDS)” to reduce divergence of beam and control irradiated beam area
(v) “Mask” to get desired beam area
(vi) “Sample holder” for powder sample.
(vii) “Anti Scatter slit (ASS)” to reduce air scattering back ground.

(viii) "Programmable Receiving slit (PRS)" to control the diffracted beam intensity and

(ix) Solar slit to stop scattered beam and pass parallel diffracted beam only.

Figure: 3.8 Internal arrangement of a PHILIPS X' Pert PRO X-ray diffractometer.

3.3.2 Interpretation of the XRD data

The XRD data consisting of θ_{hkl} and d_{hkl} values corresponding to the different crystallographic planes are used to determine the structural information of the samples like lattice parameter and constituent phase.

Lattice parameters of Mg-Cu ferrites samples were determined. Normally, lattice parameter of a composition is determined by the Debye-Scherrer method after extrapolation of the curve. In this method at least five fundamental reflections are required to determine lattice parameter. In the present case, ten reflection planes are prominent at XRD patterns and we would like to understand how the increase of Cu content in a Mg-Cu ferrite. We determine lattice spacing (inner planer distance) d using this reflection from the equation:

$$2d_{hkl}\,\mathrm{Sin}\theta = \lambda$$

$$\text{i.e. } d_{hkl} = \frac{\lambda}{2\sin\theta} \tag{3.4}$$

Where λ is the wavelength of the X-ray, θ is the diffraction angle and n is an integer representing the order of the diffraction.

The lattice parameter for each peak of each sample was calculated by using the formula:

$$a = d_{hkl} \times \sqrt{h^2 + k^2 + l^2} \tag{3.5}$$

Where h, k, l are the indices of the crystal planes. We get d_{hkl} values from the computer using software "X'- Pert HJGHS CORE". So we got ten 'a' values for ten reflection planes such as a a_1 , a_2 a_3 ….. etc. To determine the exact lattice parameter for each sample, Nelson-Riley method was used. The Nelson-Riley function [3.10] f (θ), can be written as

$$F(\theta) = \frac{1}{2}\left[\frac{\cos^2\theta}{\sin\theta} + \frac{\cos^2\theta}{\theta}\right] \tag{3.6}$$

Now drawing the graph of 'a' vs F(θ) and using linear fitting of those points will give us the lattice parameter 'a_0'. This value of 'a_0' at F(θ) = 0 or θ = 90° .These 'a_0's are calculated with an error estimated to be ± 0.0001Á.

3.3.3 X-ray Density and Bulk Density

X-ray density, (ρ_x) was also calculated usual from the lattice constant. The relation between ρ_x and 'a' is as follows [3.11]

$$\rho_x = \frac{ZM}{Na^3} \tag{3.7}$$

Where M is the molecular weight of the corresponding composition, N is the Avogadro's number ($6.023\text{X}10^{23}$ mole^{-1}), 'a' is the lattice parameter and Z is the number of molecules per unit cell,(Z = 8 for the spinel cubic structure).

Bulk Density

The bulk density (ρ_B) is measured by the formula

$$\rho_B = \frac{m}{V} \tag{3.8}$$

Where m is the mass of the disc sample and v is its volume.

3.3.4 Porosity

Porosity is a parameter which is inevitable during the process of sintering of oxide materials. It is noteworthy that the physical and electromagnetic properties are strongly dependent on the porosity of the studied samples. Therefore an accurate idea of percentage of pores in a prepared sample is prerequisite for better understanding of the various properties of the studied samples to correlate the microstructure property relationship of the samples under study. The porosity of a material depends on the shape, size of grains and on the degree of their storing and packing. The difference between the bulk density ρ_B and X-ray density ρ_x gave us the measure of porosity. Percentage of porosity has been calculated using the following relation [3.12]

$$P = (1-\frac{\rho_B}{\rho_x})\times 100\% \qquad (3.9)$$

3.4 Magnetization Measurement

Magnetization in ferrite samples originated due to the difference in the magnetic moments for the two sub-lattices. The larger the difference, the greater is the resultant magnetization, because of the anti-parallel arrangements of the moments in two sub-lattices. The magnetic moment of each sub-lattice arises due to the presence of magnetic ions such as Fe^{3+}, Fe^{2+}, Mn^{2+}, Cu^{2+}, Ni^{2+}, Co^{2+} etc. in our case, only iron ion has magnetic moment since Mg non-magnetic. Different ions occupy different two sites. So, as a whole, the two sub-lattices have their individual resultant magnetic moments. The differences in magnetic moment between the two sub-lattices give rise to net magnetic moment which in turn yields magnetization. In the present study magnetization has been performed a Vibrating Sample Magnetometer (VSM).

3.4.1 Vibration Sample Magnetometer

The principle of vibrations sample magnetometer (VSM) is the measurement of electromotive force induces by magnetic sample when it is vibrate at a constant frequency in the presence of a static and uniform magnetic field. A small part of the (10 - 50 mg) was weighted and made to avoid movements inside the sample holder shown in Figure: 3.8. VSM is a versatile and sensitive method of measuring magnetic properties developed by S. Foner [3.13] and is based on the flux change in a coil when the sample is vibrate near it.

The simplest of these is the rotating coil which rotates at a fixed angular velocity. Therefore the amplitude of the generated voltage by rotating coil is proportional to the magnetic induction and therefore the amplitude can be used to measure magnetic induction or magnetic field in free space. The signal can be read directly as an AC voltage or converted to a DC voltage which is proportional to the amplitude.

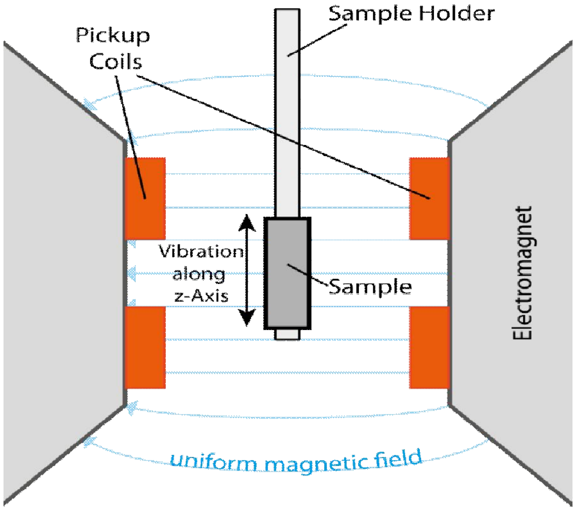

Figure: 3.9 Vibrating Sample Magnetometer - sample holder and detection mechanism

Figure: 3.9 shows VSM of Model EV7 system. The magnetic properties measurement system model EV7 is a sophisticated analytical instrument configured specially for the study of the magnetic properties of the small samples over a broad range of temperature from 103K to 800K and magnetic field from -20kOe to +20kOe. The VSM is designed to continuously measure the magnetic properties of materials as a function of temperature and the field. In this type of magnetometer, the sample is vibrated up and down in a region surrounded by several pick up coils. The magnetic sample is thus acting as a time-changing magnetic flux, varying the electric flux is accompanied by an electric field and the field induces a voltage in pick up coils. This alternating voltage signal is processed by a control unit system, in order to increase the signal to noise ratio. The result is a measure of the magnetization of the sample.

By using a compact gradiometer pickup coil configuration, relatively large oscillation amplitude (1- 3mm peak) and a frequency of 40 Hz, the system is able to resolve magnetization changes of less than 10^{-6} emu at a data rate of 1 Hz. The VSM option for the PPMS consists primarily of a VSM line a motor transport (head) for vibrating the sample, a coil set puck for detection, electronics for driving the linear motor transport and detecting the response from the pickup coils. If a sample is placed in a uniform magnetic field, created between the poles of electromagnet, a dipole moment will be induced. If the sample vibrates with sinusoidal motion sinusoidal electrical signal can be induced in suitable placed pick-up coils. The signal has same frequency of vibration and its amplitude will be proportional to the magnetic moment.

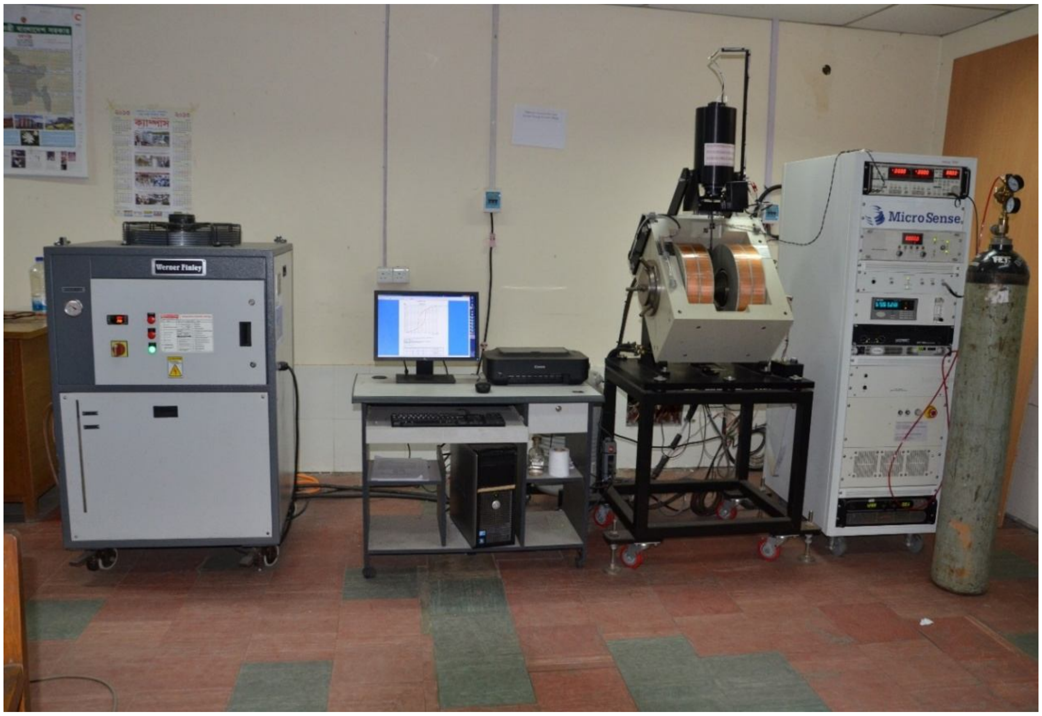

Figure: 3.10 Vibrating Sample Magnetometer at Materials Science Division, AECD

The sample is attached to the end of a sample rod that is driven sinusoidally. The center of oscillation is positioned at the vertical center of a gradiometer pickup coil. The precise position and amplitude of oscillation is controlled from the VSM motor module using an optical linear encoder signal read back from the VSM linear motor transport. The voltage induced in the pickup coil is amplified and lock-in detected in the VSM detection module.

The VSM detection module uses the position encoder signal as a reference for the synchronous detection. This encoder signal is obtained from the VSM motor module, which interprets the raw encoder signals from the VSM linear motor transport. The VSM detection module detects the in-phase and quadrature-phase signals from the encoder and from the amplified voltage from the pickup coil.

The sample is fixed to sample holder located at the end of a sample red mounted in a electromechanical transducer. The transducer is driver by a power amplifier which itself is driver by an oscillator at a frequency of 90Hz. So, the sample vibrates along the 2-axis perpendicular to the magnetizing field. The latter induce a signal in the pick-up coil system that is fed to a differential. The output of the differential amplifier is subsequently fed into a tuned amplifier and an internal lock in amplifier that receives signal supplied by the oscillator. The output of the lock-in amplifier, or the output of the magnetometer itself, is a DC signal proportional to the magnetic moment of the sample being studied. Calibration of the VSM is done by measuring the signal of a pure Ni standard of Known saturation magnetic moment placed in the saddle point. The basic instrument included the electromechanical system and the electronic system including in personal computer. Laboratory electromagnet coils of various maximum field strengths may be used.

3.5 Experimental Procedure for Microstructure Study

Magnetic properties of the Mg-Cu sample are strongly dependent upon the sensitive control of the microstructure permeability is directly proportional to the grain size of the samples. At least up to a critical diameter of the grains causes the permeability to increase monotonically. Resistivity and density of the ferrite samples are also dependent on the porosity of the samples. Resistivity of the samples increases with the trapped intra-granular pores. Hence the microstructure studies of the samples are required for making prediction about the result of permeability and resistivity of the ferrite samples. For microstructure study the ferrite samples were polished step by step. Primarily the samples were polished by using Megaserv Universal Polisher; model No C200/5V, Volts 240, Amp. 0.75 Secondly, using another polishing machine 99 phoenix .Aue, Enfield, CT06082 USA, Model No LABPOL 8/12, keeping a aped of 300 - 450 rev/sec for about 1 hour using different grades of Al_2O_3 fine powders mixing with water. In the tertiary stage the polished samples were classed ultrasonically for $\frac{1}{2}$ hour using an ultrasonic cleaner FEITSCH @ Laboratte, Model 17:202, No 1030. After the fine polishing and ultrasonic cleaning the samples were etched thermally under suitable temperature for the different samples down below 150 to 100°C of the sintering temperature for 2 minutes in air for every sample. As the thermal etching was finished the samples were readily for the microstructure study. The microstructure measurements of the samples were done by using Philips XL30 Scanning Tunneling Microscope at AECD, Dhaka, Bangladesh. The following figure 3.10 shows the pictorial diagram of SEM.

The SEM microstructures of samples sintered at 1200°C (furnace cooled) were studied by using Philips XL30 Scanning Tunneling Microscope. To observe the microstructure the ferrite samples were ground and then polished with fine Al_2O_3 powder followed by thermal etching near to the sintering temperature 2 minutes. When the etching was completed, the grains were seen clearly by the SEM and photographed.

Figure: 3.11 Scanning Tunneling Microscope

3.6 Experimental Procedure for Mössbauer Spectrometer

Mössbauer experiments on the Mg-Cu ferrite powder sample were performed Materials Science Division, AECD. Mössbauer measurement can be made in two different geometries, transmission and scattering configuration. In the present work only transmission geometry was used. In transmission type measurements, the intensity of γ-ray transmitted through a thin absorber are measured with the help of a suitable detector like proportional counter. γ-ray source is driven electromagnetically by a transducer so as to Doppler shift the energy spectrum is obtained by counting transmitted γ-rays by small and known amounts. The absorption Mössbauer spectrum is obtained by counting transmitted γ-rays as a function of the source to absorber velocity. The Mössbauer effect allows for very precise measurements of γ-rays resonance. In combination with the Doppler shift, it can be used to observe the hyperfine splitting of the ^{57}Fe nucleus and thus determine the internal filed of the ^{57}Fe nuclei. A measurement of the line width can also be made. In our experiment, a Fe-Co nucleus decays into an excited state of the ^{57}Fe nucleus shown in figure 3.12

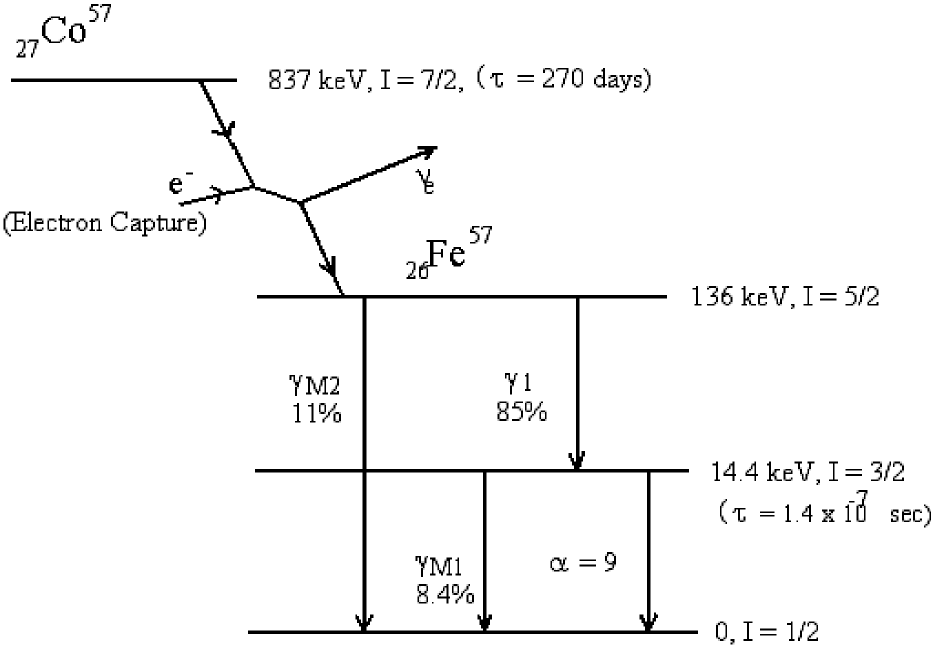

Figure: 3.12 Energy level scheme of Fe^{57} Mössbauer spectroscopy involves the 14.4 KeV transition. Interstices are given in % decays.

Since Fe-Co is not ferromagnetic, the decaying nucleus does not experience any Zeeman splitting and emits 14.4KeV γ-rays. the emitted γ-rays are incident on an absorber with roughly 2.2% abundance of $_{57}$Fe nuclei. This concentration is sufficient that any absorbing nucleus experiences Zeeman splitting due to the magnetic field from surrounding $_{57}$Fe atoms. If the source is at rest relative to the absorber, the splitting of energy levels in the absorber prevents resonant absorption. If the relative velocity of the source in the direction of the absorber increases, Doppler shift γ-rays can be made to much resonance conditions with the split levels in the absorber. By changing the velocity of the source, resonance conditions can be reached for each of the different transitions in the absorber when in resonance, the absorber will absorb much more of the γ-rays. The shape of the excess absorption peaks may be compared to theoretical estimates and the natural line width may be determined.

The detector counts and source velocity are synchronized by a micro processor system. The counts accumulate in 576 channels for one complete cycle which contain two complete spectra; one for positive acceleration and one for negative acceleration of the source. As the acceleration is constant the time interval is equal for all velocity intervals hence each channel records for the same amount of time. During analysis the full spectrum is folded around a central point to produce a single spectrum.

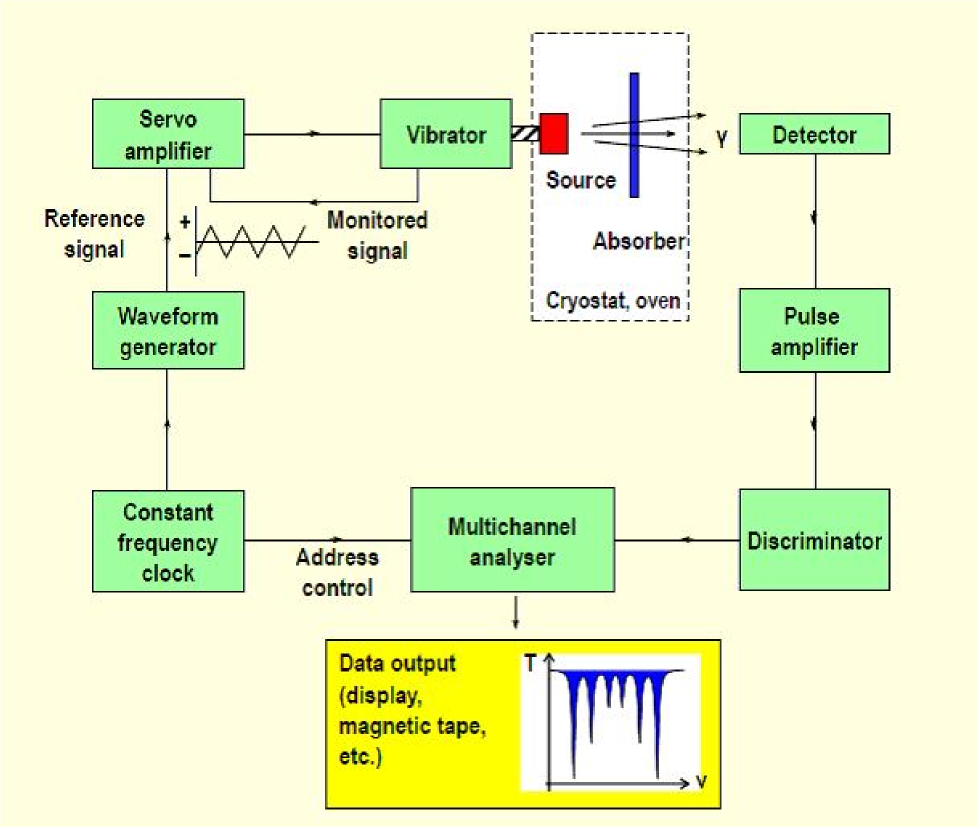

Figure 3.13 Scheme of Mössbauer Spectroscopy

This increases the number of counts (and hence gives better statistics) and flattens the background profile produced by the difference intensity of the source radiation as the source move relative to the absorber and detector. The experimental apparatus is drawn in figure 3.13. A radioactive Fe-Co source is mounted on a vibrating shalf that mores in the direction of a Geiger Muller tube (detector). An absorber placed between the numbers of γ-rays that reach the detector. Several pieces of electronic equipment are used to control the motion of the source and correlate it with the signal from the detector.

Figure 3.14 Sample preparations for Mössbauer measurement

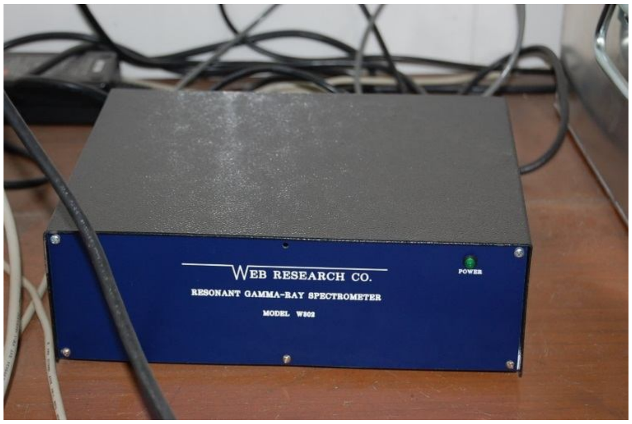

Figure 3.15 SEE Co.MS4 Spectrometer recording a Mössbauer spectrum

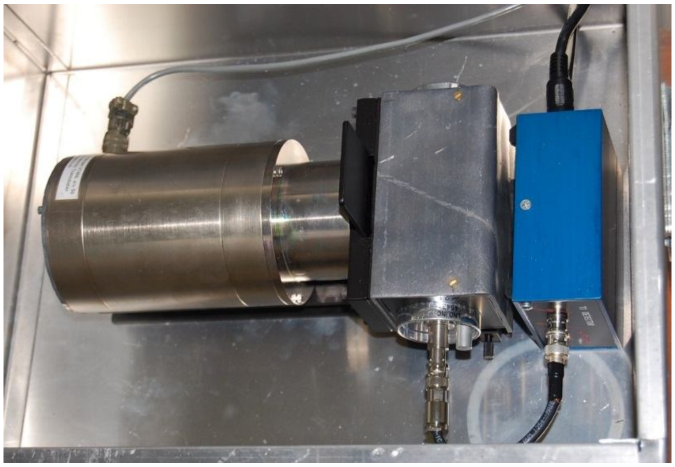

Figure 3.16 Velocity Transducer with the sample at room temperature.

RESULTS AND DISCUSSION

4.1 Structural and Physical Characterization of Mg-Cu Ferrites

The spinel ferrites having general formula $Mg_{1-x}Cu_xFe_2O_4$ [x = 0.0, 0.1, 0.2, 0.3, 0.4 & 0.5] have been prepared by the standard solid state reaction technique using reagents of analytical grate. The substitution of nonmagnetic Cu in Mg-Cu ferrites has a significant influence on the structural and physical properties such as lattice constant, X-ray density, balk density, porosity etc. XRD patterns reveal that the samples are of single phase cubic spinel structure. Lattice parameter 'a' of the samples was found to be compare than base ferrites. The porosity was calculated from the X-ray density and bulk density. The possible experimental and theoretical reasons responsible for the change in substitution of the above mentioned properties have been discussed below.

4.1.1 Phase Analysis

X-ray diffraction (XRD) studies of the samples were performed by using Philips X' PERT PRO X-ray Diffractometer using Cu-K_α radiation in the range of $2\theta = 15°$ to $65°$ in steps of 0.02°. The XRD patterns for the series of samples $Mg_{1-x}Cu_xFe_2O_4$ (x = 0.0, 0.1, 0.3, 0.4 and 0.5) sintered at 1100°C for 3 hours is shown in Figure 4.1(a, b, c, d, e, f). All the samples show good crystallization with well defined diffraction lines. A phase analysis using XRD technique was performed to confirm the formation of single-phase cubic spinel structure with no extra lines corresponding to any other crystallographic phase. The results obtained from XRD pattern for all the samples of $Mg_{1-x}Cu_xFe_2O_4$ with the (h k l) values corresponding to the diffraction peaks of different planes (220), (311), (400), (422), (511), and (533) which represent either odd or even indicating the samples are spinel cubic phase. The analysis of XRD patterns indicated that the studied Mg-Cu ferrites samples have spinel cubic structure with a single phase. The Miller indices (i.e. h, k, l) in this range of compositions are unmixed, which shows that the crystal structures are phase centered cubic (FCC) using XRD data. The lattice parameter 'a' and have the X-ray density were calculated.

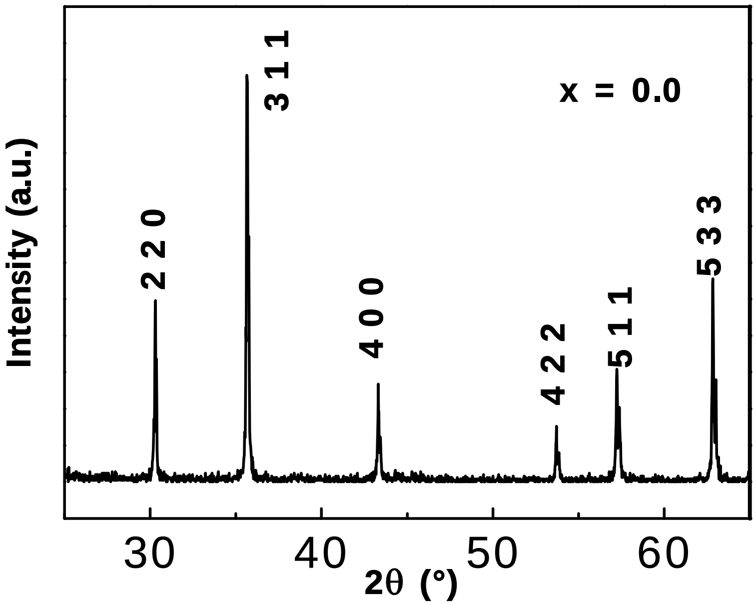

Figure 4.1(a): X-ray diffraction patterns for $Mg_{1-x}Cu_xFe_2O_4$ for x = 0.0 sintered at 1100°C for 3 hours.

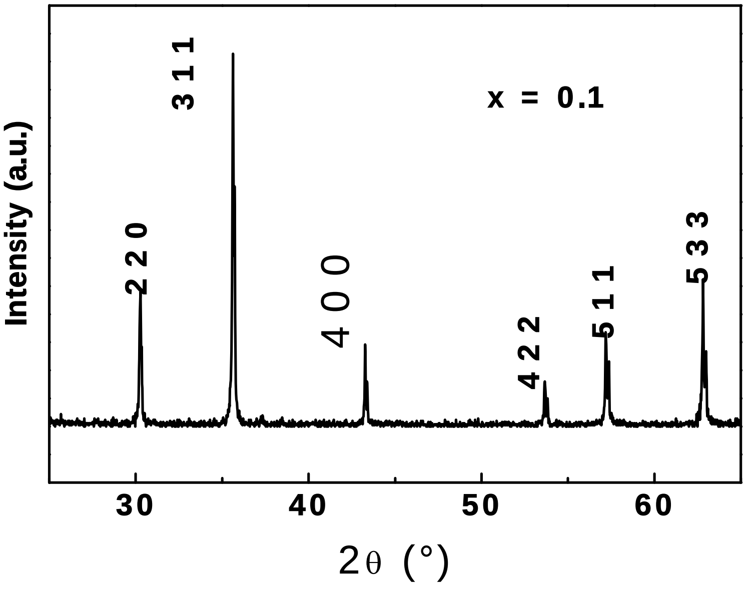

Figure 4.1(b) X-ray diffraction patterns for $Mg_{1-x}Cu_xFe_2O_4$ for x = 0.1 sintered at 1100°C for 3 hours.

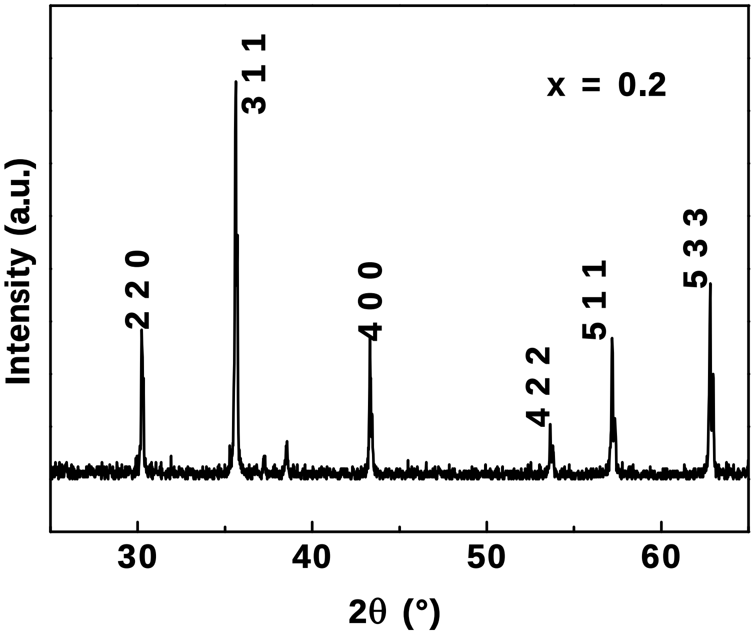

Figure 4.1(c): X-ray diffraction patterns for $Mg_{1-x}Cu_xFe_2O_4$ for x = 0.2 sintered at 1100°C for 3 hours.

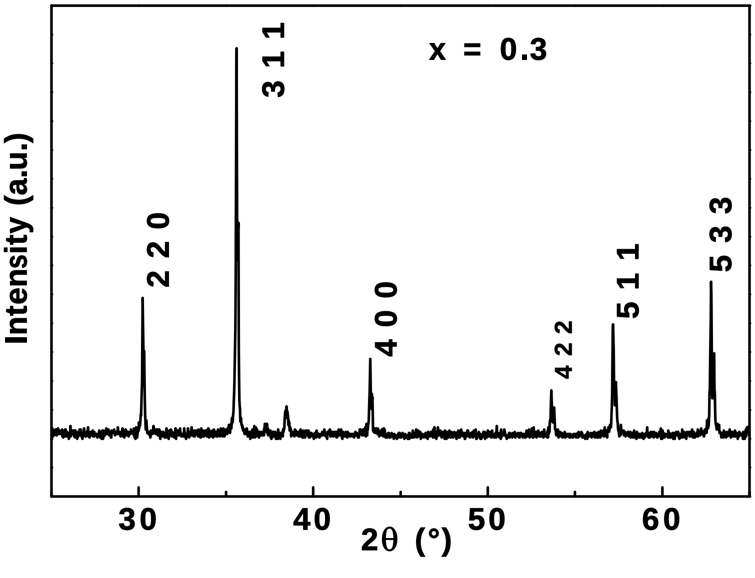

Figure 4.1(d) X-ray diffraction patterns for $Mg_{1-x}Cu_xFe_2O_4$ for x = 0.3 sintered at 1100°C for 3 hours.

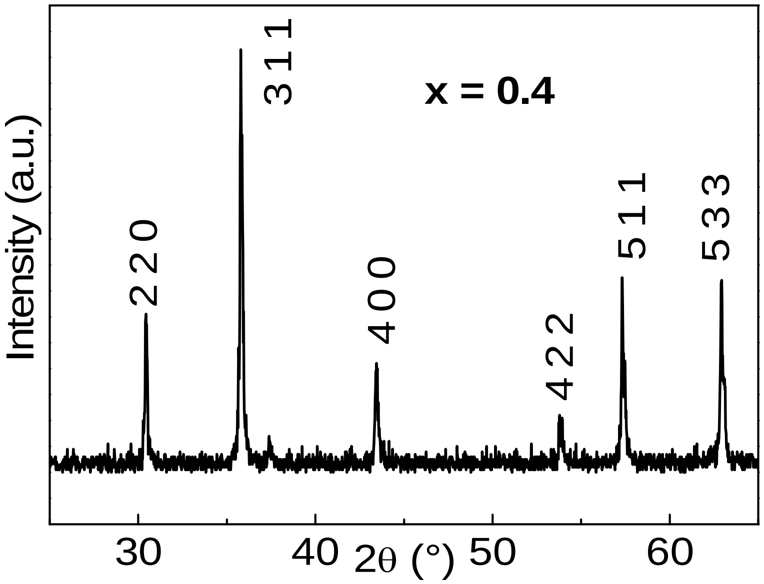

Figure 4.1(e) X-ray diffraction patterns for $Mg_{1-x}Cu_xFe_2O_4$ for x = 0.4 sintered at 1100°C for 3 hours.

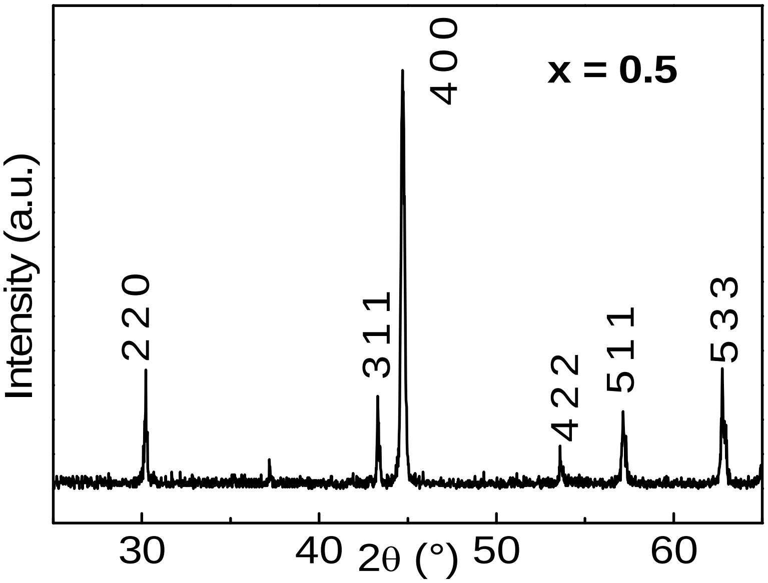

Figure 4.1(f) X-ray diffraction patterns for $Mg_{1-x}Cu_xFe_2O_4$ for x = 0.5 sintered at 1100°C for 3 hours.

4.1.2 Lattice Parameters

The lattice parameter or lattice constant from the calculated lattice parameter 'a' corresponding to each plane of XRD pattern using Nelson –Riley function [4.1]

$$F(\theta) = \frac{1}{2}[\frac{\cos^2\theta}{\sin\theta} + \frac{\cos^2\theta}{\theta}] \tag{4.1}$$

Where θ is the Bragg's angle, by extrapolating the lattice parameter values to F(θ) = 0 or θ = 90°. For the calculation of exact lattice parameter the graph of apparent lattice parameter 'a' vs. the values of Nelson – Riley function F(θ) are plotted in Figure 4.2 (a) to (f) . The Y-axis values at F(θ) = 0 gives the exact values of lattice parameters. The equations of the linear fitting of the points are shown in the graph. Variation of lattice parameters 'a' as function of Cu-contents x is shown in figure 4.3 and also shown in table 4.1. The lattice parameter of $Mg_{1-x}Cu_xFe_2O_4$ ferrites is nearly same cu-contents up to values x = 0.4 and $x \geq 0.4$ is increases shown in figure 4.3. Since the ionic radii of Mg^{2+} and Cu^{2+} ions are 0.72Å and 0.73 Å. When the larger Cu^{2+} ions enter into the lattice, the unit cell expands resulting in enhancement of lattice parameter

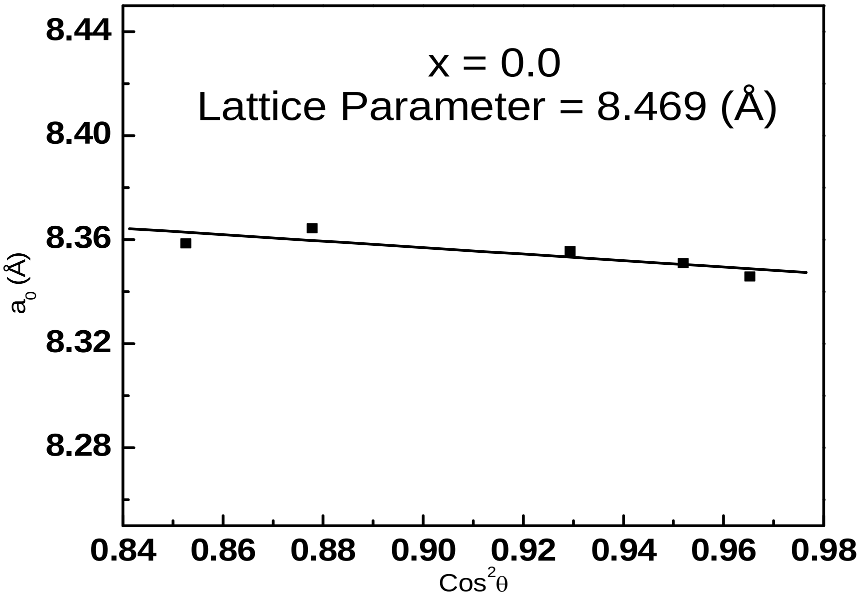

Figure: 4.2(a) Variation of the lattice parameter 'a' Å as N-R function F(θ) for x = 0.0 and T_s = 1100°C

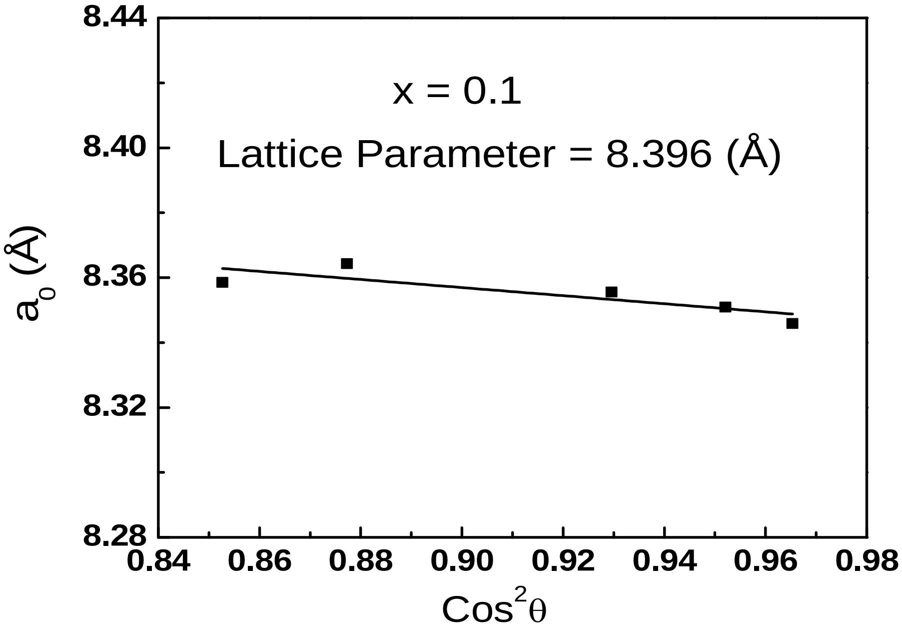

Figure 4.2(b): Variation of the lattice parameter 'a' Å as N-R function F(θ) for x = 0.1 and T_s =1100°C

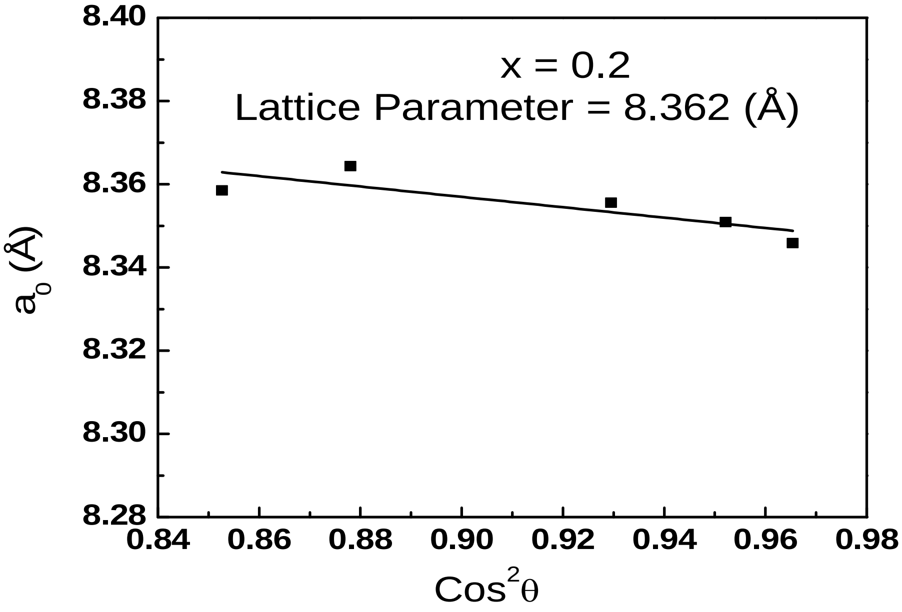

Figure 4.2(c): Variation of the lattice parameter 'a' Å as N-R function F(θ) x = 0.2 and T_s=1100°C

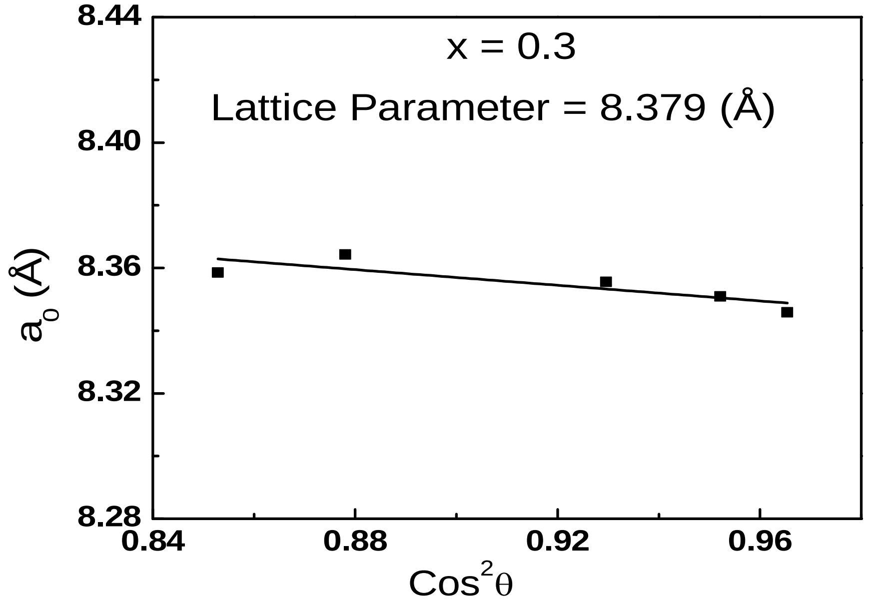

Figure 4.2(d): Variation of the lattice parameter 'a' Å as N-R function F(θ) for x = 0.3 and T_s =1100°C

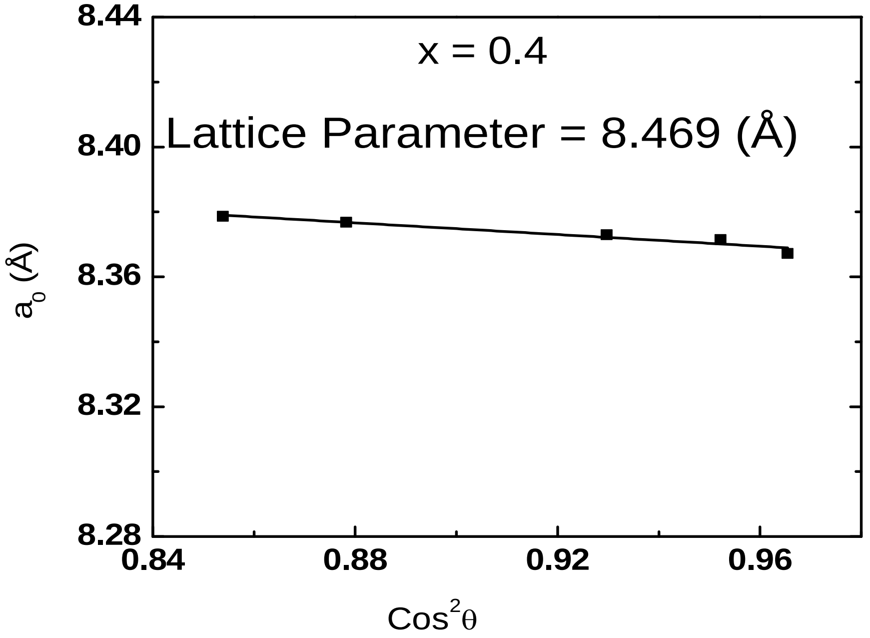

Figure 4.2(e): Variation of the lattice parameter 'a' Å as N-R function F(θ) for x = 0.4 and T_s =1100°C

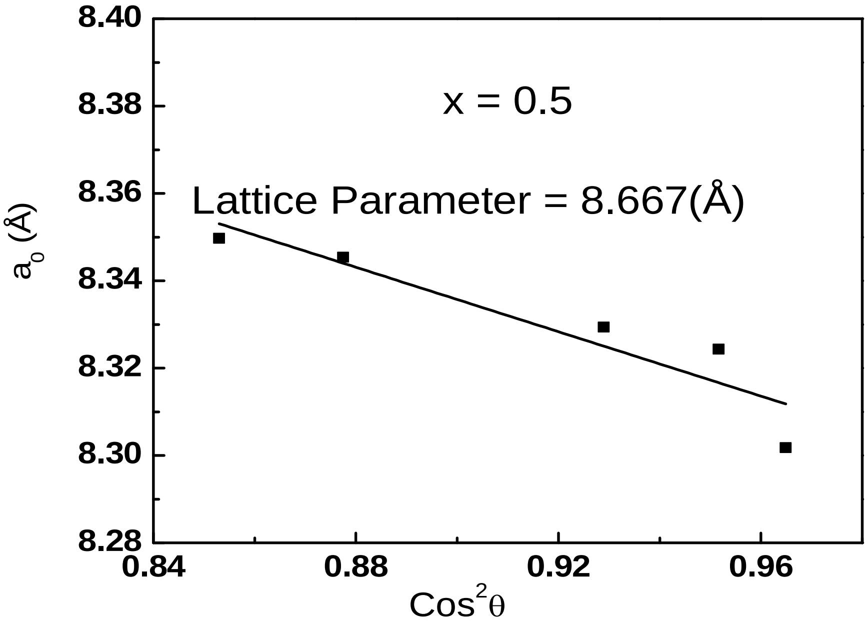

Figure 4.2(f): Variation of the lattice parameter ‘a’ Å as N-R function F (θ) for x = 0.5 and T_s = 1100°C

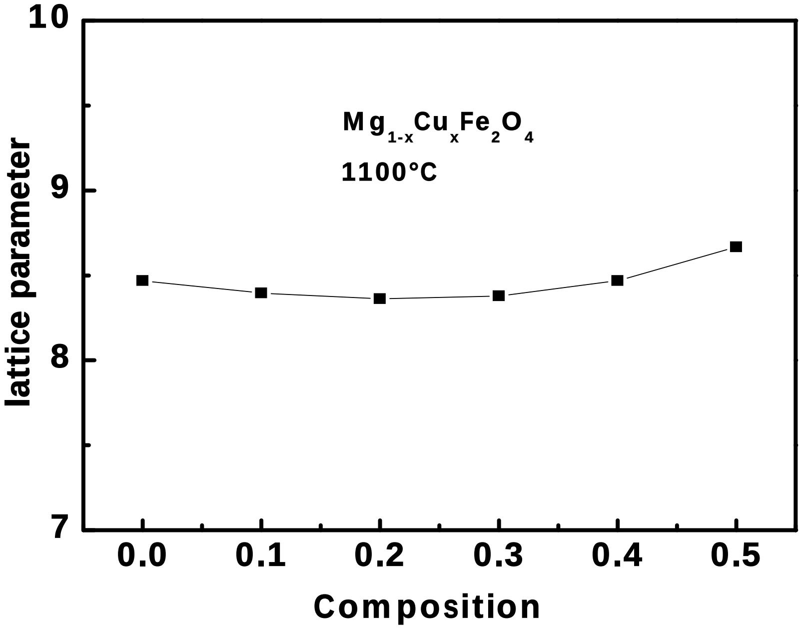

Figure 4.3: Variation of the lattice parameter ‘a’ Å for the sample $Mg_{1-x}Cu_xFe_2O_4$ with Cu-content.

It is well known that the distribution of cations on the octahedral B sites and tetrahedral A-sites determine to a great extent the physical, magnetic, electrical and Mössbauer parameters of Mg-Cu ferrites. These exists a correlation between the ionic radius and the lattice constant, the increase of the lattice constant is proportional to the increase of the ionic radius [4.2]

4.1.3 Density and Porosity

Density plays a vital role in controlling the properties of polycrystalline ferrites. The effect of Cu substitution on the physical properties such as X-ray density, bulk density, and porosity for all the studies sample $Mg_{1-x}Cu_xFe_2O_4$ (x = 0.0, 0.1, 0.2, 0.3, 0.4 & 0.5) where the formula:

X-ray density $\rho_x = \frac{8M}{Na^3}$ gm/cm^3 (4.2)

Porosity $\rho_x = 1 - \frac{\rho_B}{\rho_x}$ (4.3)

The bulk density, ρ_B was measured by usual mass and dimensional consideration whereas X-ray density ρ_x was calculated from the molecular weight and the volume of the unite cell derived from the lattice for each sample. The calculated values of the bulk density and theoretical or X-ray density of the studied ferrite system are presented in Table-4.1.

Table 4.1: Lattice parameter, X-ray density, bulk density and porosity for different composition of the sample $Mg_{1-x}Cu_xFe_2O_4$ sintered at 1100°C

Composition	Lattice parameter a_o in Å	X-ray Density (ρ_x) (gm/cc)	Bulk Density (ρ_B) (gm/cc)	% Porosity
X = 0.0	8.469	4.373	2.477	43.36
X = 0.1	8.396	4.556	2.305	49.41
X = 0.2	8.362	4.722	2.663	43.61
X = 0.3	8.379	4.782	3.126	34.63
X = 0.4	8.469	4.717	3.463	26.58
X = 0.5	8.667	4.481	3.415	23.79

An increasing trend in X-ray density and decreasing trend in porosity has been observed with the substitution of Cu shown in figure 4.4 and figure 4.5. The X-ray density of the sample sintered at 1100°C increases monotonically with the increase of Cu-constant. The highest X-ray density is observed for x = 0.5 ($\rho_x =$ 3.939gm/cc) and the lowest density is observed at x = 0.00 ($\rho_x =$ 3.478 gm/cc). The bulk density ρ_B=increases with the increases of Cu- contents. It is also observed that the bulk density is lower than the corresponding X-ray density. This may be due to the existence of pores, which were formed and developed during the sample preparation or sintering process [4.3]. The increase in X-ray density is also due to the difference in ionic radii between Mg and Cu. The X-ray density increase slightly with the Cu-substitution, which is due to the atomic weight and density.

The percentage of porosity was calculated using the equation (4.3). The porosity of the present studied sample $MgFe_2O_4$ is found 43.36%. The porosity has decreased in Mg-Cu ferrites systems by Cu substitution, which may due to the creation of more oxygen vacancies with the substitution of Cu-ions in the samples and virtually less cation are created [4.4]. It is also known that the porosity of ferrite samples results from two sources, inter granular porosity (P_{intra}) and, inter granular porosity (P_{intra}) [4.5]. Thus the total porosity (P%) could be written as the sum of the two types.

i.e. $P(\%) = P_{intra} + P_{intra}$ (4.4)

The intra-granular porosity mainly depends on the grain size.

The porosity of the sample $Mg_{1-x}Cu_xFe_2O_4$ sintered at 1100°C decreases with the increase of Cu- contents. It is observed that the lowest porosity is obtained for the sintering temperature 1100°C for x = 0.5, which is 23.79% and the highest porosity is seen to occur when x = 0.1.

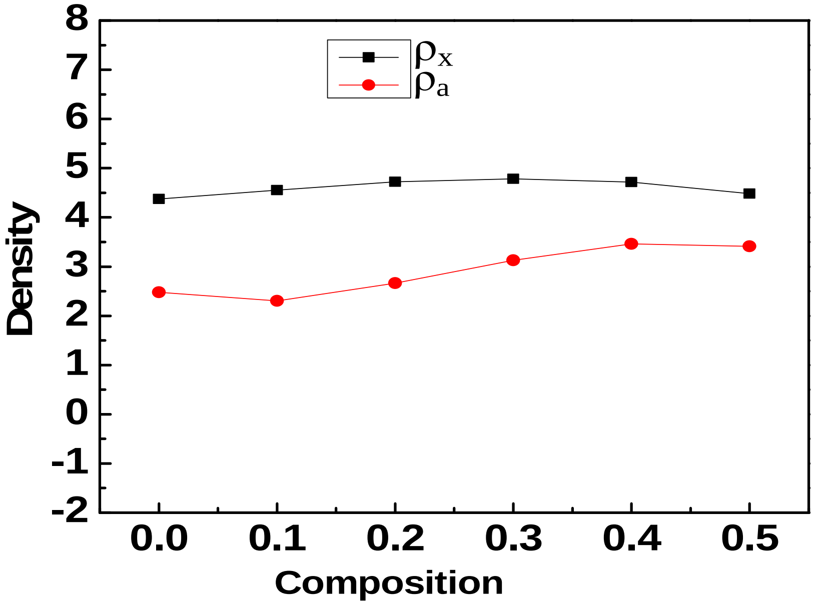

Figure 4.4: Comparison of the X-ray density and bulk density for the sample $Mg_{1-x}Cu_xFe_2O_4$

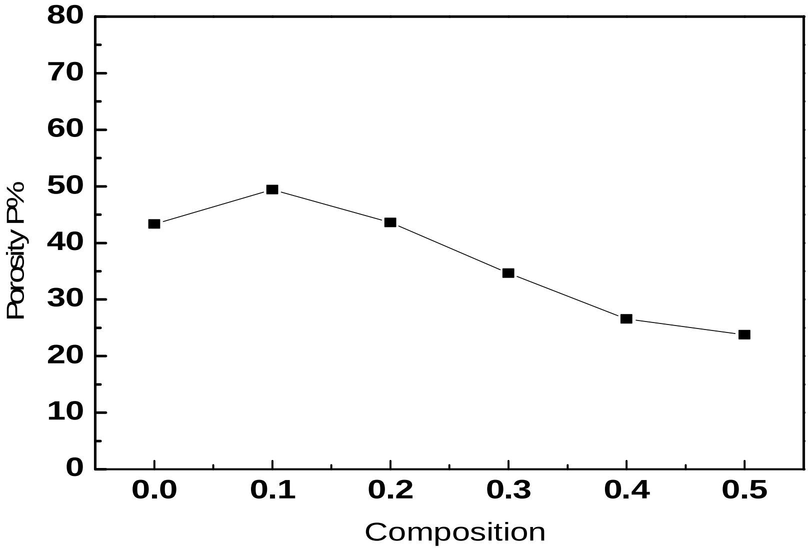

Figure 4.5: Variation of porosity (%P) for different composition of $Mg_{1-x}Cu_xFe_2O_4$ sintered at 1100°C.

4.2 Microstructure Analysis of Mg-Cu Ferrites

Magnetic and electric properties sensitively depend on the microstructure of ferrites. Between the grain size and porosity of microstructure, grain size is more important parameter affecting the magnetic properties of ferrites. Grain growth is closely related to the grain boundary mobility. Re-crystallization and grain growth involve the movement of grain boundaries. Figure 4.6 (a, b, c, d, e & f), Figure 4.7 (a, b, c, d, e & f) and 4.8 (a, b, c, d, e & f) shows the SEM microstructures of $Mg_{1-x}Cu_xFe_2O_4$ ferrites sintered at 1200°C, 1200°C (surface) and 1200°C (quenched). It is clear that the microstructure of Mg-Cu ferrites strongly depends on the amount of CuO present in the samples. CuO influences the microstructure Mg-Cu ferrites by the formation of liquid phase during sintering. It facilities the grain growth by increasing the rate of cation inter diffusion as a result of its segregation to the grain boundaries [4.5]. The behavior of grain growth reflects the completion between the driving force for grain boundary movement and the retarding force exerted by pores [4.6].

During the sintering, the thermal energy generates a force that drives the grain boundaries to grow over pores, thereby decreasing the pore volume and making the materials dense. When the driving force of the grain boundary in each grain is homogeneous, the sintered body attains a uniform grain size distribution. Abnormal grain growth occurs if this driving force is inhomogeneous. Moreover, the strength of the driving force depends upon the diffusivity of individual grains, sintering temperature and porosity. During the phase sintering, grain growth occurs via a dissolving solution precipitation process. Energetically, small grains are less stable then large grain due to their higher specific surface areas. As a consequence, small grains would be dissolved in the liquid-phase layers. Once the concentration of the dissolved phase reached a critical level, precipitation would take place. This means that larger grains grow at the expense of smaller grains. It seems that small grains have to “swim” through a barrier (liquid-phase layer) to combine with a large grain.

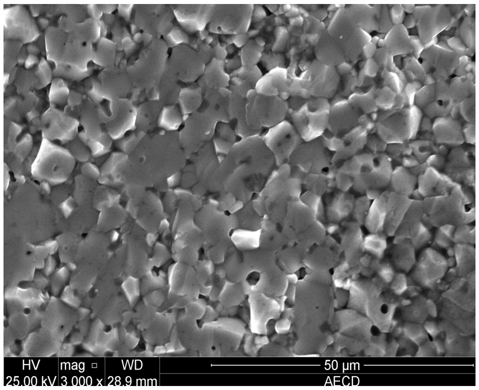

Figure 4.6 (a): Microstructure of $Mg_{1-x}Cu_xFe_2O_4$ sample sintered at 1200°C for x = 0.0

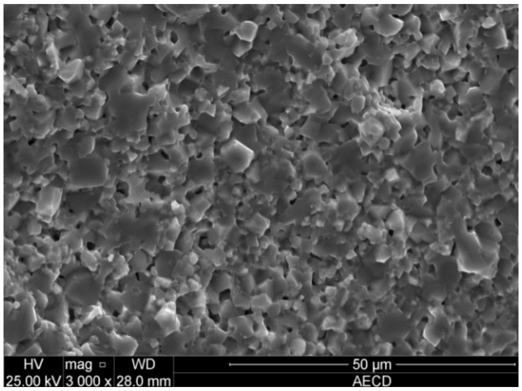

Figure 4.6 (b): Microstructure of $Mg_{1-x}Cu_xFe_2O_4$ sample sintered at 1200°C for x = 0.1

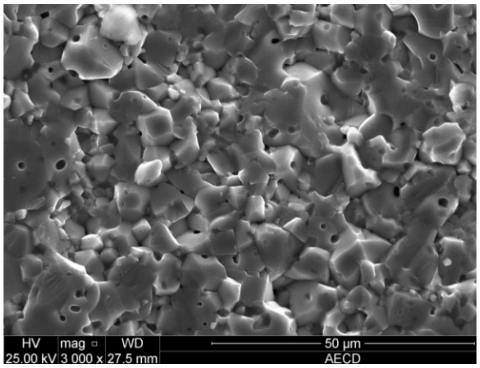

Figure 4.6 (c): Microstructure of $Mg_{1-x}Cu_xFe_2O_4$ sample sintered at 1200°C for x = 0.2

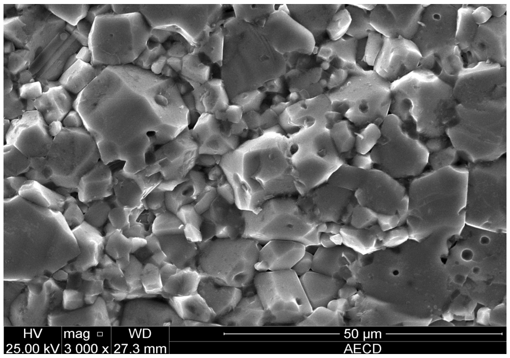

Figure 4.6 (d): Microstructure of $Mg_{1-x}Cu_xFe_2O_4$ sample sintered at 1200°C for x = 0.3

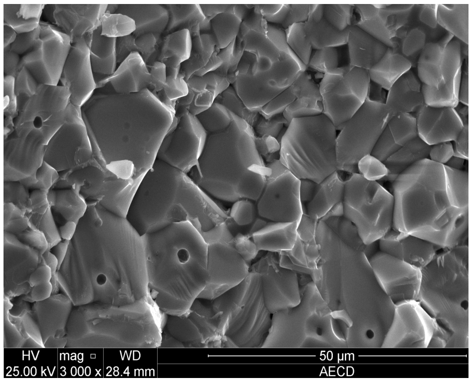

Figure 4.6 (e): Microstructure of $Mg_{1-x}Cu_xFe_2O_4$ sample sintered at 1200°C for x = 0.4

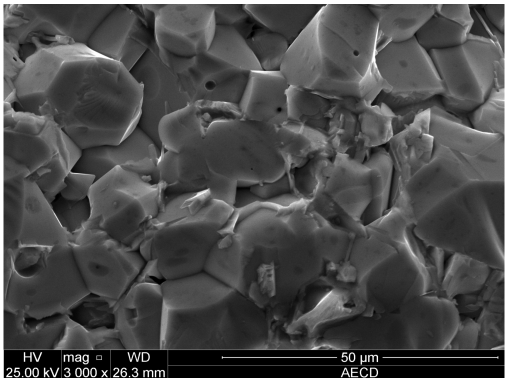

Figure 4.6 (f): Microstructure of $Mg_{1-x}Cu_xFe_2O_4$ sample sintered at 1200°C for x = 0.5

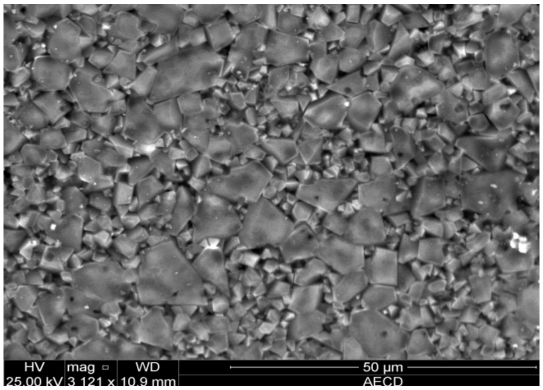

Figure 4.7 (a): Microstructure of $Mg_{1-x}Cu_xFe_2O_4$ sample sintered at 1200°C (surface) for x = 0.0

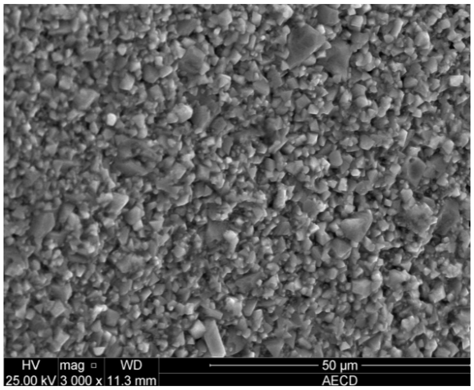

Figure 4.7 (b): Microstructure of $Mg_{1-x}Cu_xFe_2O_4$ sample sintered at 1200°C (surface) for x = 0.1

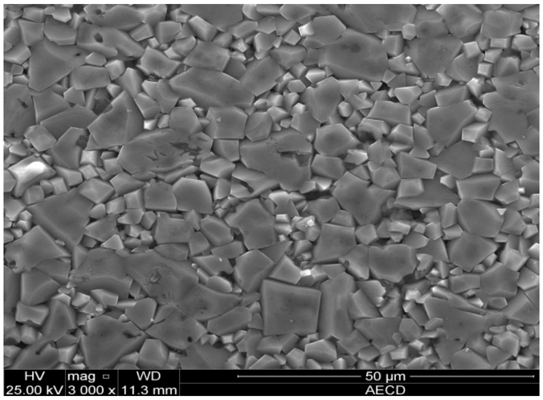

Figure 4.7 (c): Microstructure of $Mg_{1-x}Cu_xFe_2O_4$ sample sintered at 1200°C (surface) for x = 0.2

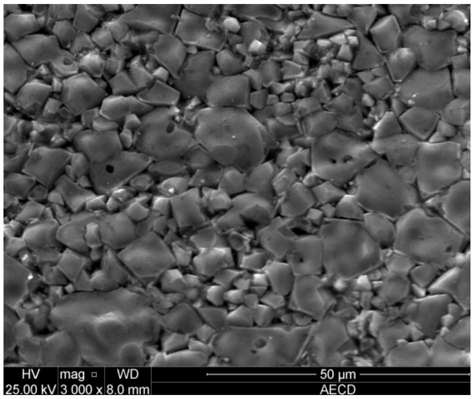

Figure 4.7 (d): Microstructure of $Mg_{1-x}Cu_xFe_2O_4$ sample sintered at 1200°C (surface) for x = 0.3

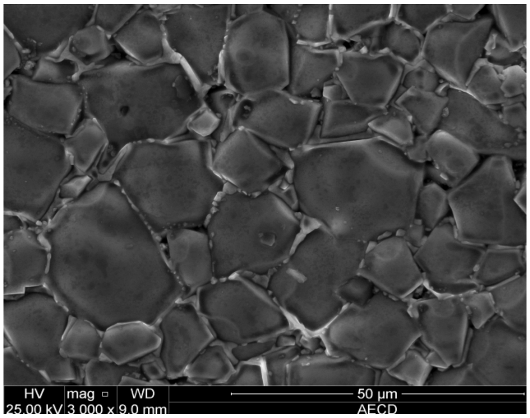

Figure 4.7 (e): Microstructure of $Mg_{1-x}Cu_xFe_2O_4$ sample sintered at 1200°C (surface) for x = 0.4

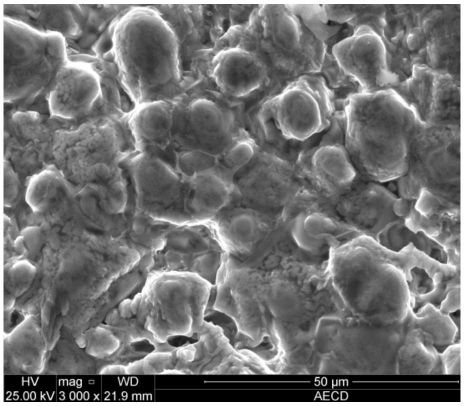

Figure 4.7 (f): Microstructure of $Mg_{1-x}Cu_xFe_2O_4$ sample sintered at 1200°C (surface) for x = 0.5

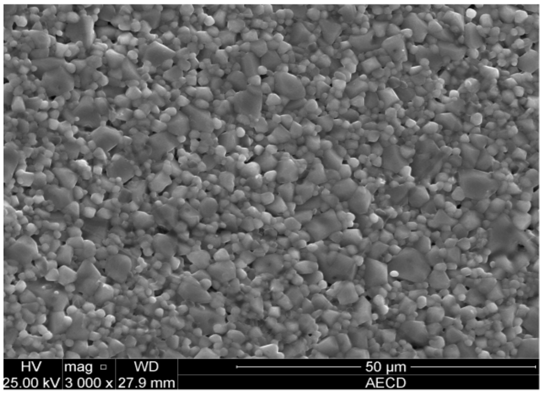

Figure 4.8 (a): Microstructure of $Mg_{1-x}Cu_xFe_2O_4$ sample sintered at 1200°C (quenched) for x = 0.0

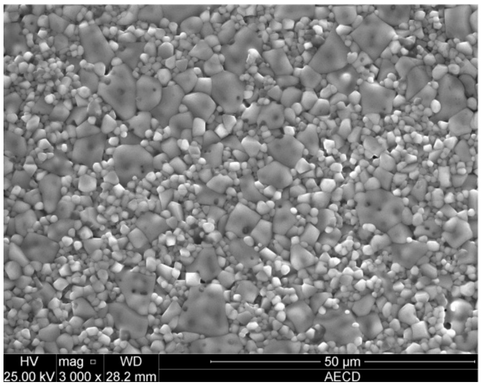

Figure 4.8 (b): Microstructure of $Mg_{1-x}Cu_xFe_2O_4$ sample sintered at 1200°C (quenched) for x = 0.1

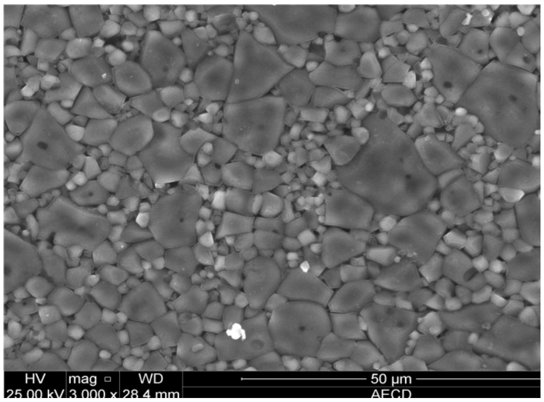

Figure 4.8 (c): Microstructure of $Mg_{1-x}Cu_xFe_2O_4$ sample sintered at 1200°C (quenched) for x = 0.2

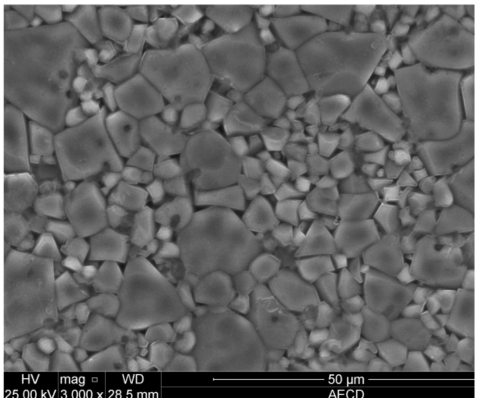

Figure 4.8 (a): Microstructure of $Mg_{1-x}Cu_xFe_2O_4$ sample sintered at 1200°C (quenched) for x = 0.3

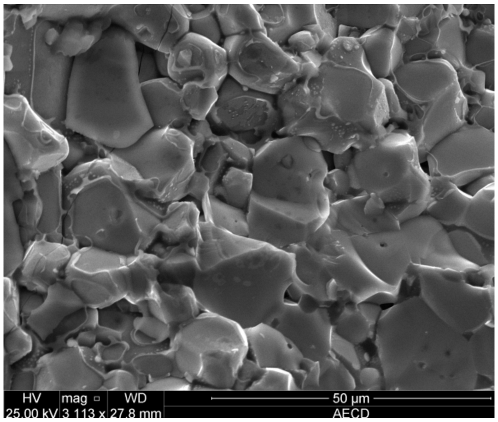

Figure 4.8 (c): Microstructure of $Mg_{1-x}Cu_xFe_2O_4$ sample sintered at 1200°C (quenched) for x = 0.4

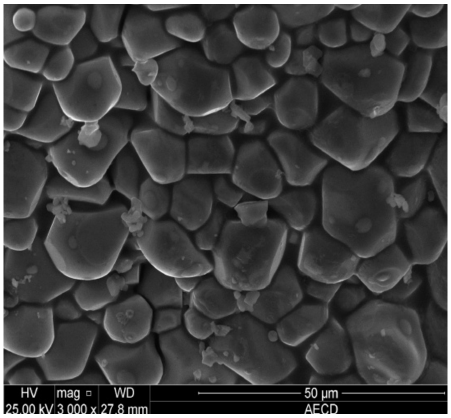

Figure 4.8 (c): Microstructure of $Mg_{1-x}Cu_xFe_2O_4$ sample sintered at 1200°C (quenched) for x = 0.5

The driving force for grain growth is the surface tension of grain boundaries [4.7]. Considerable amount of pores can be seen in the microstructure sample sintered at 1200°C for x = 0.0. It is observed that an increase in the amount of cu content result in an increase in the coverage of the grains by the liquid –phase layers and this is beneficial to grain growth. As a result, the average grain size increases with increasing of concentration of Cu content with the exception at x = 0.1 which might be attributed to experimental errors.

It is seen from figure that the sample without copper shows a homogeneous microstructure with small grain size and a uniform size distribution. A gradual increase in grain size distribution is observed with increased Cu content. Considerable increase in grain size with sample x = 0.2, 0.3, 0.4 and 0.5 shows the onset of uniform grain growth sintered at 1200°C. Figure 4.8 shows the increase in grain size with quenched sintering temperature 1200°C is clearly visible.

The grain growth in the samples with higher copper content has remarkably enhanced, giving rise to a microstructure with exaggerated grain growth which accelerates as sintering temperature. The rapid grain growth may be due to the formation of larger amount of liquid phase in the Mg-Cu ferrites. The migration of the pores to the grain boundary and hence contributed to the reduction of the sintered density. From figure 4.6 to figure 4.8 shows the grain sizes markedly increased with the Cu content and sintered with the Cu content and sintered 1200°C, 1200°C (surface) and 1200°C (quenched) respectively. It is clear visible from the micrographs that the dense microstructure are obtained higher context Cu for x = 0.4 and x=0.5 o0f 1200°C (quenched) $Mg_{1-x}Cu_xFe_2O_4$ ferrites.

4.3 Variation of Saturation Magnetization at Room Temperature at Different Sintering Temperature

The magnetic properties measured by Vibration Sample Magnetometer (VSM) at room temperature $Mg_{1-x}Cu_xFe_2O_4$ (x = 0.0, 0.1, 0.2, 0.3, 0.4 & 0.5) ferrites sintered at 1100°C, 1200°C and 1200°C (quenched) for 3 hours. The room temperature magnetic hysteresis (M - H) loop of the samples has been measured and is presented in figure 4.9 to figure 4.11. The hysteresis loops show a little hysteresis effect. No sample exhibited a coercively value indicating that all the samples belong to the family of soft ferrites. It is observed that saturation magnetization are saturated with an applied field of around 5kOe of all sintered and sintered (quenched) temperature. Figure 4.9 and Figure 4.10 shows the variation of saturation magnetization (M_s) of $Mg_{1-x}Cu_xFe_2O_4$ ferrites as a function of Cu content. It is observed from the figure that virgin nearly same as saturation magnetization up to x = 0.4 at sintering temperature at 1100°C and M_s-up to x = 0.3 at constant sintering temperature 1200°and then if increases with increasing Cu content of $Mg_{1-x}Cu_xFe_2O_4$ ferrites. The observed variation in saturation magnetization can be explained on the basis of cation distribution and the exchange interactions between A and B sites respectively. The increase in M_s with increased Cu-content is due to the increase of resultant sublattice magnetic moment, which can be explained on the basis of Neel's two sub lattice model. Neel [4.9] considered three types of exchange interactions between unpaired electrons of two ions lying in A and B sites.

In perfect ferrites, the A-A, B-B and A-B nearest neighbor exchange coupling are normally antiferromagnetic and the A-B exchange coupling is usually heavily predominant. Therefore, the spins at the A-sites will be anti parallel to the spins at B-sites below a transition temperature (called Curie temperature). The net magnetization is therefore the different between the magnetic moments of B and A sublattice, i.e. $M = M_B - M_A$ and will normally be parallel to the B-sublattice magnetization because the number of cation on B-sites is twice the number of cation on A-sites. The magnetization of each composition depends on the distribution of Fe^{3+} ions between two sub lattices A and B, where the Mg^{2+} and Cu^{2+} ions are nonmagnetic. When B-B or A-A interaction is dominant, Neel found that the above transition will not take place, and he concluded that the substance remains paramagnetic down to the lowest temperature. But Yatel and Kittel [4.10] claimed that there exists kind of strong magnetic ordering at low temperature. They formulated this discrepancy in the Neel's theory by non collinear model of ferrimagnetism.

It is seen from the figure 4.11 that the value of M_s gradually increases with increasing Cu-content, becomes maximum for x = 0.3 and then remains constant except x = 0.4 of $Mg_{1-x}Cu_xFe_2O_4$ ferrites at sintering temperature 1200°C (quenched). The porosity is minimum of the sample $Mg_{1-x}Cu_xFe_2O_4$ shown in Table - 4.1 x = 0.4 which might be attributed to experimental error.

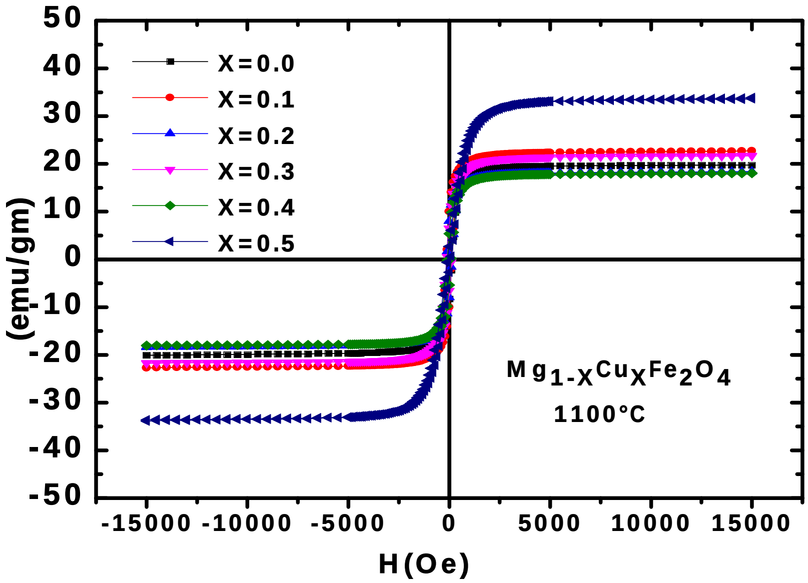

Figure 4.9: The magnetization (M_S) versus the applied magnetic field (H) curves of $Mg_{1-x}Cu_xFe_2O_4$ ferrites sintered at 1100°C for 3 hours.

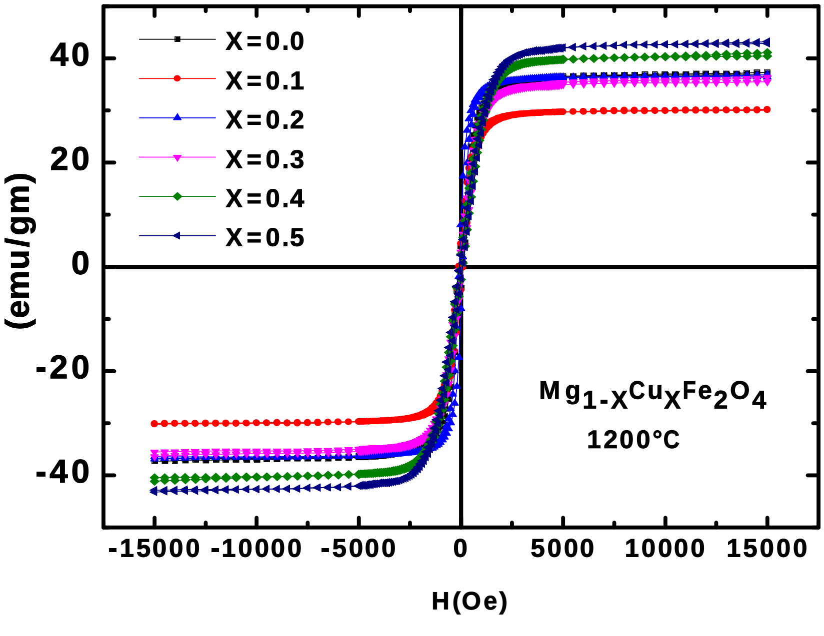

Figure 4.10: The magnetization (M_S) versus the applied magnetic field (H) curves of $Mg_{1-x}Cu_xFe_2O_4$ ferrites sintered at 1200°C for 3 hours.

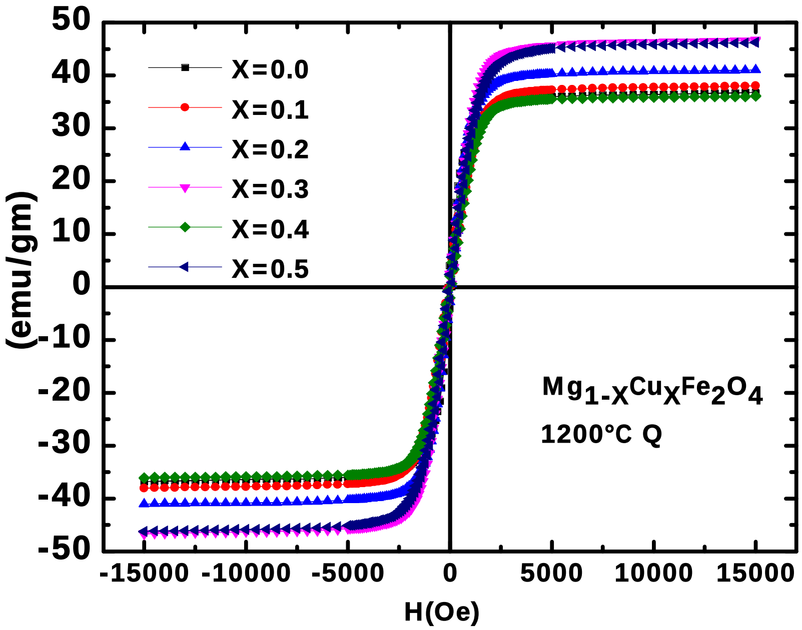

Figure 4.11: The magnetization (M_S) versus the applied magnetic field (H) curves of $Mg_{1-x}Cu_xFe_2O_4$ ferrites sintered at 1200°C (quenched) for 3 hours.

From the cation distribution, it is clear that Cu replaces the magnetic ions Fe^{3+} from A-site to B-site but the difference between the A and B site moments increase; as a result, M_s increases initially. The steady in the magnetization after $x > 0.3$ indicates the possibility of a non-collinear spin canting effect in the quenched sample [4.11-4.12]. The saturation magnetizations (M_S) of the $Mg_{1-x}Cu_xFe_2O_4$ ferrites as a function of Cu content at room temperature for different sintering temperature are shown in Figure 4.12 and Table-4.2. The magnetization behavior cannot be explained by Neel's two sublattice model due to presence of spin canting on B-sites, which increases of B-B interaction and consequently decreasing the A-B interaction. Hence the present system of ferrites, frustration and randomness increases as Fe- content increases in the Mg-Cu ferrites and shows significant departure from Neel's collinear model.

Table 4.2: Data of saturation Magnetization (M_S) for different sintering temperature

Atom fraction of Cu X=	1100°C	1200°C	1200°C Q
0.0	20.09	37.28	36.77
0.1	22.73	30.22	38.10
0.2	18.44	36.88	41.10
0.3	21.79	36.41	46.80
0.4	18.10	41.14	36.20
0.5	33.90	43.23	46.30

Table 4.2 gives the summary of M_S for different sintering temperature for Mg-Cu ferrites. For samples sintered at 1100°C, the M_S increases with increases of Cu-contents which is the samples sintering temperature increases. The increase of density lower porosity and as a consequence lowers the internal shape anisotropy, which leads to the increase of permeability [4.13]. The rotation of magnetization becomes easier in the less porous specimen.

4.4 Experimental Results and Analysis of Mössbauer for Mg-Cu Ferrites

Mössbauer spectroscopy is used for the identification of magnetic field distribution of magnetic atoms in Mg-Cu ferrites. Structural and magnetic changes in $Mg_{1-x}Cu_xFe_2O_4$ as induced by high energy hand milling were investigated by Mössbauer spectroscopy. The as-prepared powder displays sharp peaks expected for well crystallized cubic spinal. The continuous improvement of computation capabilities for spectral analysis and the introduction of sophisticated software for the treatment of Mössbauer data have enabled researchers to obtain rise and valuable information from the Mössbauer experiments as well as to study the structure of with higher accuracy and from complementary points of view. In the absence of Magnetic order, Mössbauer spectra from Fe ions on either A- or B- sites of spinel would show one or a set of doublets with particular values of isomer shift and quadruple splitting. On the other hand magnetically ordered Fe ions would yield sextants of six absorptions lines each, reflecting hyperfine magnetic splitting. The line widths are often sensitive sample crystallinity and compositional effect.

In the case of ^{57}Fe there is magnetic field acting at ^{57}Fe nuclei. This causes the upper level to split to two levels. Using the selection rule $\Delta m = 0, \pm 1$ for transitions to occur, we get six possible transition. In order to match the source energy to each of six different velocity of the source. This is automatically achieved in constant acceleration mode. Room temperature Mössbauer spectra, typical of Mg-Cu ferrites, are obtained and changes in the spectra corresponding to the different compositions of the system $Mg_{1-x}Cu_xFe_2O_4$ (x = 0.0, 0.1, 0.2, 0.3, 0.4 & 0.5) ferrites are sintered at 1100°C, 1200°C and 1200°C (quenched) are shown in figure 4.12 (a, b, c, d, e, z &f), figure 4.13(a, b, c, d & f) and figure 4.14 (a, b, c, d & f) respectively. The fitting of spectral lines were preformed assuming Lorentzian absorption line shapes using the Mössbauer spectral fitting software WMOSS by web research. In which allows for fitting to continuous distribution. In the figures shown below, the outer sextets corresponds to Fe^{3+} ions in octahedral position and the inner sextets corresponds to Fe^{3+} ions in tetrahedral position. The sextet pattern arises due to the interaction of γ-ray with the magnetic field of the sample. The appearance of sextet indicates presence of internal magnetic fields which is on significant characteristic of ferromagnetic materials. The spectral parameters such as isomer shift (δ) quadruple splitting (ΔE_q) and hyperfine field (H_{hf}) are computed and summarized in Table 4.3, Table 4.4 & Table 4.5 are shown sintered Temperature 1100°C, 1200°C & 1200°C (quenched) respectively.

The columbic interaction after the energy separation between the ground state and the excited state of the nuclei, thereby causing a slight shift in the position of the observed centroid of the spectrum, which are different for various Mg-Cu ferrites with different compositions give rise to isomer shifts. The isomer shifts in these table are quoted relative to metallic iron at room temperature. The δ's given relative to the centroid of these spectrum are shown in Table 4.3, Table 4.4 and Table 4.5. The δ's of the Fe atom in Mg-Cu ferrites with composition $Mg_{1-x}Cu_xFe_2O_4$ are observed to be range 0.217 to 0.369 mm/s sintered at 1100°C, 0.260 to 0.459 mm/s sintered at 1200°C and 0.251 to 0.378 mm/s sintered at 1200°C (quenched), indicting the isomer shift values for all samples are typical of the high spin Fe^{3+} ions [4.13] small effect on the isomer shifts values which indicates that the S-electron change distribution of the Fe^{3+} ions change with Cu substituting.

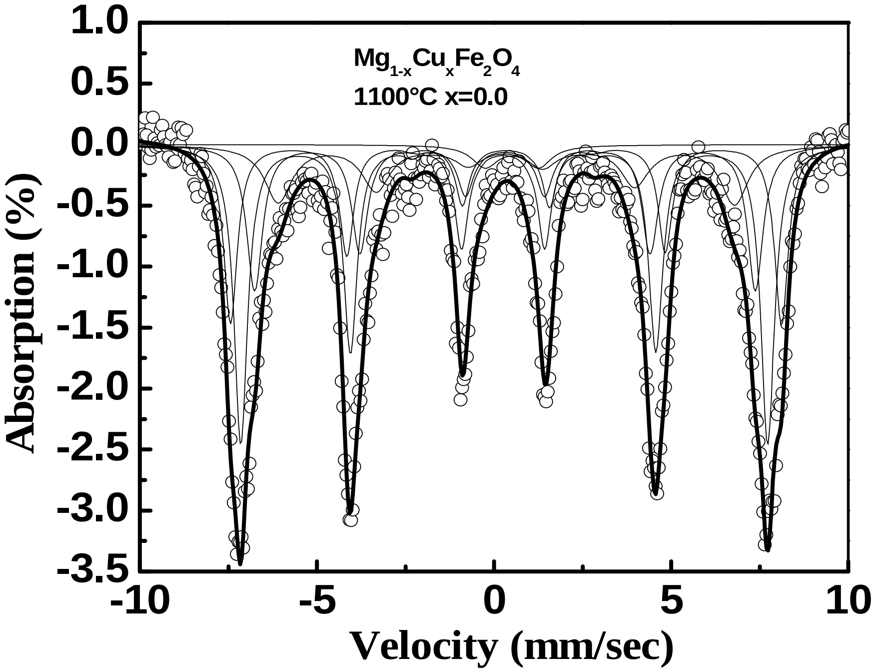

Figure 4.12 (a) Mössbauer spectra of $Mg_{1-x}Cu_xFe_2O_4$ for x = 0.0 sintered at 1100°C

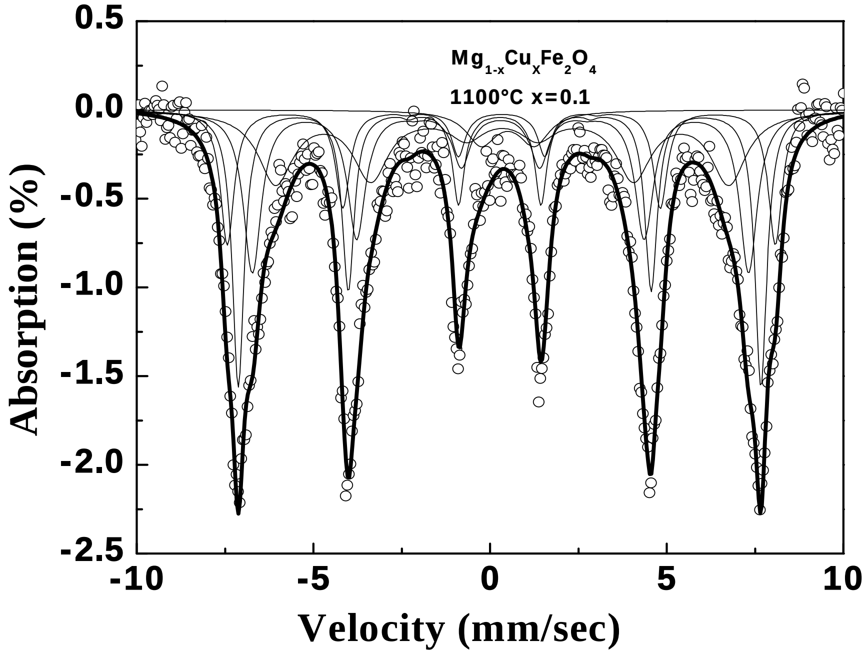

Figure 4.12 (b) Mössbauer spectra of $Mg_{1-x}Cu_xFe_2O_4$ for x = 0.1 sintered at 1100°C

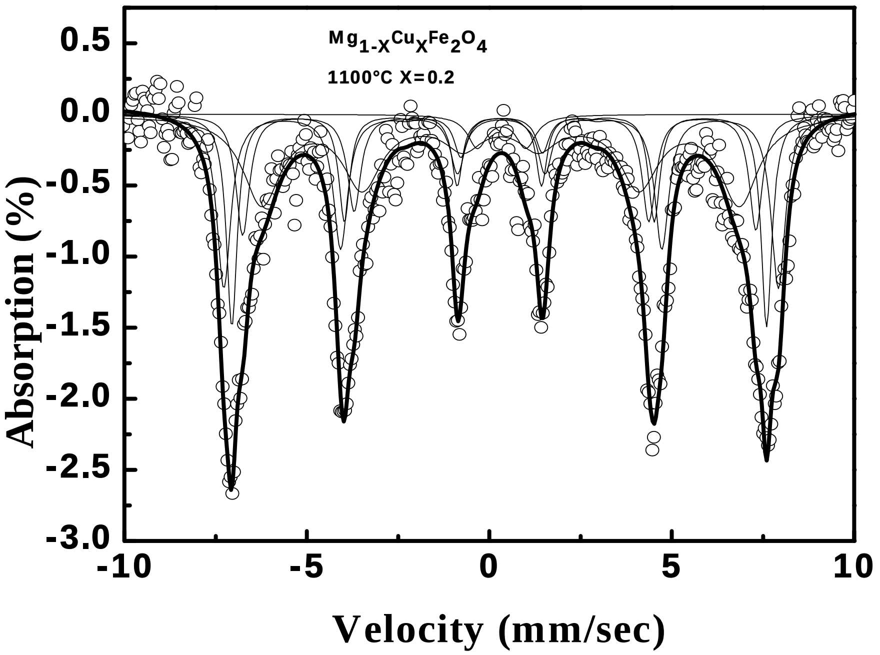

Figure 4.12 (c) Mössbauer spectra of $Mg_{1-x}Cu_xFe_2O_4$ for x = 0.2 sintered at 1100°C

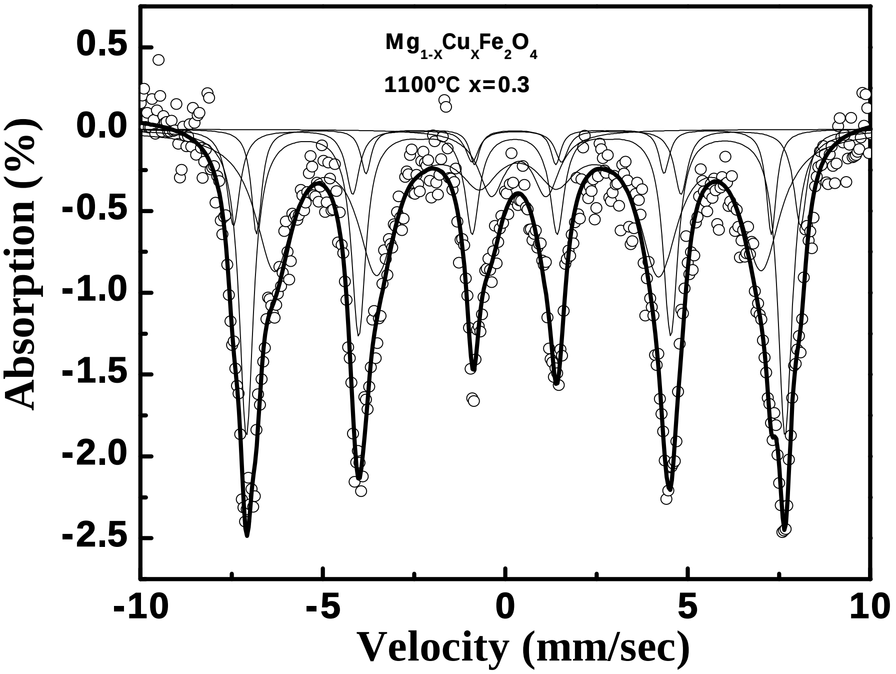

Figure 4.12 (d) Mössbauer spectra of $Mg_{1-x}Cu_xFe_2O_4$ for x = 0.3 sintered at 1100°C

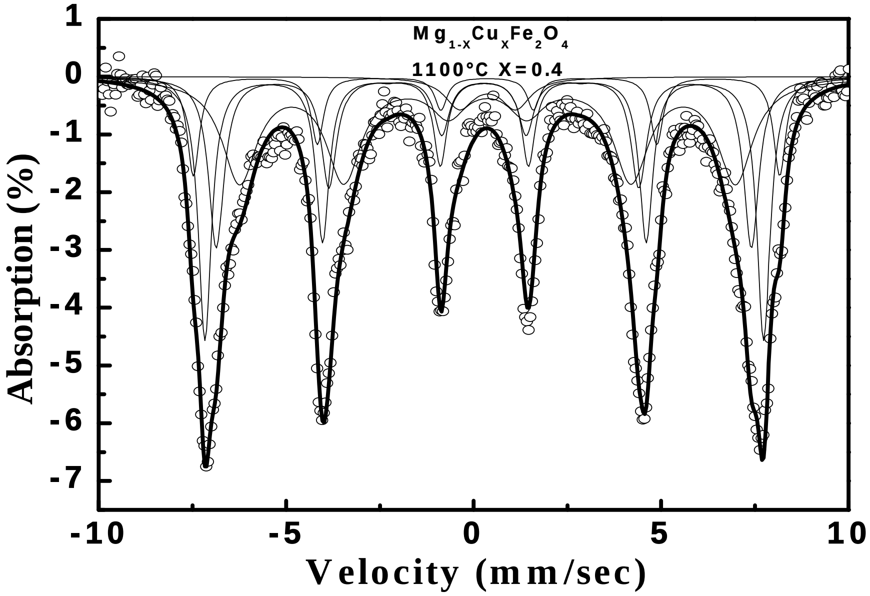

Figure 4.12 (e) Mössbauer spectra of $Mg_{1-x}Cu_xFe_2O_4$ for x = 0.4 sintered at 1100°C

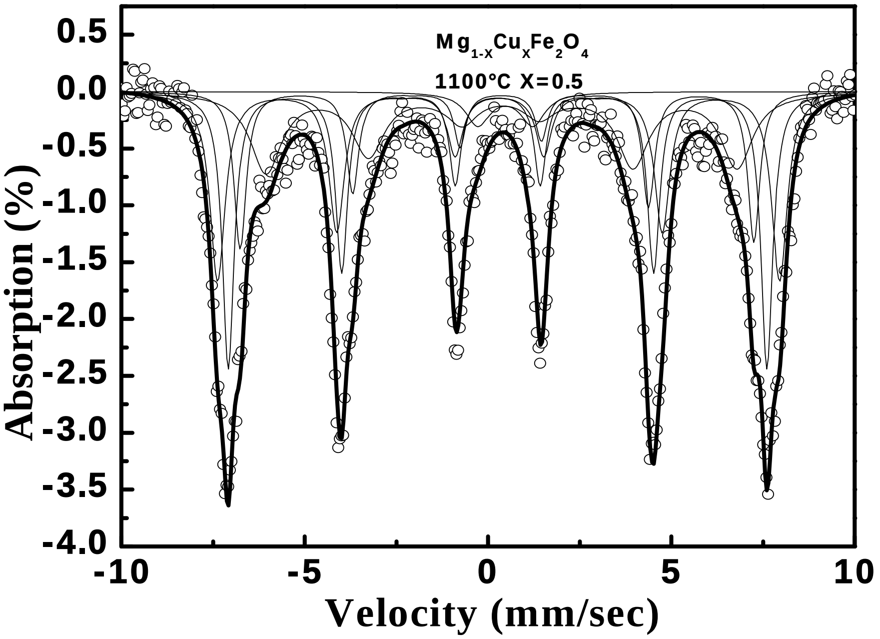

Figure 4.12 (f) Mössbauer spectra of $Mg_{1-x}Cu_xFe_2O_4$ for x = 0.5 sintered at 1100°C

Figure 4.12 (a, b, c, d, e, f) Room temperature Mössbauer spectra of $Mg_{1-x}Cu_xFe_2O_4$ (x = 0.0, 0.1, 0.2, 0.3, 0.4, 0.5) ferrites sintered at 1100°C for 3 hours.

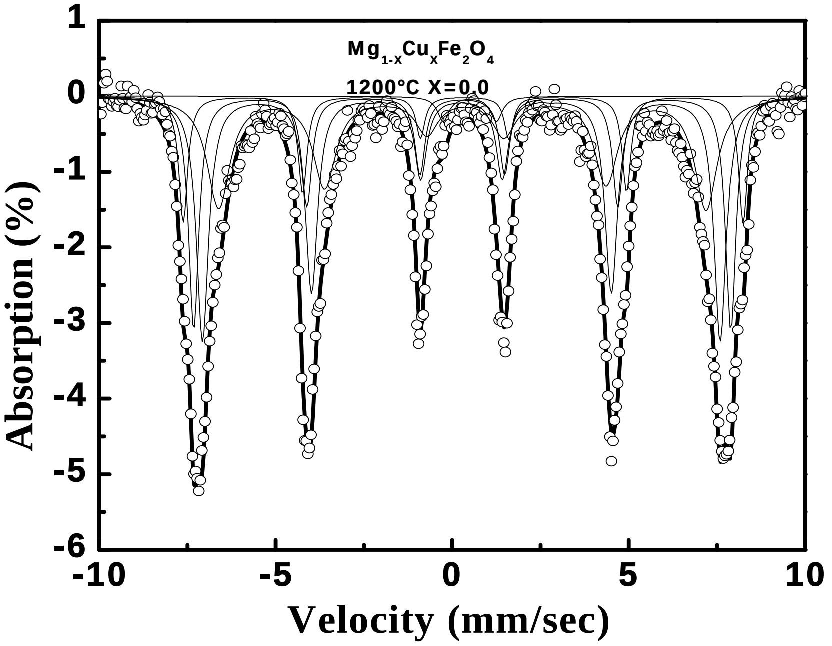

Figure 4.13 (a) Mössbauer spectra of $Mg_{1-x}Cu_xFe_2O_4$ for x = 0.0 sintered at 1200°C

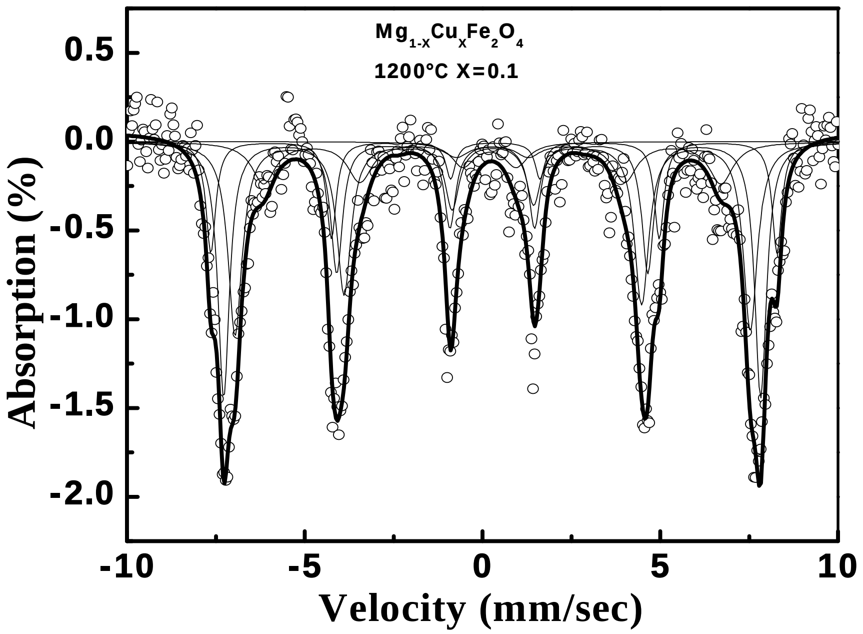

Figure 4.13 (b) Mössbauer spectra of $Mg_{1-x}Cu_xFe_2O_4$ for x = 0.1 sintered at 1200°C

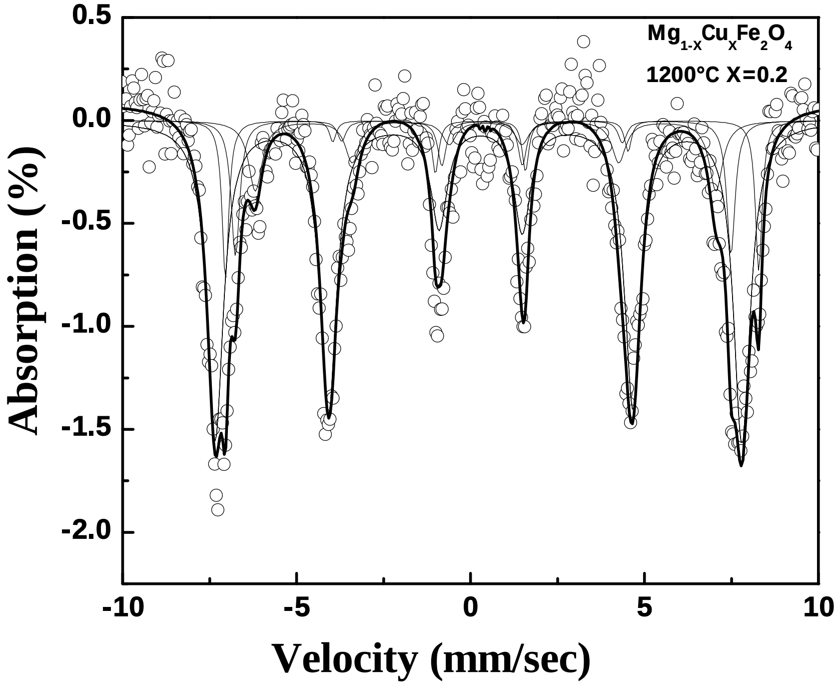

Figure 4.13 (c) Mössbauer spectra of $Mg_{1-x}Cu_xFe_2O_4$ for x = 0.2 sintered at 1200°C

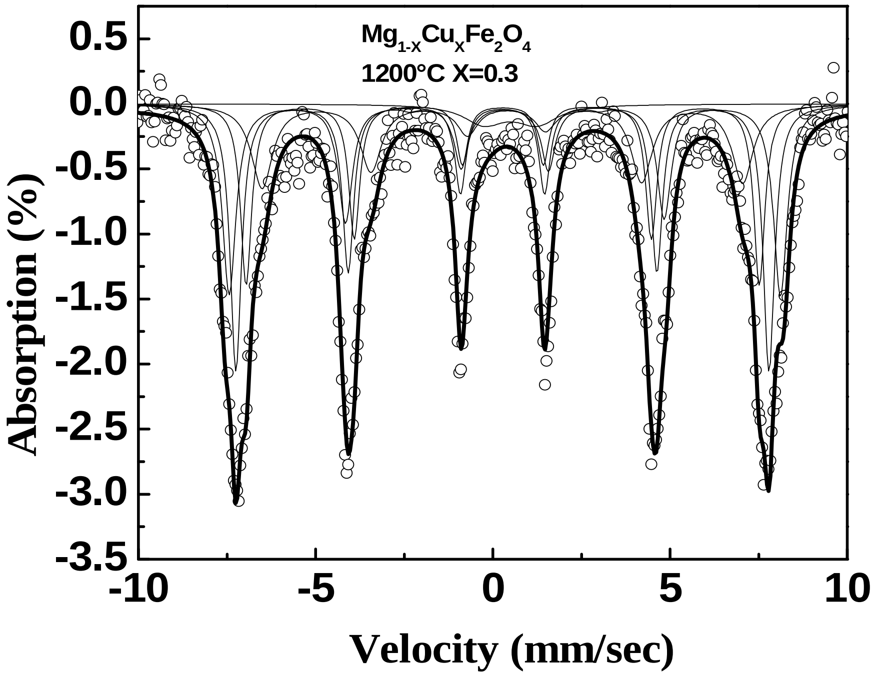

Figure 4.13 (d) Mössbauer spectra of $Mg_{1-x}Cu_xFe_2O_4$ for x = 0.3 sintered at 1200°C

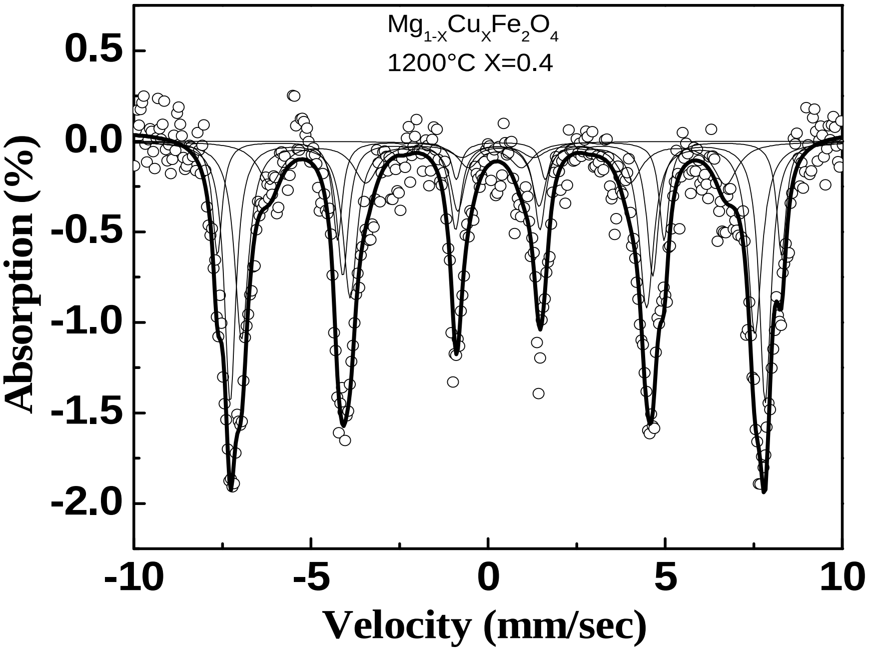

Figure 4.13 (e) Mössbauer spectra of $Mg_{1-x}Cu_xFe_2O_4$ for x = 0.4 sintered at 1200°C

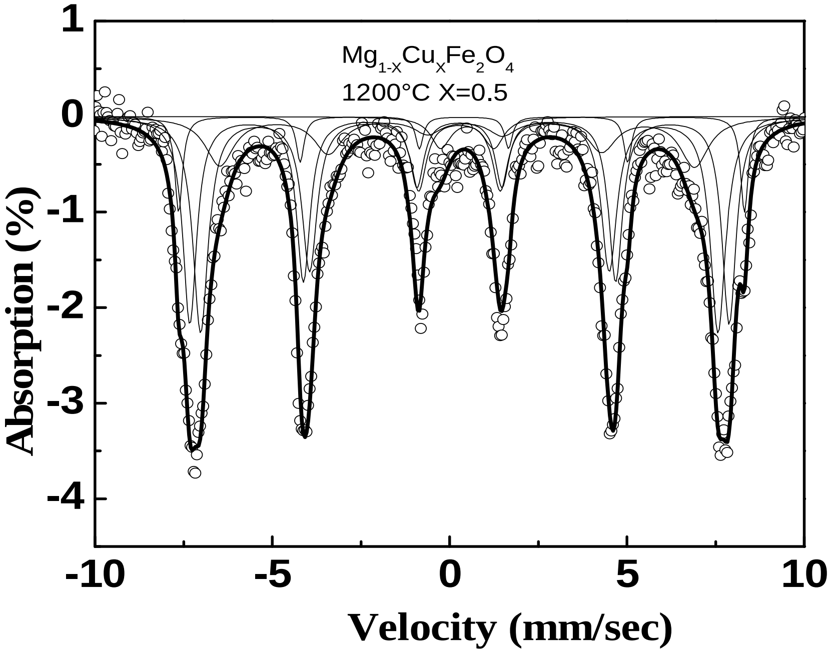

Figure 4.13 (f) Mössbauer spectra of $Mg_{1-x}Cu_xFe_2O_4$ for x = 0.5 sintered at 1200°C.

Figure 4.13 (a, b, c, d, e, f) Room temperature Mössbauer spectra of $Mg_{1-x}Cu_xFe_2O_4$ (x = 0.0, 0.1, 0.2, 0.3, 0.4, 0.5) ferrites sintered at 1200°C for 3 hours.

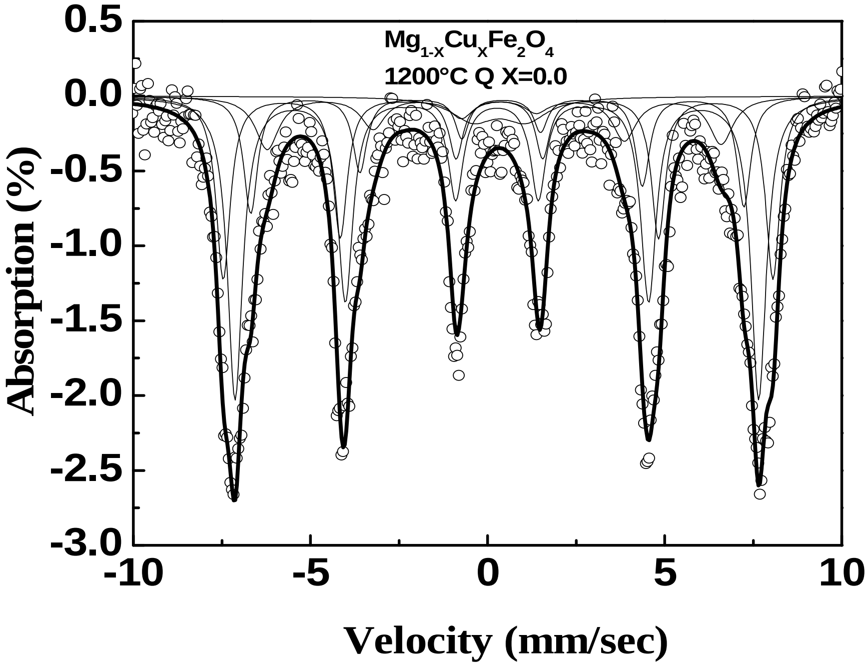

Figure 4.14 (a) Mössbauer spectra of $Mg_{1-x}Cu_xFe_2O_4$ for x = 0.0 sintered at 1200°C (quenched).

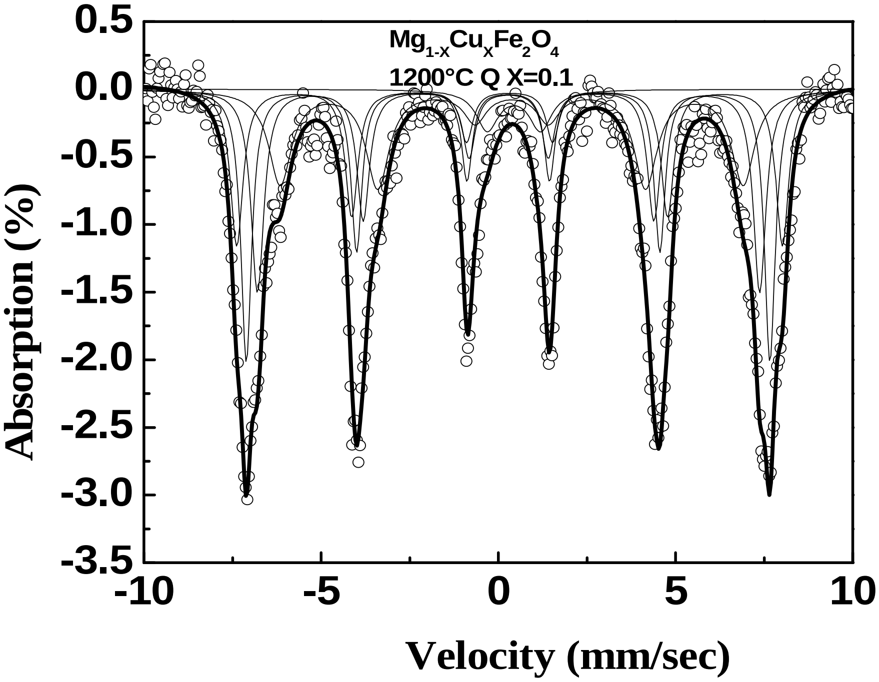

Figure 4.14 (b) Mössbauer spectra of $Mg_{1-x}Cu_xFe_2O_4$ for x = 0.1 sintered at 1200°C (quenched).

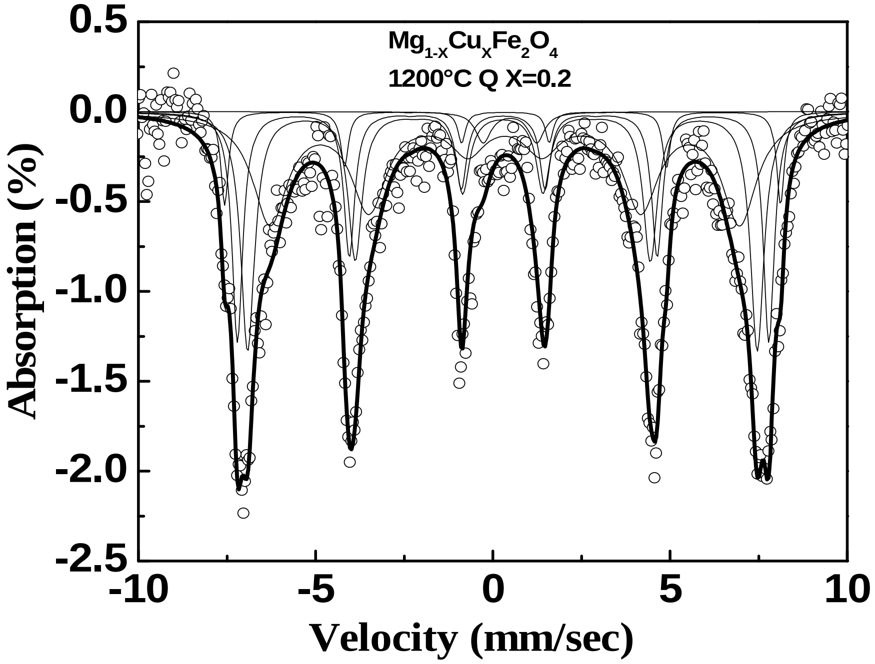

Figure 4.14 (c) Mössbauer spectra of $Mg_{1-x}Cu_xFe_2O_4$ for x = 0.2 sintered at 1200°C (quenched).

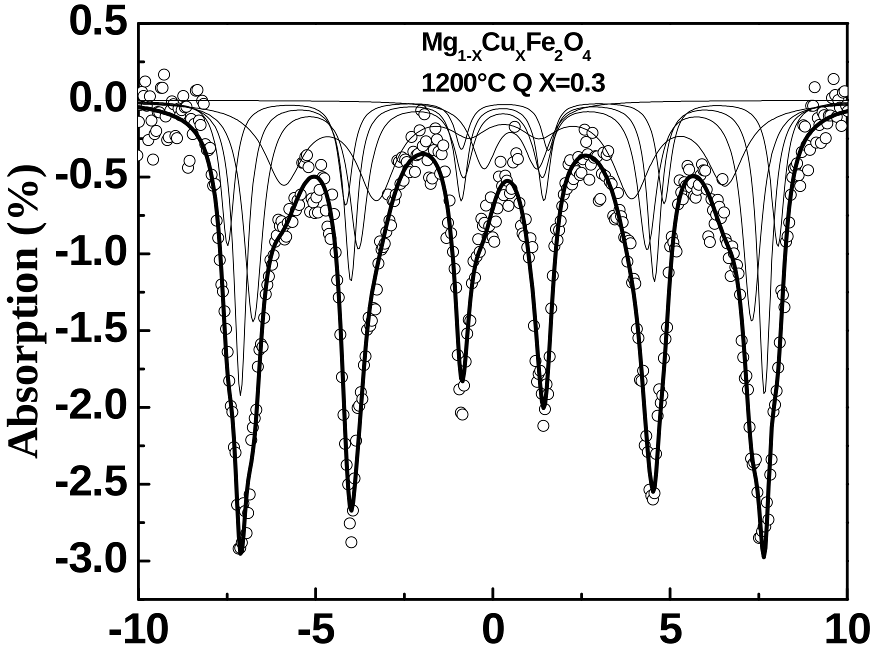

Figure 4.14 (d) Mössbauer spectra of $Mg_{1-x}Cu_xFe_2O_4$ for x = 0.3 sintered at 1200°C (quenched).

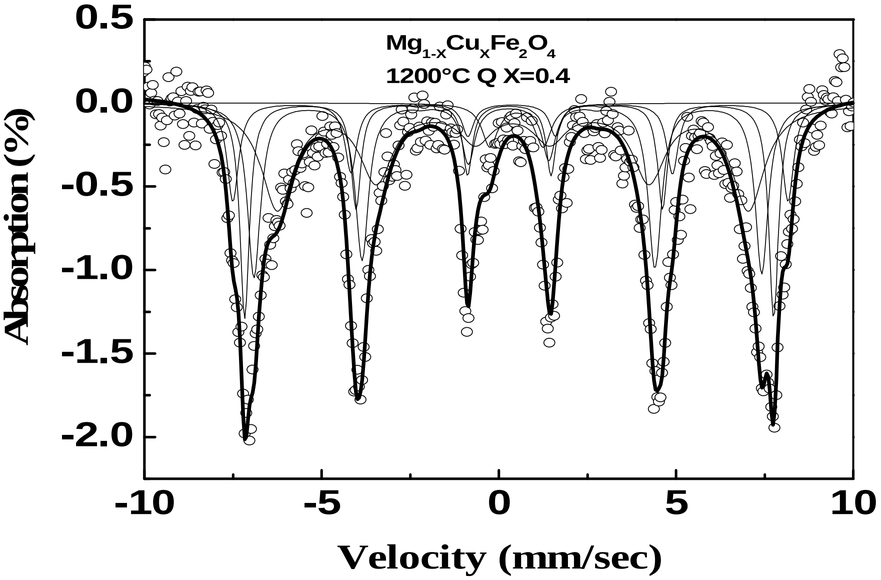

Figure 4.14 (e) Mössbauer spectra of $Mg_{1-x}Cu_xFe_2O_4$ for x = 0.4 sintered at 1200°C (quenched).

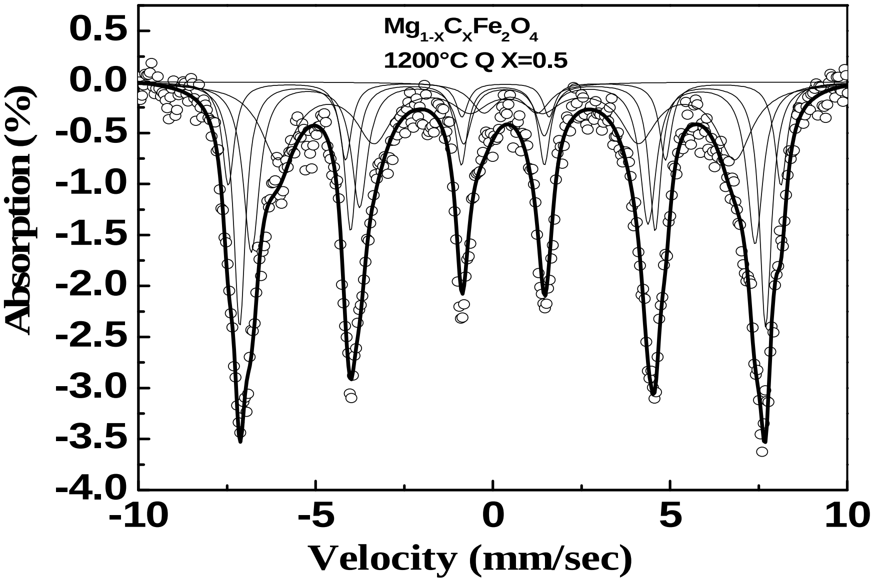

Figure 4.14 (f) Mössbauer spectra of $Mg_{1-x}Cu_xFe_2O_4$ for x = 0.5 sintered at 1200°C (quenched).

Figure 4.14 (a, b, c, d, e, f) Room temperature Mössbauer spectra of $Mg_{1-x}Cu_xFe_2O_4$ (x = 0.0, 0.1, 0.2, 0.3, 0.4, 0.5) ferrites sintered at 1200°C (quenched) for 3 hours.

Table 4.3: Hyperfine parameters of Mossbauer spectroscopy at room temperature without any applied field sintered at 1100°C for 3 hrs.

Concentration	Site Occupancy	Isomer Shift (δ) mm/sec	Quadruple splitting (ΔE_q) mm/sec	Hyperfine field (H_{int}) kG	Rel. Area
X = 0.0	B	0.336	0.389	-483.68	0.247
	B	0.272	0.037	-463.163	0.424
	A	0.309	0.000	-440.175	0.244
	A	0.334	0.987	-396.468	0.169
X = 0.1	B	0.320	0.0295	-482.885	0.175
	B	0.272	0.000	-460.646	0.298
	A	0.343	0.000	-399.296	0.254
	A	0.294	0.000	-437.315	0.276
X = 0.2	B	0.324	0.005	-473.188	0.287
	B	0.274	0.000	-456.313	0.233
	A	0.308	0.000	-407.409	0.385
	A	0.306	0.691	-435.965	0.191
X = 0.3	B	0.316	0.002	-483.793	0.114
	B	0.217	0.032	-459.678	0.383
	A	0.253	0.096	-439.262	0.0823
	A	0.342	0.161	-415.333	0.514
X = 0.4	B	0.351	0.039	-486.916	0.108
	B	0.286	0.000	-463.982	0.301
	A	0.369	0.000	-411.785	0.362
	A	0.274	0.000	-444.38	0.228
X = 0.5	B	0.299	0.048	-477.263	0.287
	B	0.263	0.000	-457.417	0.310
	A	0.357	1.118	-393.894	0.254
	A	0.295	0.615	-434.751	0.180

Table 4.4: Hyperfine parameters of Mossbauer spectroscopy at room temperature without any applied field sintered at 1200°C for 3 hrs.

Concentration	Site Occupancy	Isomer Shift (δ) mm/sec	Quadruple splitting (ΔE_q) mm/sec	Hyperfine field (H_{int}) kG	Rel. Area
X = 0.0	B	0.330	0.232	-493.583	0.135
	B	0.286	0.000	-473.591	0.246
	A	0.330	0.431	-429.129	0.303
	A	0.262	0.000	-456.518	0.363
X = 0.1	B	0.383	0.362	-479.924	0.000
	B	0.428	1.152	-475.169	0.000
	A	0.459	0.444	-450.737	-0.0283
	A	0.273	0.433	-363.255	0.000
X = 0.2	B	0.452	1.499	-468.198	0.119
	B	0.260	0.293	-471.252	0.897
	A	0.349	1.037	-438.897	0.129
	A	0.434	0.000	-412.217	0.142
X = 0.3	B	0.323	0.009	-490.436	0.222
	B	0.272	0.000	-468.369	0.301
	A	0.324	1.216	-415.907	0.192
	A	0.282	0.000	-450.879	0.214
X = 0.4	B	0.339	0.080	-495.884	0.170
	B	0.273	0.000	-470.346	0.387
	A	0.276	0.000	-400.490	0.161
	A	0.291	0.388	-413.624	0.411
X = 0.5	B	0.369	0.138	-496.815	0.0787
	B	0.278	0.000	-473.511	0.355
	A	0.323	0.757	-414.853	0.164
	A	0.276	0.000	-454.298	0.395

Table 4.5: Hyperfine parameters of Mossbauer spectroscopy at room temperature without any applied field sintered at 1200°C (quenched) for 3 hrs.

Concentration	Site Occupancy	Isomer Shift (δ) mm/sec	Quadruple splitting (ΔE_q) mm/sec	Hyperfine field (H_{int}) kG	Rel. Area
X = 0.0	B	0.314	0.080	-483.181	0.254
	B	0.265	0.000	-460.30	0.428
	A	0.251	1.499	-389.011	0.116
	A	0.331	0.828	-430.809	0.152
X = 0.1	B	0.316	0.000	-479.369	0.224
	B	0.278	0.000	-460.032	0.297
	A	0.375	0.000	-406.684	0.265
	A	0.290	0.000	-441.204	0.267
X = 0.2	B	0.314	0.191	-488.309	0.0663
	B	0.291	0.000	-466.933	0.234
	A	0.337	0.000	-412.492	0.394
	A	0.277	0.020	-447.696	0.308
X = 0.3	B	0.308	0.202	-483.249	0.146
	B	0.274	0.000	-460.480	0.268
	A	0.321	0.269	-387.688	0.269
	A	0.27	0.020	-438.040	0.291
X = 0.4	B	0.344	0.090	-487.695	0.141
	B	0.294	0.000	-464.775	0.227
	A	0.265	0.462	-445.160	0.308
	A	0.393	0.008	- 413.646	0.414
X = 0.5	B	0.343	0.050	-485.470	0.141
	B	0.281	0.070	-462.075	0.306
	A	0.378	0.000	-401.219	0.288
	A	0.303	0.738	-440.170	0.303

Quadrupole splitting is the electric quadrupole interaction between the quadrupole moments of the nuclei and the electric field gradient at the nucleus due to the symmetric distribution change on the ions. This provides information on the nature chemical bonds. The ΔE_q of Fe atom in the ferrites with composition $Mg_{1-x}Cu_xFe_2O_4$ are observed in the range 0.00 to 1.118 mm/s sintered at 1100°C, 0.00 to 1.152mm/s sintered at 1200°C and 0.00 to 1.499 mm/s sintered at 1200°C (quenched) are shown in Table 4.3, Table 4.4 and Table 4.5 respectively. The observed trend of Mössbauer line wide and the average quadrupole splitting points to a gradual decrease to increase in structural disorder produce an appreciable broadening with increase of Cu-content. Quadrupole interaction has values close to zero for both A and B sites. As in the presence of a strong magnetic interaction the distribution of quadrupole interaction, which arise from chemical disorder of the individual Zeeman lines for both the octahedral and tetrahedral patterns, but does not produce observable quadrupole line shifts [4.14].

The general trend of decreasing the hyperfine fields value are shown in Table 4.3, Table 4.4 and Table 4.5, respectively presumably due to the weakening of A-B exchange interaction caused by the substitution of Cu^{2+} with the non-magnetic Mg^{2+} ions, which also results in a decrease of the Curie temperature. The Mössbauer phenomenon on and the hyperfine interactions have characteristic sintering temperature and the spectrum observed in any situation depends on whether the properties of nuclear environment or the position of the nucleus in changing sites.

Information on the cation distribution can be derived the area ratio of A and B sites to Mössbauer spectra. A difficult arises for samples having similar Mössbauer parameters A and B sites [4.15]. In order to improve the resolution Mössbauer measurements were carried out in a high external magnetic field. Spinel ferrite is known to have a collinear structure such that the B-site moments are oriented parallel and those at the A-site antiparallel to the external field direction. Since the internal field at the Fe nucleus is negative, the magnetic hyperfine splitting at the A-site increases with the applied field; while the B-site splitting decreases. Figure 4.11, figure 4.12 and figure 4.13 are shows Mössbauer spectra for the investigated samples are taken sintered at 1100°C, 1200°C and 1200°C (quenched) respectively, clearly detect a resolved splitting of the outer lines of the spectrum to the magnetic hyperfine field at the B-site. Increase intensity with respect to the B-site peak. This trend is consistent with the picture that the relative number of Fe^{3+} ions has changed. At sintering temperature the recoilless fractions for Fe ions on the A and B sites are essentially equal and therefore, the occupation numbers of the Fe ions can be considered proportional to the corresponding areas of their Mössbauer spectra. Consequently the relative numbers of Fe^{3+} ions in A and B site are determined from the ratios of the area under the two sublattices with respect to Cu-content.

The observed decrease in hyperfine field can possibly be explained by considering that substitution of Cu^{2+} ions in the system moves not only Fe^{2+}but also Mg^{2+} and or Cu^{2+} ions from B to A sites. This indirectly causes A sublattice dilution since Cu^{2+} and Mg^{2+} have a lesser magnetic moment than that of Fe^{3+} and contributes to an increase in the hyperfine field. It is well known that the internal hyperfine magnetic field at the Fe-nucleus is antiparallel to the atoms magnetic moment. Consequently, Fe ions with antiparallel moments contribute to the external peak and Fe ions with parallel moments contribute to the sextet corresponding to other peak.

The physical origin of this spin arrangement is from the canting of the spins in the B-sublattice due to weakening of the inter sublattice interaction J_{BB} on nonmagnetic Cu-substitution in the A-sublattice. As in the case of spinels, J_{BB} is antiferromagnetic, the B-sublattice splits into two sublattice forming Y-K angles between the directions of the spins resulting in a decrease of net B-sublattice magnetization. This happens because the replacement of large Fe^{3+}sites ions by smaller Cu^{2+} ions small reduce the influence of the internal hyperfine field at nearest Fe^{3+} through transferred hyperfine field.

CONCLUSION

5.1 Conclusion

The synthesis, characterization and detail study of structural, magnetic properties and Mössbauer spectroscopic analysis have been carried out on $Mg_{1-x}Cu_xFe_2O_4$ (where x = 0.0,0.1, 0.2, 0.3, 0.4 & 0.5) ferrites samples using conventional double sintering method, sintered at 1100°C, 1200°C and 1200°C (quenched) at 3 hours. The formation of single phase ferrite is confirmed by X-ray diffraction. The X-ray density of the sample sintered at 1100°C increases monotonically with increase of Cu-constants. The highest X-ray density is observed for x = 0.5 (ρ_x = 3.939 gm/cc) and the lowest density is observed for x=0.0 (ρ_x = 3.478 gm/cc). The bulk density (ρ_B) = increases with the increase of Cu contents ($x \leq 0.4$), the value of ρ_B decreases slightly afterward. The lower bulk density of the sintered samples may be attributed to inevitable existence of pores during the sample processing. The porosity of the sample $Mg_{1-x}Cu_xFe_2O_4$ sintered at 1100°C decreases with the increase of Cu contents up to values x = 0.4 which is 28.78% and the highest porosity is seen to occur when x = 0.0, The lattice parameter of these samples nearly same up to x = 0.4 and $x \geq 0.4$ is increases, since the ionic radii of Mg^{2+} and Cu^{2+} ions are 0.72Å and 0.73Å. The unit cell expands resulting in enhancement of lattice parameter that the distribution of cations on octahedral B-sites and tetrahedral A-sites of Mg-Cu ferrites. This enhancement of lattice parameter obviously expands the lattice resulting in decrease of the strength J_{AB} interaction.

The particle morphology of Mg-Cu ferrites sample sintered at 1100°C, 1200°C and 1200°C (quenched) has been investigated using scanning electron microscope (SEM). Throughout the study it has been observed that with the simultaneous addition of CuO remarkably increased the grain size as well as densities. During the investigation it has also been observed that sintering temperature has a significant effect on the microstructure of Mg-Cu ferrites. It is observed that an increase in the amount of Cu-content results in an increase in the coverage of the grains by liquid phase layers, and this is beneficial to grain growth. However, from the observation it may be expected clear visible from the micrograph that the dense microstructures are obtained higher content Cu of 1200°C quenched Mg-Cu ferrites.

Magnetization (emu/gm) has been measured using a VSM for all the samples. The value of saturation magnetization (M_S) increases with increasing Cu-content, becomes maximum for x = 0.5 and then remains constant. A large increase of M_S value for x = 0.5 compared with their base counterpart has been observed. This increase of magnetization was attributed to non-magnetic substitution of Cu^{2+} as a result of their preferential A-site occupancy and modification of cation distribution of Fe^{3+}. The M_S of each composition depends on the distribution of Fe^{3+} ions between two sublattice, A and B, where the Mg^{2+} and Cu^{2+} ions are non magnetic, where B-B or A-A interaction is dominant. Saturation M_S increases with increasing Cu-content with a value of M_S =36.77 emu/gm for x= 0.0 compared with M_S = 46.3 emu/gm for x = 0.5 at sintered temperature 1200°C quenched.

The Mössbauer spectra for the samples clearly show Lorentzian shaped lines in sextet broad distribution of magnetic hyperfine field (H_{hf}) is compared to pure 57_{Fe} foils. The formation of sextets indicated the $Mg_{1-x}Cu_xFe_2O_4$ ferrites are ferromagnetic. Mössbauer parameters such as isomer shift, quadruple splitting, hyperfine field and cation distribution at tetrahedral (A) and octahedral (B) sites were also determined. The isomer shifts of $Mg_{1-x}Cu_xFe_2O_4$ ferrites to the pure Fe standard are in the range 0.217 to 0.459 mm/s indicating the Fe^{3+} ions. The average magnetic H_{hf} of the Mg-Cu ferrites decrease due to the weakening of A-B exchange interaction caused by the substitution of non magnetic Mg^{2+} with Cu^{2+} ions, which also our observation the replacement of large Fe^{3+} sites through transferred hyperfine field. On the other hand, magnetically ordered Fe ions would yield sextets of six absorption line such each, reflecting hyperfine magnetic splitting. The line widths are often sensitive to sample crystallinity and sintering temperature. In a ferromagnetic order, all Fe ions with antiparallel moments reside on the A-sites, hence the areal fractions of the sextet provide reasonable estimate for the inversion parameter and the possibility of magnetization reversal on B-site. There are concurrent changes to the magnetic state and greater tendency of magnetization to stabilize at sintering temperatures. This behavior is consistent with a diluted exchange coupling between magnetic Fe-ions on the A and B- sites.

5.2 Scope for Future Work

With the development and advancement of ferrites a tremendous surge in research on miniaturization and high frequency electronic devices is taking place. For these efficient devices we need soft magnetic materials as its basic magnetic component. Soft ferrites materials are extensively used in inductor cores which form a basic requirement in modern technology. Mg-Cu ferrites are suitable for these devices for future. Fabrication and characterization of multilayer chip inductor using improved Mg-Cu ferrites is of high demand. Magnetic properties including zero field measurement, temperature variable Hall Effect, dielectric measurement should be developed in order to obtain a more reliable result of its performance in materials science and electronic application. Moreover, different compassion, sample forming techniques and sintering temperature should be future investigated in order to optimize all properties.

REFERENCE

CHPATER-I

[1.1] Culity B. D. and Graham C. D.; "Introduction to magnetic materials",2nd edition, A. Willey & Son Publication, U. S. A., 2009

[1.2] Hilpert S., Deutseh. Ber. Chem. Ges. BD2, 42, 2248,1909

[1.3] Snoek J. L.; "New developments in Ferromagnetism & Antiferromagnetism"; Annales de physique, 3, 137, 1948.

[1.4] Smith J. and Wijn H. P. J., "Ferrites", Wiley LONDON, p-140, 1959

[1.5] Meena khisun daram A., Gunaselcaran N., Srinivasan S.; Physics Status Solidi (a) 69, KIS, 1982.

[1.6] Akther Hossain A. K. M., Seki M., Kawai T., Tabata H.; J. Appl. Physics 96(2), 1273, 2004.

[1.7] Balayachi A., Dormann J. L. and Nogues M. "Critical analysis of magnetically semi disordered systems: Critical exponents at various transitions"; J. Phys.: Condens Matter. 10, 1599, 1998.

[1.8] Hakim M. A., Manjurul Haque M., Huq M., Manjura Hoque S. and Nordblad P.; " Reentrant spin glass and spin glass Behavior of Diluted Mg-Zn ferrites"; CP 1003, International Conference on Magnetic Materials, AIP, p-295, ICMM-2007.

[1.9] Martinho H., Moreno N. O., Sanjurijo J. A., Rettori W., Chaeong S. N.; Phys. Rev. B64, 024408, 2001.

[1.10] Raj A. M. E., Som T., Ganesan V., Jayachandran M., Selvan G., Swaminathan V., Sanjeeviraja C.; Nuclear Instruments and Methods in Physics Research B 266, 2564, 2008.

[1.11] Brabers V. A. M., Hirsch A. A., Vleuten W. C. V., Doremalen P. V.; IEEE Trans. Magn.14(5), 895, 1978.

[1.12] Mazen S. A., Rahiem A. E., Sabrah B. A.; J. Mat. Sci., 23, 2917, 1988.

[1.13] Liu. D. M.; J. Mat. Sci., 29, 1507, 1994.

[1.14] Naknao N., Nakahata I., Murse T.; J. Jpn. Soc. Powder Metall. 48(2), 131, 2001.

[1.15] Jain M., Majumder S. B., Katiyar R. S., Bhalla A. S.; Mat. Let. 57, 4232, 2003.

[1.16] Yue Z., Zhou J., L. Li, Wang X., Gui Z.; Mat. Sci. Engg. B86, 64, 2001.

[1.17] Rezlescu N., Rezlescu E., Popa P. D., Craus M. L., Rezlescu L.; J. Magn. Magn. Mater, 182, 199, 1998.

[1.18] Rezlescu E., Rezlescu N., Popa P. D., Rezlescu L., Pasnicu C., Craus M.L.; Mat. Res. Bull. 33(6), 915, 1998.

[1.19] Bhosale D. N., Sawant S. R., Gangal S. A., Mahajan R. R., Bakare P. P.; J. Magn. Magn. Mater. 173, 51, 1997.

[1.20] Bhosale D. N., Sawant S. R., Gangal S .A., Mahajan R. R., Bakare P. P.; Mat. Sci. Engg. B.65, 79, 1999.

[1.21] Hiti M. A. E.; J. Magn. Magn. Mater. 192, 305, 1999.

[1.22] Hoque S. M., Choudhury Md. A., Islam Md. F.; J. Magn. Magn. Mater. 251, 292, 2002.

[1.23] Haque M. M., Haq M., Hakim M. A.; Mat. Chem. Physics 112, 580, 2008.

[1.24] Banerjee D., Bachadur D., Suresla K. G., Nigam A. K.; Physica B, 378-380, 1091, 2006.

[1.25] Mahmoud M. H., Abdalls A. M., Hamdelv H. H., Hikal W. M., Tahar S. M., Ho J. C.; "Mössbauer Spectroscopic evaluation of high energy bull milled $CdFe_2O_4$"; J. Magn. Magn. Mater. 263, 269-274, 2003.

[1.26] Prup S. M., Topsoc B.; J. Appl. Phys. 11, 63, 1976.

[1.27] Daniels J. M., Rosencwaiy A.; Can. J. Phys. 48, 381, 1970.

[1.28] Srivastava J. K., Muralecdharam K., Vijatarghavan R.; Phys, Left 24, 482, 1984.

[1.29] Sattar A. A., Wafix A. H., Ei-Shokrofy K. M. El-Tubby M. M.; Phys. Stat. Sol (a) 171, 563, 1999.

[1.30] Mahmoud M. H., Satter A. A.; "Mössbauer study of Cu-Zn ferrite substituted with rare earth ions"; J. Magn. Magn. Mater. 277, 101-105, 2004.

[1.31] Rodmorcq, Piecuch B.M., Jonta Chr., Machal G. and Manging Ph.; Phys. Rev. B21, 1911, 1980.

[1.32] Chappert J. J., Coey M. D., Lienard A. and Rebouillat J. P.; J. Phys. Fll, 2727, 1981.

[1.33] Chien C. L. and Unruch K. M.; Nucl. Instrum method, 199, 193, 1982.

[1.34] Gubben P. C., Appeldom J. H. F., Vander Kraan A. M. and Buschow K. H. J.; J. Phys. F4, 921, 1974.

[1.35] Mazen S. A., Abdullah M. H., Nakhla R. I., Zuki H. M. and Metawe F.; "X-ray analysis and IR absorption spectra of Li-Ge ferrite"; Mater. Chem. Phys., 34, 35, 1993.

[1.36] Yousif A. A., Elzain M. E., Mazen S. A., Sutherland H. H., Abdullah M. H. and Mansour S.F.; "A Mössbauer and X-ray diffraction investigation of Li-Ti ferrites"; J. phys. Condensed Matter, 6, 5717, 1994.

[1.37] Wafix A. H., Mazen S.A. and Mansour S. F.; "composition dependence of discontinuous magnetization in Li- Ti ferrites"; J. Phys., D26, 2010, 1993.

[1.38] Mazen S. A., Wafix A. H. and Mansour S. F.; "The effect of Ti^{4+} ions on some magnetic properties of lithium ferrite"; J. Mater. Sci.; 31, 2661, 1996.

[1.39] Nakamura T.; "Low temperature sintering of Ni-Zn-Cu ferrite and its permeability spectra"; J. Magn. Magn. Mater,; 168, 285, 1997.

[1.40] Rezlescu N., Rezlescu E., Popa P. D. , Craus M. L. and Rezlescu L.; "Copper ions influence on the physical properties of a Magnesium- Zinc ferrite"; J. Magn. Magn. Mater. 182, 199, 1998.

[1.41] Tsay C. Y., Liu K. S. and Lin T. F.; "Microwave sintering of Ni-Cu-Zn ferrites and multilayer chip inductors"; J. Magn. Magn. Mater.; 209, 189, 2000.

[1.42] Prakash C. and J. S. Baijlal ; "Dielectric Behavior of tetravalent titanium substituted Ni-Zn-ferrites", J. Less Comm. Met. 107, 51, 1985.

[1.43] Mansour S.F.; "Frequency and composition dependence on the dielectric properties for Mg-Zn ferrite"; Egypt. J. Sol.; 28(2), 263, 2005.

[1.44] Smit J., Wijn H. P. J.; "Ferrites", John Wiley & sons, New York, 1959.

[1.45] Goldman A.; "Recent Advances in Ferrite Materials Technology"; in Modern Ferrite Technology, Van Nostrand Reinhold, New York, 1990.

[1.46] Goev G., Masheva V., Ilkov L., Nihtianova D.,Mikhov M.; Proceedings of the fifth General Conference of the Balkan Physical Union BPU-5, 687, 2003.

[1.47] Low K. O., Sale F. R.; J. Magn. Magn. Mater. 256, 221, 2003.

[1.48] Hakim M. A., Haque M. M., Huq M., Hoque M. Sk. And Nordblad P.; "Re entrant spin glass and spin glass behavior of diluted Mg-Zn ferrites"; Cp 1003, Magnetic Materials, International Conference on Magnetic Materials, AIP, 295, 2007.

[1.49] Yue. Z., Zhou J., Li L., Wang X., Gui Z., Mat. Sci. Engg. B.86, 64, 2001.

[1.50] Rezlescu N., Rezlescu E., Popa P. D., Craus M. L., Rezlescu L.; J. Magn. Magn. Mater. 182; 199, 1998.

[1.51] Rezlescu E., Rezlescu N., Popa P. D., Rezlescu L., Pasnicu C., M. L. Craus; Mat. Res. Bull. 33(6); 915, 1998.

[1.52] Khan Z. H., Mahbubur Rahman M., Sikder S. S., Hakim M. A., Shireen Akhter, Das H. N. and Anuman B.; "Thermal Hysteresis of Cu substituted $Ni_{0.28}Cu_{0.10+x}Zn_{0.62-x}Fe_{1.98}O_4$ ferrites"; Advanced Chemistry letters; vol. pp 1-6, 2013.

[1.53] Low K. O. and Sale F. R.; J. Magn. Magn. Mater., 30, 246, 2002.

[1.54] Khan Z. H., Mahbubur Rahman M., Sikder S. S., Hakim M. A., Saha D. K.; "Complex Permeability of Fe- deficient Ni-Cu-Zn ferrites"; Journal of Alloys and compounds; 548, 208-215, 2013.

[1.55] Haque M. M., Huq M. and Hakim M. A.; "Effect of Zn^{2+} substitution on the magnetic properties of $Mg_{1-x}Zn_xFe_2O_4$ ferrites"; Physica, B404, 3915, 2009.

[1.56] Saroaut Noor, Hakim M. A., Sikder S. S., Manjura S. Haque, Kazi Hanium Marja, Per Nordblad; "Magnetic Behavior of Cd^{2+} & substituted Cobalt ferrites"; Journal of Physics and Chemistry of Solids; 73, pp 227-231, 2011.

[1.57] Farea A. M. M., Shatendra Kumar, Khalid Majasam Batoo, Ali Yousef, Alimuddin; " Influence of frequency, temperature and composition on electrical properties of polycrystalline $Co_{0.5}Cd_xFe_{2.5-x}O_4$ ferrites"; Physica B403, 684, 2008.

[1.58] Mahmoud M. H., Satter A. A. ; "Mössbauer study of Cu-Zn ferrite substituted with rare earth ions"; J. Magn. Magn. Mater., 277, 101-105, 204.

[1.59] Hakim M. A., Sikder S. S. ,Asgar M. A., Srivastava B. K. and Krishamurthy A.; "The Study of hyperfine field of amorphous ribbon with composition $Co_{80-x}Fe_xB_{10}Si_{10}$ by Mössbauer technique"; Nuclear Science and Applications; Vol. 13,No-12, November 2004.

[1.60] Mohan M., Shaikh I., Kulkarni R. G.; "Magnetic properties of the Mixed Spinal $CoFe_{2-X}Cr_x O_4$"; Physics B, 403, 684, 2008.

[1.61] Mahmoud M. H., Abdallas A. M, Hamideh H. H., Hikal W. M., Taher S. M., Ho J. C.; "Mössbauer spectroscopic evaluation of high energy Ball milled $CdFe_2O_4$"; J. Man. Magn. Mater.; 263, 269-274, 2003.

[1.62] Dalt S. D., Takim A. S., Volkmer T. M., Sousa V. C., Bergmann C. P.; Powder Technol., 210, 103-108, 2011.

[1.63] Chul Sung Kim, Woo-Chul Kim, Sung Young an, Senng Wha Lee; “Structure and Mossbauer Studies of Cu doped Ni-Zn Ferrite”; J. Magn .Magn. Mater.; 215, 213-216, 2000.

[1.64] Arshed M., Siddique M., Anwer-ul-islam, Butt N. M., Abbas T., Almed M.; Solid State Commun.; 939, 599, 1995.

[1.65] Naknao A., Nakahata I., Murse T.; J. Jpn. Soc. Powder Powder Metal: 48(2) 131, 2001.

[1.66] Brabers V. A. M., Hirsch A. A., Vleuten W. C. V., Doremalen P.V. ; IEEE Trans. Magn. 14(5), 895, 1978.

[1.67] Liu D. M.; J. Mat. Sci. 29, 1507, 1994.

CHAPTER-II

[2.1] Jevadevan B., Chinnasamy C. N., Shinoda K., Tohji K.; “Mn-Zn ferrite with higher magnetization for temperature sensitive magnetic fluid”; J. Appl. Phys.., Vol-93, pp 8450, 2003.

[2.2] Jackson J. D.; “Classical Electrodynamics”; 3rd Ed. John Wisley & Sons, New York, 1998.

[2.3] Vijaya M. S. and Rangarajan; “Materials Science”; Mc Graw-Hill Publ. Com. Ltd., New Delhi., 447, 1999-2000.

[2.4] Hadfield D.; Lliffe Books, LTDT, London, John Wiley and Sons; “Permanent Magnets and Magnetism”; Inc., New York, 1961.

[2.5] Rollin J. Parker and Robertj Stadders; John Wiley and sons; “Permanent Magnets and Their Applications”; Inc., New York, 1962.

[2.6] Rollin J. Parker; John Wiley and Sons, “Advances in Permanent Magnetism”; Inc., New York, 1990.

[2.7] Malcolm Mc Caig, John Wiley and Sons; “Permanent Magnets in Theory and Practice”; Inc., Toronto, 1977.

[2.8] Parasnis D. S., Harper and Brothers, “Magnetism: From Lodestone to Polar Wandering”; New York, 1961.

[2.9] Kittel C.; “Introduction to Solid State Physics”; 7th Ed. John wiley & sons; New York, 1996.

[2.10] Omar M. A.; “Elementary Solid State Physics (Principles & applications)”; Addison Wesley Amsterdam; 1962.

[2.11] Morish A. H.; "The Physical Principle of magnetism"; John Wiley & Sons, 1965.

[2.12] Reitz J. R., Milford F. J. and Chrisly R. W.; "Foundation of Electromagnetic Theory"; 3rd Ed. Addison- Wealey London, 1979.

[2.13] Smit J. and Wijn H. P. J.; "Ferrites", John Wiley & Sons, New York, 1959.

[2.14] Standly K. J.; "Oxide Magnetic Materials"; 2nd ed., Oxford University Press, 1972.

[2.15] Bragg W. H.; "The structure of magnetic and the spinels"; 95, 561, 1915.

[2.16] Livingston J. D.; "Driving Forces: The Natural Magic of Magnets"; Harrand University Press: Cambridge, 1996.

[2.17] Cullity B. D.; "introduction to magnetic Materials"; Addition-Wesley Publishing Com.; 1972.

[2.18] Alex Goldman; "Modern Ferrite Technology", Van nosttrand Reinhold, New York, 1990.

[2.19] Li F. S., Wang L., Wang J. B., Zhou Q. G., Zhou X. Z., Kunkel H. P. and Williams G.; J. Magn. Magn. Mater., 268, 332, 2004.

[2.20] Chen C. W.; "Magnetism and Matallurgy of Soft Magnetic Materials"; New York 1977

[2.21] Chan R. W., Haasan P., Kramar E. I.; "Materials Science and Technology"; Vol.3B VCH Publishers Inc., New York, NY(USA) and Verlagsges ellschaff mbH, Weinheim (Federal Republic of Germany), 1994.

[2.22] Craik D. J.; "Magnetic Oxide"; Part-I, John Wiley and Sons, Ltd., Bristol England 1957.

[2.23] Verway E. J. W. and Heilmann E. L.; J. Chem. Phys. 15(4), 174, 1947.

[2.24] Neel L.; "Magnetic properties of ferrites: Ferrimagneticm and Anti ferromagnetism"; Annales de Phys., 3, 137-198, 1948.

[2.25] Muncu G., Sertel K., Volakis J. L., Figrtin A. and Vitebsky I.; " R. F. Propagation in ferrite thickness nonreciprocal magnetic photonic crystals" ; IEEE Antenna Propagant. SOC. Symp. 2, 1395, 2004.

[2.26] Land A.; "Quantum Mechanics"; Pitman, London, 1951.

[2.27] Van Vleck J. H.; "Theories of Electric and Magnetic Susceptibility"; Claredon Press, Oxford, 1932.

[2.28] Weiss P.; "L'hypothese du champ molecular et lu propriete ferromagnetic"; J. Phys. Theror. Appl., 6, 661, 1907.

[2.29] Vowles, Hugh P.; "Early evolution of Powder Engineering"; 17(2), 412, 1932.

[2.30] Fowler. Michael; "Historical Begimmry of Theories of Electricity and Magnetism"; Retrived, 2008.

[2.31] Cahn R. W., Haasen P., Kramer E. J.; "Materials Science and Technology"; Spring Verlag Naorosa Publishers House, New Delhi, 1990.

[2.32] Halliday D., Resnick R and Walker J.; "Fundamentals of Physics", 6th Ed. John Wiley & Sons, New York, 2002.

[2.33] Romeign F. C., Philips Res. Rep. 8, N-R-5, 304, 1953.

[2.34] Cahn R. W., Haasen P., Kramer E. J.; "Materials Science and Technology"; spring Verlag Naorosa Publishers house,, New Dilhi , 1990.

[2.35] Verway E. J. W. and Heilmann E. L.; J. Chem. Phys., 15(4), 174, 1947.

[2.36] Yafet Y. and Kittel C.; "Anti ferromagnetic arrangements in ferrites"; Phys. Rev. 87, 290, 1952.

[2.37] Leyons D. H., Keplan T. A., Dwight K. and Menyuk N.; "Classical theory of the ground spin state in cubic spinels"; Phys. Rev. 126, 540, 1962.

[2.38] Alex Goldman; "Modern ferrite Technology"; Van Nostrand Reinhold, New York, p15, 1940.

[2.39] William D. Callister; The University of Utah: Materials Science and Engineering 6th Ed., Wiley 2003.

[2.40] Gunther K.Werthein; "Mössbauer effect: Principle and Application"; Academic Press, New York, 1964.

[2.41] Gonser U., Ed., Topics in Applied Physics, Spring erverlag, Berlin Heidelberg, New York, 1973.

[2.42] Kistner O. C. and Sunyar A. W.; Phys. Rev. Letters 4, 229, 1960.

[2.43] May L.; "An introduction to Mossbauer Spectroscopy"; Plenum Press., New York, 1971.

[2.44] Cohen M. H. and Reift R.: Solid State Physics, 5, 321, 1957.

[2.45] Koferman H.; Kernmoments Akad, Verlagesges; M. Franfrut 1956.

[2.46] Sternabeimer R. M.; Phys. Rev., 84, 244, 1951.

[2.47] Wertheim G. K.: "Mössbauer effect: principles and Appliction; Academic Press, New York, 1964.

[2.48] Anjali Krishna Morthy; " Mossauer Study of Electric filed Gradients in Natural Mica and Synthetic Spinel System"; Ph. D. Thesis, University of Rajsthan, Jaipur, 1980.

[2.49] Fermi E.; Z. Physics, 60, 320, 1930.

[2.50] Ferrel R. A.; AJ. 28, 484, 1960.

Chapter III

[3.1] Kong L. B., Li Z. W., Lin G. Q. and Gan Y. B.; “Magneto-Dielectric properties of Mg-Cu-Co ferrites Ceramic: II Electrical, dialectical and magnetic properties”, J. Am. Ceram. Soc., 90(7), 2014, 2007.

[3.2] Sharma S. K., Kumar R., Kumar S. Knobel M., Menses C.T., Kumar V. V. S., Reddy V. R. , Singh M. and Lee C. G.; “ Role of inter partical interactions on the magnetic behavior of $Mg_{0.95}Mn_{0.05}Fe_2O_4$ ferrite nanoparticales”; J. Phys. Conden. Matter. , 20, 235214, 2008.

[3.3] Zahi S., Hashim M. and Daud A. R.; “Synthesis magnetic and microstructure of Ni-Zn ferrite by Sol-gen technique”; J. Magn. Magn. Mater., 308, 177, 2007.

[3.4] Hakim M. A., Saha D. K. and Fazle Kibria A. K. M. ; “Synthesis and temperature dependent structural study of nanocrystalline Mg- ferrite materials”; Bang. J. Phys., 3, 57, 2007.

[3.5] Bhaskar A., Rajini Kanth B. and Murthy S. R.; “Electrical properties of Mn added Mg-Cu- Zn ferrites prepared by microwave sintering method”; J. Magn. Magn. Mater.; 283, 109, 2004.

[3.6] Yue Z., Zhou J., Li L. and Gui Z.; “ Effects of MnO_2 on the electro-magnetic properties of Ni-Cu-Zn ferrites prepared by sol-gel auto combustion”; J. Magn. Magn. Mater., 233, 224, 2001.

[3.7] Burke J.E. ; “Kinetics of High Temperature Processes”, Kingery W. D. ed. (wiley, NY) 1959

[3.8] Slick P. I.; “ Ferrites for Non-microwave applications”, ferromagnetic materials, Ed. E. P. Wolfarth, North Holland Pub Co_2, 1980

[3.9] Kittel C.; Introduction to Solid State Physics, 7th edition, John Wiley and Sons, Inc., Singapore, 1996

[3.10] Nelson J. B., Riley D. P; “An experimental investigation of extrapolation methods in the derivation of accurate unit-cell dimensions of crystals”, Proc. Phys. Soc. London 57, 160, 1945.

[3.11] Gadkari A. B., Shinde T. T. and Vasambekar P. N. ; “Structural and Magnetic properties of nanocrystalline Mg-Cd ferrites prepared by oxalate Co-precipitation methods”; J. Mater. Sci. Mater. Electron, 21(1), 96 - 103, 2010.

[3.12] Tahir Abbas, Islam M. U. and Ashraf M.; Ch. Mod. Phys. Letts. B, 9(22), 1419, 1995.

[3.13] Simon Forner; “Versatile and sensitive Vibrating Sample Magnetometer”, Rev. Sci. Instr. 30, P.548, 1959

Chapter IV

[4.1] Nelson J. B., Riley D. P.; “An experimental investigation of extrapolation methods in the derivation of accurate unit-cell dimensions of crystals”; Proc. Phys. Soc. London 57, 160, 1945.

[4.2] Hemida O. M., Barakal M. M. ; “Effect of hopping rate and jump length of hopping electrons on the conductivity and dielectric properties of Co-Cd ferrites”; J. Magn. Magn. Mater., 223, 127, 2001.

[4.3] Muhammad A. and Maqsood A. ; “Structural electrical and magnetic properties of $Cu_{1-x}Zn_xFe_2O_4$ ($0 \leq x \leq 1$)” ; J. Alloy Compds. 460, 54 - 59, 2008.

[4.4] Abbas T., Islam M. U. and Choudhury M. A. ; “Study of sintering behavior and electrical properties of Cu-Zn-O system”; Modern Phys. Lett. ; B9, 1419-1426, 1995.

[4.5] Satter A. A., El-sayed M. M., El-Shokrofy K. M. and El-Tabey M. M.”; Improvement of the magnetic properties of Mn-Ni-Zn ferrite by the non-magnetic Al^{3+}ions substitution”; J. Appl. Sci. 5(1), 162-168, 2005.

[4.6] Low K. O., Sale F. R.; “Electromagnetic properties of gel-derived Ni-Cu-Zn ferrites”; J. Magn. Magn. Mater., 246, 30, 2002.

[4.7] Bellad S. S., Watawe S. C., Chouguli B. K.; “Microstructure and permeability studies of Mixed Li-Cd ferrites”; J. Magn. Magn. Mater., 195, 57, 1999.

[4.8] Coble R. L., Burke J. E.; in J. E. Burke (Ed.) Sintering in ceramics, Progress in ceramic science, Vol.3, P.474.

[4.9] Neel I., Ann. Phys. 3, 137, 1948.

[4.10] Yatet Y. and Kittel C.; “ Antiferromagnetic arrangements in ferrites”, Phys. Rev. 87, 290, 1952.

[4.11] Geller S.; “Comments on Molecular-Field theory for Randomly substituted ferromagnetic Garnet systems By Nowik”, Phys. Rev, 181, 980, 1969.

[4.12] Patton C. E., Liu Y.; “Localized canting models for substituted magnetic oxides”. J. Phys. C: Solid State Physics, 16, 5995, 1983.

[4.13] Brown F. and Gravel C .L.; Physics Rev., 97, 55, 1955.

[4.14] Kim C. S., Lee S. W., Park S. L., Perk J. Y., Oh Y. J.; J. Appl. Phys. 79, 5428, 1996.

[4.15] Daniels J. H., Roseacwsic Can A.; J. Phys. 48, 1970.

[4.16] Morish A. H., Clari P. E.; Phys. Rev. Bll, 278, 1975.